NOVEL DWT-DAPSK BASED TRANSCEIVERS FOR DVB-T TRANSMISSION AND NEXT GENERATION MOBILE NETWORKS

By

Yahya Ali Lafta Al-hussiany

BSc. (Avionic Electronic Eng.), MSc. (Electronic & Comm. Eng.)

A thesis submitted in partial fulfilment of the requirements of Liverpool John Moores University for the degree of Doctor of Philosophy.

December 2012

NOVEL DWT-DAPSK BASED TRANSCEIVERS FOR DVB-T TRANSMISSION AND NEXT GENERATION MOBILE NETWORKS

By

Yahya Ali Lafta Al-hussiany

ABSTRACT

Digital wireless communication has become one of the most exciting research topics in the electronic engineering field due to the explosive demands for high-speed wireless services, such as cellular video conferencing. The second generation Terrestrial Digital Video Broadcasting (DVB-T2) has been demonstrated to provide digital communication services with very high spectral efficiency and significantly improved performance. Orthogonal Frequency Division Multiplexing (OFDM) systems have been increasingly deployed in mobile networks for their spectral efficiency and optimum bit error rate. An OFDM system is a multi-carrier system which transmits signals from a single source at different frequencies simultaneously as parallel components. A distinguishing feature of the OFDM system is its ability to preserve high bandwidth efficiency in high speed data streams. Among the different types of OFDM systems, wavelet based systems have been demonstrated to have much better bandwidth and channel performance compared to the Discrete Fourier transform (DFT) and Discrete Cosine Transform (DCT) based systems. The DFT and DCT systems suffer from several disadvantages including less bandwidth efficiency due to the need for guard interval and highly complex system design.

Discrete Wavelet transform (DWT) based OFDM systems naturally overcome these disadvantages by their design methodology and the technique of transmitting concentrated energy over small spectral coefficients. Several types of modulation schemes such as DPSK, QAM are employed in OFDM systems, which introduce certain penalties such as increased bandwidth and complexity of the system design. So a multilevel differential modulation technique namely Differential Amplitude and Phase Shift Keying (64 DAPSK) has been proposed as an alternative solution. DAPSK-OFDM is very suitable for high date-rate digital mobile radio channel with additive white Gaussian noise (AWGN). In this research work it has been demonstrated that a combination of DWT-OFDM with DAPSK modulation can be employed to achieve very low peak-to-average power ratio (PAPR), improved bit error ratio (BER), and much reduced inter symbol interference (ISI) & inter-carrier interference (ICI) in wireless mobile network applications. A mathematical model has been proposed for the DWT-OFDM system with DAPSK modulation scheme in this work. The system performance has been evaluated via simulation using Matlab Simulink package and also verified using Matlab programming. This proposed DWT-OFDM with 64DAPSK hybrid system is demonstrated to have better BER (by an order of magnitude for an SNR of 25dB) performance and improved PAPR (by 7.2dB) and interference values. It is also demonstrated that including companding with this system results in further reduction of PAPR. Finally, the simulation results also demonstrate that DWT-DAPSK scheme can be successfully employed in DVTB-T2 systems due to its very high spectral efficiency, much improved BER and significantly reduced PAPR performance.

Acknowledgements

Table of Contents

List of Figures

List of Tables

Abbreviations/acronyms

ADL	asymmetric digital subcarrier
ASK	amplitude shift key
AWGN	additive white Gaussian nose
BER	bit error-rate
BPSK	binary phase shift key
BEP	bit- error probability
BW	bandwidth
CCDF	complementary cumulative distribution function
CFO	carrier-frequency offset
CP	cyclic prefixes
DAB	digital Audio Broadcasting
DCT	discrete cosine transform
DFT	discrete Fourier transform
DVB	digital Video Broadcasting
DWT	discrete wavelet transform
EVM	error vector magnitude
GU	guard interval time
ICI	intercarrier interference
IDCT	inverse discrete cosines transform
IDFT	inverse discrete Fourier transform
IDWT	inverse discrete wavelets transform
ISI	intersymbol interference
MCM	multicarrier modulation
NSAMP	number samples
OBI	Out-of-band
OFDM	orthogonal frequency-division multiplexing
P	average power
PAM	phase amplitude modulation
PAPR	peak to Average Power Ratio
PSD	power spectrum density
PSK	phase shift key
QAM	quadrature amplitude modulation
QPSK	quadrature Phase Shift Keying
SIR	signal interference ratio
VDSL	very high bit rate Digital Subscriber Line
WIMAX	worldwide Interoperability for Microwave Access
WLAN	wireless Local Area Networks

Chapter 1

INTRODUCTION

1.1 Introduction

In broad band mobile multimedia applications the transmission techniques give rise to some drawbacks due to the time-variant and the frequency selective behaviour of the radio channels. Multimedia applications require transmitting mixed type of data such as text, video, graphics, speech etc. using the same radio link. Adapting the transmission itself might lead to very different requirements of the individual services in terms admissible BER [Quality of service (QoS)], maximum delay and data rate. Moreover, it can be expected that there will also be a huge demand for mobile or at least wireless access to multimedia services, for future developments. However, in the case of radio transmission, high data rates lead to additional technical considerations. Therefore, a broad-band radio channel is characterized [Rohling, H., et al (1999)] both by time variant behaviour caused by a moving receiver or transmitter and by frequency selective fading, which is caused by multipath propagation. As a result, more users will be able to receive better quality of service using such a system than by using the traditional code division multiple access (CDMA) systems, additive white Gaussian (AWGN) channel is used by various radio communication technologies. All the demands posed by high data rate transmission could be addressed using orthogonal frequency-division multiplexing (OFDM) as a transmission technique and various broad-band communication system and services. This solution will be able to support data rates higher than that supported by Universal Mobile Telecommunications System (UMTS) and thus can be used in our future mobile communication systems.
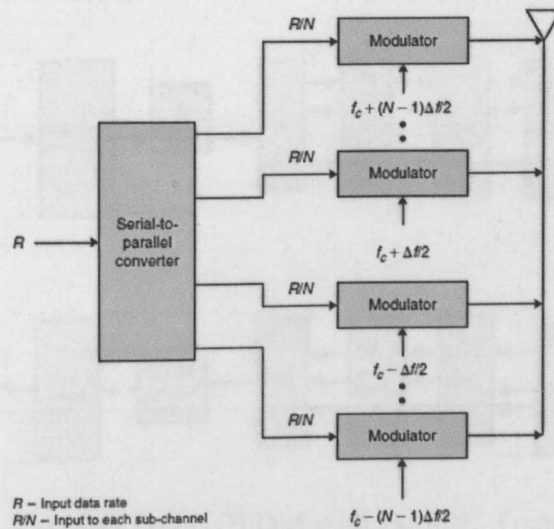
Figure 1-1-1 Orthogonal Frequency Division Multiplexing (OFDM)
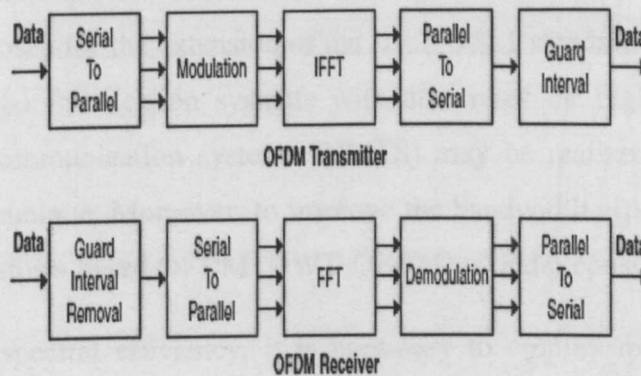
Figure1-1-2 OFDM Transmitters and Receiver systems

In 4G communication systems, bandwidth is a precious commodity, and service providers are continuously met with the challenge of accommodating more users within a limited available bandwidth (Gupta et al 2008, Xiaclong et al 2002). Fourier based multi-carrier modulation (MCM) (often called orthogonal frequency division multiplexing (OFDM) is a strong candidate for the next generation wireless network which requires high data bit rate (Kumbasar, and Kucur, 2008, Li and Stuber, 2006). The main advantage of OFDM is that it is immune to multi path fading (Kumbasar, and Kucur, 2008, Li and Stuber, 2006).
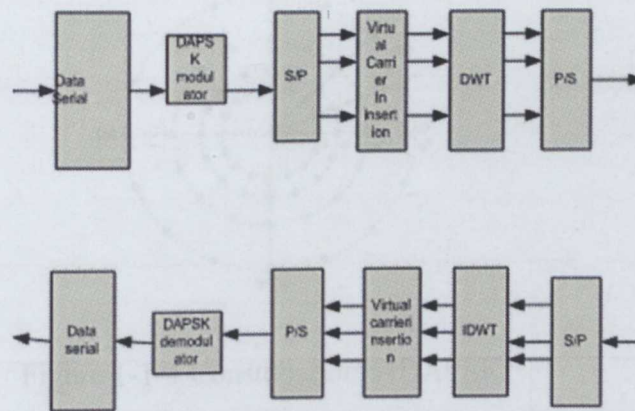
Figure 1-1-3 Hybrid DWT-OFDM with DAPSK Transmission system

Currently, the OFDM transmission technique has been adopted in Europe, for digital video broadcasting (DVB) and digital terrestrial video broadcasting (DTVB). Also, ETSI-BRAN has selected OFDM technique for HIPERLAN 2 (High performance local area networks), and it has also been chosen for the extension of the IEEE 802.1 standard for 5GHz frequency range. Future mobile communication systems with data rates far higher than that of the universal mobile telecommunication systems (UMTS) may be realized using OFDM as a suitable modulation technique. Moreover, to improve the bandwidth efficiency, ISI, and ICI, Discrete Wavelet Transform based OFDM (DWT-OFDM) is under consideration.

To obtain high spectral efficiency, it is necessary to employ multilevel modulation schemes with variable amplitudes (e.g. DAPSK, QAM). These modulation schemes require coherent demodulation that needs to estimate and track parameters of fading channels (Kang et at 2007). Further, a differential modulation technique does not require any explicit knowledge about the radio channel equalization process. As a result, therefore, different modulation techniques do not require a frequency-domain equalizer in the receiver, which reduces the computation complexity.

However, its behavior in dividing the total bandwidth into narrow sub channels results in a detrimental effect of delays being spread due to multipath propagation. The effects of the delay spread can be minimized using appropriate modulation technique. Therefore, OFDM allow the DWT with DAPSK could allow high data rate transmission over highly frequency–selective channels which will implementation cost to be recovered.
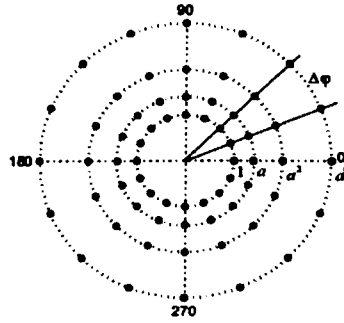
Figure 1-1-4 Constellation 64DAPSK

OFDM systems using discrete Fourier transform (DFT) and discrete cosine transform (DCT) transform have been implemented and are in use in practical systems. A block diagram of such a system is shown in Fig.1.1. However, these cosine Fourier based systems suffer from less bandwidth efficiency due to the need for guard intervals, and thus require a highly complex system design. Therefore, if a conventional single carrier system is used for this purpose, the channel equalization can be very complex. A discrete wavelet transform (DWT) based OFDM systems overcome these disadvantages by transmitting concentrated energy over small spectral coefficients. Many research investigations have led to the conclusion that the wavelet based OFDM is more advantageous than the Fourier based OFDM (Abdullah and Hussian, 2007, Sandberg and Tzannes, 1995, Akansu and Xueming, 1998, Strang and Nguyem, 1994). However, a major disadvantage of the OFDM system on the whole is that the transmitted signal has a high peak-to-average power ratio (PAPR).

1.2 Research Motivation

In recent years, describing complex algebraic functions and analysing empirical continuous data obtained from different types of signals at different scales of resolution have seen significant development. The most widespread application of the wavelet transform so far has been for data compression. This is associated with the fact that the DFT is closely related to sub band decomposition.

Various modulation schemes such as the differential phase shift keying (DPSK), quadrature amplitude modulation (QAM) have been employed in the OFDM systems. However, these modulation schemes have certain drawbacks such as increased BW, complex system design, etc. So an alternative, multilevel differential modulation technique called Differential Amplitude and Phase Shift Keying (64 DAPSK) has been proposed by (Liu, and

Wei, 2001, Tan, 2006, Hanzo et al 1999). Since then it has been shown that (Webb, W. T., 1992) DAPSK-OFDM is very suitable for high data rate digital mobile radio, which uses additive white Gaussian noise (AWGN) channels. This research work draws inspiration from the research models described above, and proposes combining a DWT-OFDM system with DAPSK modulation scheme in order to achieve a low peak-to-average power ratio (PAPR), improved bit error ratio (BER), improved inter symbol interference (ISI) and inter-carrier interference (ICI) in wireless mobile systems. A mathematical model for the DWT-OFDM system with the DAPSK modulation scheme is also proposed in this work. Furthermore, the system performance in terms of BER, PAPR, ISI and ICI is also evaluated via simulation using Simulink/Matlab software package.

1.3 Research Objectives

The principal objectives of this research can be summarized as follows: 1. To compare and evaluate the performance of DCT , DFT and DWT-OFDM techniques in combination with QAM, DPSK and DAPSK in terms of BER, PAPR and SNR; 2. To design a hybrid system of DWT-OFDM with DAPSK modulation and to develop a mathematical model for the system; 3. To simulate the mathematical model by using MATLAB code and verify using the Simulink model; 4. To evaluate the performance of the proposed system in terms of reduced PAPR obtained in the proposed system and the performance of ICI & ISI.

1.4 Contributions

In this research work, a mathematical model that describes hybrid DWT-OFDM with DAPSK scheme has been developed and presented. This hybrid system has been shown to perform better in terms of spectral efficiency, compared to that of the DFT and DCT based systems for high data rate applications such as mobile communication networks. Moreover, the DWT is widely used for data compression. Wavelet based still image compression methods not only out-perform traditional methods in the rate-distortion sense, but also possess built-in scalability such that single bit stream can be transmitted progressively and decoded from coarse to fine resolution (Guo, H., 1998) While DWT-OFDM provides many advantages, the transmitted signal does not have a constant envelope. In this work, reduction in the power contained in the side-lobes has been demonstrated using a new companding transform technique for combination of DWT OFDM with 64DAPSK.

Moreover, the proposed hybrid system is demonstrated to have improved the bandwidth efficiency, ISI, and ICI.

1.5 Thesis layout

The layout of this PhD thesis is as follows: After an introduction in Chapter 1, Chapter 2 presents the literature review on OFDM techniques and the associated modulation schemes. Chapter 3 presents the background information on OFDM systems with different transformations techniques and modulation schemes. Chapter 4 presents the mathematical model and the analysis for the novel hybrid OFDM system consisting DWT system with DAPSK scheme that can be used for wireless communication system for optimum performance. Chapter 5 presents the simulation and analysis of the proposed system, and its performance evaluation using Matlab/Simulink software package. The results and discussion for simulation are presented in Chapter 6, while Chapter 7 summarises the conclusion and provides suggestions for future extension of the work. Finally, the references are listed and two appendices are included as well.

Chapter 2

Literature Review on OFDM techniques and modulation scheme

Multicarrier modulation techniques such as orthogonal frequency division multiplexing (OFDM) are attractive for a number of reasons. They have high spectral efficiency since the sub-carriers are orthogonal in frequency and also adaptive bit loading techniques can be employed.

As the OFDM techniques are suitable for both flat fading and frequency selective fading communication channels, they have been implemented in communication systems since the 90s (Lee and Williams, 2000). The OFDM technique imposes high demands on the accuracy of frequency synchronization. An approach of the OFDM is to change the spectral occupancy by using pulse shaping techniques. Furthermore, OFDM appears to cope with issues such as narrowband jamming, and also serves as a natural solution when the available spectrum is not contiguous, for the overlay system (Mounir and Swami, 2008).

The OFDM is not without its disadvantages. One of the major disadvantages of OFDM is its characteristically high peak-to-average power ratio (PAPR). Severe signal distortions will result, when high PAPR signals are transmitted through non-linear power amplifiers. Another disadvantage is the power and bandwidth penalty imposed by the closely spaced subcarriers and thus the cyclic guard interval makes the link performance sensitive to oscillator frequency offset and phase noise. This means that OFDM systems require more expensive power amplifiers. , and therefore techniques for reducing the PAPR of OFDM signals have been studied extensively (Jun and Stuber, 2002) by researchers.

In OFDM system design, a number of parameters need to be considered, such as the guard time's symbol duration, number of subcarriers, subcarriers spacing, the type of forward

error correction coding, and modulation type per subcarrier. The choice of parameters is influenced by system requirements such as required bit rate, available bandwidth, Doppler values and tolerable delay spread. Some requirements pose conflicting demands. For instance, a large number of subcarriers with small subcarrier spacing are desirable to get a good delay spread tolerance, however the opposite is true for good tolerance against phase noise and Doppler spread (van Nee, 1996).

2.1 DFT, DCT, and DWT OFDM Systems,

2.1.1 DFT based OFDM

For analysing harmonic signals for which there is no need for local information, the Fourier transform theory has been very useful. The Fourier series is called the discrete Fourier transform (DFT) if it used in this way to represent finite-length sequences. In the following discussions, t_s represents one period finite-duration of a DFS sample within the finite-duration sequence.

Fast Fourier transform (FFT) algorithms are based on the fundamental principle of decomposing the computation of the discrete Fourier transform of length into successively smaller DFT components. The way this principle is implemented leads to a variety of different algorithms, all with comparable improvements in computational speed. Generally, we have two types. The first, called decimation in time, derives its name from the fact that in the process of arranging the computation into smaller transformations, the sequence x[n] (generally thought of as a time sequence) is decomposed into successively smaller sub time sequences. In the second general class of algorithms, the sequence of DFT coefficients X[k] in which a frequency coefficient is decomposed into smaller sub frequency sequences – hence its name, decimation in frequency (Oppenheim, A. V., et al., 1998).

Already the traditional DFT based OFDM has been successful in generating research interest in its application to high performance local area networks (HIPRLAN) (Peng and Beaulieu, 2006), European digital video/audio systems (DVB, DAB) (Tao et al., 2007), and in the physical layers of many wireless network standards, such as IEEE.802.11a, IEEE 802.16a. (Tao et al., 2007). It has also found applications in asymmetric digital subscriber loop (ADLS), and in wire-line digital communications system(Bingham, 2000). The OFDM system's digital demodulations and modulations can be realised as DFT and the inverse DFT (IDFT), respectively (Weinstein and Ebert, 1971).

2.1.2 DCT based OFDM

The discrete cosine transform (DCT) scheme is synthesised based on a set of cosinusoidal functions that can be used in an orthogonal basis to achieve multicarrier modulation (MCM) (Gupta et al., 2008). DCT has better compression capability for bit rate reduction compared to other techniques like transform coding or predictive coding (Gharge and Krishnan, 2007). Compression plays a significant role in transmission and signal or image processing. Most video compression standards such as MJPEG, HDTV, JPEG and H. 261, use DCT as the standard transform coding scheme(Chiu and Liu, 1992).

The DCT-OFDM can sometimes, offer additional benefits over the DFT-OFDM, since the fast DCT algorithms provide fewer computational problems than FFT algorithms, as proposed in(Wang and 1984). The upper bound of throughput for the DFT- based OFDM system is less than that of the DCT-based OFDM system, in the case of exponentially and static decaying channel profiles by using the circular convolution property of the DCT, as reported for the DCT-OFDM system feeding a symmetrically extended data sequence (Peng and Beaulieu, 2006).

However, both DFT and DCT based OFDM systems need to add guard interval time (GI) or cyclic prefixes (CP) to the signal before transmitting it, in order to spread the successive frame symbols with an immunity against inter-symbol interference (ISI), which decreases the spectral containment of the channel (Abdullah et al., 2009).

2.1.3 DWT based OFDM

In recent years, describing complex algebraic functions and analysing empirical continuous data obtained from different types of signals at different scales of resolution have seen significant development. The most widespread application of the wavelet transform so far has been in data compression. This is associated with the fact that the DWT is closely related to sub band decomposition.

The discrete wavelet transform OFDM (DWT-OFDM) does not require cyclic prefixing (CP) (Dilmaghani and Ghavami, 2008) so that the spectral containment of the channels is better for DWT than DFT and DCT-OFDM systems. Then, as alternative platforms for replacing FFT and IFFT, the DWT and IDWT have been proposed in (Dilmaghani and Ghavami, 2008). The DWT-OFDM system saves 20% in bandwidth (BW) efficiency compared to DFT and DCT systems due to the elimination of CP (Tellambura, 2001). Also, DWT-OFDM can better combat narrowband interference due to its very high spectral containment properties of wavelet filter, and its inherent robustness with respect to inter carrier interference (ICI) than the traditional DFT (Tellambura, 2001)

In addition, using wavelet in OFDM systems results much lower levels of ICI compared to DFT OFDM (Sandberg and Tzannes, 1995) systems, due to the huge reduction in power contribution to the side-lobes..

2.2 Modulation schemes

The process of transforming the information generated by a source into a signal format that is suitable for transmission over a physical channel is denoted by the term modulation.

The information is represented by a sequence of bits b_i of period T_b, in the case of digital transmission (Benvenuto et al., 2007). The modulation theory employs frequency and time domain analyse systems for demodulation and modulation of information-bearing signals (Zimer et al., 1990). The main modulation techniques used in modern digital communication systems are QPSK, QAM, DPSK, DAPSK, etc.

2.2.1 QPSK modulation scheme

The quadrature phase shift keying (4-PSK) termed as QPSK, uses 2 basis functions for its modulation. The input bit sequence is split into two bit sequences, i.e. in-phase and quadrature sequences. The two binary sequences are then separately modulated by two carriers, which are in quadrature. The two modulated signals, each of which can be considered as a BPSK signal, are summed to produce a QPSK signal. Each coordinate in its constellation quarter represents a point in real and imaginary terms in the signal space. Thus, the transmitted signals can be represented in terms of two orthonormal functions (Zimer et al., 1990).

The QPSK scheme is proposed in the DFT-OFDM system to improve measurement parameters such as Bite Error Rate (BER) and avoid ICI (Ryu et al., 2005).

2.2.2 QAM modulation scheme

The quadrature amplitude modulation (QAM) is a signalling scheme that allows multiple signals to be transmitted using quadrature carriers (Benvenuto et al., 2007). It is a multilevel modulation scheme that can be represented in M-QAM where M is equal to 2^n, n= 1, 2... 8.

Although, conventional QAM requires exact channel estimation for coherent demodulation it can also achieve high bandwidth efficiency (Kai-ming et al., 2005). However, the channel estimation may lead to severe performance degradation when estimation error increases and requires relatively high computational effort (Xiaoyi et al., 1999).

There have been several research proposals to use QAM modulation scheme in conjunction with DFT, DCT and DWT based OFDM systems. For example, DWT-OFDM and DFT-OFDM systems with QAM modulation have been implemented in the system demonstrated by (Abdullah et al., 2009).

However, there are certain drawbacks in using the 64QAM modulation in HF communication systems. For example the complex equalization algorithms and channel estimation required for this system, result in an increased cost of receiver and demands a large amount of computation. Moreover, the small angular separation between the constellation points imply high sensitivity to carrier synchronization, and a nonlinear distortion in both amplitude and phase is caused when the power amplifiers are operated close to saturation region in order to improve power efficiency.

2.2.3 DPSK modulation scheme

The differential phase shift key (DPSK) is a differential encoding of the message sequence at the transmitter (Zimer et al., 1990). Each bit of the encoded sequence is calculated by holding the current digit as a reference for the following bit in the sequence. A '1' is encoded as no change of state, and a '0' is encoded as a transition from the state of the reference bit to the opposite state in the encoded message sequence. The encoded message sequence then phase-shift keys a carrier with phase π and 0 (Zimer et al., 1990). The M-DPSK modulation is proposed in (Divsalar and Simon, 1990).

For the DPSK modulation scheme, the constellation diagram describes the transition between phase states. For the 64DPSK, a phase difference of 5.625^0 exists between the adjacent phase states in the constellation diagram. Due to the noise disturbances an additional phase deviation of 2.8125^0 occurs in the radio channel, which leads to an increased BER in the receiver and thus may result in a false decision.

2.2.4 DAPSK modulation scheme

The differential amplitude and phase shift keying (DAPSK) is a multilevel differential modulation technique, which is constituted from amplitude shift keying (ASK) and DPSK (Rohling and Engels, 1995). It reduces the computational complexity as it does not require any explicit knowledge of the radio channel properties in the differential channel equalization process; therefore it is not necessary to implement channel estimation and frequency-domain equalizer.

The data bits to be transmitted are directly mapped to the phase difference and the amplitude ratio of two consecutive modulation symbols in the same subcarrier in the frequency domain for an OFDM symbol. But the information is contained in the difference between the two consecutive subcarriers in the same OFDM symbol in the time direction for an OFDM symbol.

64-DAPSK was first proposed for digital terrestrial video broadcasting (DTVB) application (Rohling and Engels, 1995) as an alternative modulation technique. Also, the 64DAPSK is a very attractive technique for high data-rate transmission in mobile radio environment due to reduced complexity in its receiver design.

2.3 Performance measurements of BER, PAPR, ISI, ICI

2.3.1 Performance measurements of ICI and ISI

The choice of performance measurement parameters often results in a trade-off between conflicting requirements. For example, we can consider bandwidth, bit rate, and delay-spread. To start with, the delay-spread directly dictates the guard time to be about two to four times the root-mean-squared value of the delay-spread. In practical scenario, the guard value depends on the type of coding and QAM modulation. Higher order QAM (like 64-

QAM) is more sensitive to ICI and ISI than QPSK; while heavier coding naturally reduces the sensitivity to interference such as (ICI, ISI)(Nee, 2000). Now that the guard time has been set, the symbol duration can be fixed. To minimize the reduction in the signal-to-noise ratio (SNR) caused by the guard time, it is desirable to have the symbol duration much larger than that of the guard time. It cannot be increased by an arbitrary value, however, because of the possible increase in implementation complexity, and sensitivity (ICI, ISI) to phase noise and frequency offset (Pollet et al., 1995) as well as increased peak-to-average ratio (Pauli, 1997) (Rapp, 1991a). Hence, a practical design choice is to make the symbol duration at least five times the guard time, which implies a –3dB SNR loss because of the guard time.

The received signal may contain more than one replica of the transmitted signals arriving at different time delays, causing degradation of the overall system performance and ISI, therefore the mobile radio channel is characterized by multipath reception in addition to direct LOS (Latif and Gohar, 2006). The sensitivity of the OFDM receiver to carrier frequency offset (CFO) introduces ICI in the system, this carrier frequency offset can be compensated by frequency offset estimation. However, estimation residue frequency offset (caused by frequency differences between oscillators in the transmitter and receiver or frequency selective fading) usually exists in OFDM system, and is inevitable. Therefore, schemes that are robust to frequency offset (Latif and Gohar, 2006) need to be investigated. Applying a raised-cosine window to the ISI free part of the received OFDM symbol is proposed in (Beaulieu and Peng, 2007) to reduce ICI.

The DCT operation distributes more energy to the desired subcarrier and less energy to the interfering subcarrier channels as opposed to the DFT operation. Therefore, the desired subcarrier suffers from less ICI coming from neighbouring subcarriers in DCT-OFDM than in the DFT-OFDM system (Peng and Beaulieu, 2006).

The DCT-OFDM gives smaller ICI power and greater signal-to-interference ratio (SIR) than the DFT-OFDM when the system is operating in the presence of CFO over an AWGN channel. One can also consider the SIR defined by (Peng and Beaulieu, 2006) .

The ICI and SIR analysis suggests that the desired subcarrier suffers less ICI coming from neighbouring subcarriers in DCT-OFDM than in DFT-OFDM. The reduced interference will lead to better bit–error probability (BEP) performance, which can be observed from the exact BEP expression and simulation results demonstrated by (Peng and Beaulieu, 2006). A full range of CFO estimation is achieved due to the anti-symmetry introduced in DCT-OFDM. The DCT-OFDM can provide more robust and accurate estimation than the DFT-OFDM(Tao et al., 2007).

2.3.2 BER and PAPR Performance

The probability of error in terms of the number of erroneous bits per bit number is described as Bit Error Rate (BER), which is a commonly used performance metric.

The OFDM system of the data-conjugate shows, with respect to the PAPR and BER, the best performance compared with the original OFDM, OFDM with the data-conversion method and convolution coding (Ryu et al., 2005).

In certain environments, the BER performance of MCM systems with a wavelet orthogonal base is better than those employing a Fourier base, though their PAPR is higher than that of the MCM system employing a Fourier base. As demonstrated earlier (Zhang et al., 2007), if the transmitted peak power is limited, no matter by regularity or application constraint, the average power allowed by MCM will be reduced. This will in turn reduce the transmission range of MCM systems. Thus, to maintain spectral efficiency, a linear amplifier with a large dynamic range is needed. This would greatly degrade the power efficiency, which should be avoided. Therefore, to increase the efficiency of wavelet based MCM

systems, appropriate methods are required to reduce the PAPR to conserve the power consumption (Zhang et al., 2007).

In fact, the PAPR may be reduced by increasing the average power of signals while keeping the peak unchanged, but the reduction in PAPR may be very limited under certain BER performance constraints. In order to arrive at an optimum trade-off between BER performance and the reduction in PAPR in practical OFDM systems, (Xiao et al., 2002) has proposed the use of piecewise scales transform (PST) using the complementary cumulative distribution function (CCDF) of PAPR of signals. Although, several researchers have tried to address the reduction of PAPR in the continuous- time OFDM signal (continuous-time PAPR or convenience) (Tellambura, 2001) (Hua and Gang, 2003), only Wang and Poor have proposed using complex modulation scheme to reduce PAPR (Wong et al., 2008) in discrete time domain.

Different wavelets (harr, coieflets, and symlets) have been analysed in (Khalid and Shah, 2006) to find that DWT-OFDM has lesser peak to average power ratio (PAPR). Also, reduction by using wavelet packet tree (BWPT) structures for PAPRs of Harr, Db-4 and DB-6 binary phase shift keying (BPSK)-wavelet OFDM(WOFDM) are compared to conventional Mallat structures in (Kumbasar and Kucur, 2008).

Based on the detailed literature review presented, it is confirmed that while a large selection of research work is available on DWT-OFDM systems and DAPSK modulation schemes independently, there is no serious proposal to combine the two for high bit-rate communication with reduced PAPR. Therefore, this research work proposes a hybrid DWT-OFDM with 64DAPSK modulation in order to achieve much reduced PAPR and to improve ISI and ICI due to interference in high speed mobile networks.

Chapter 3

OFDM Systems and modulation techniques

3.1   Introduction

In conventional OFDM system guard intervals (GIs) or cyclic prefixes (CPs) are used to prevent Inter-symbol Interference (ISI) and Inter-carrier Interference (ICI) which converts the linear convolution into a cyclic one). This kind of conversion can be exploited to simplify the equalisation in the receiver by substituting frequency-domain equalisation (Zou, W.Y., and Wu, Y., 1995, Jarot, S.P.W., and Nakagava, M., 2001). Another advantage of using GIs or CPs lies in the fact that ISI caused by sidebands of pulse shaping filter can be diminished. As the GI or CPs must be discarded at the receiver, system throughput is greatly reduced (Zhang, H. et al 2007). Also, this will have an adverse effect on bandwidth of the system. The Discrete Fourier Transform based OFDM (DFT-OFDM) has currently drawn the most attention in the area of wireless communication. However, in order to combat ISI, a cyclic prefix (CP) is inserted between the DFT-OFDM symbols, and this will take up nearly 20% of the bandwidth efficiency. Another promising MCM system, known as the DCT based OFDM has been proposed by AL-Dhahir, N. et al 2006, where it is shown that the DCT-OFDM can under certain circumstances, offer additional benefits over the DFT-OFDM. In particular, the bandwidth required for DCT is half of that required for DFT, for the same number of sub-carriers (Tan, J., and Stiber G. L., 2002). Whereas, DWT-OFDM offers improved narrowband interference due to very high spectral containment properties of wavelet filters, and is inherently more robust against ICI than the DFT based OFDM systems (Khalid, S., and Shah, S. I.,2006, Ahmed, N., 2000). In addition, DWT-OFDM is implemented using overlapped wavelets to preserve data rate (Ahmed, N., 2000). The great reduction in

side-lobe levels is also a motivation behind the recent trend towards wavelet based

OFDM systems.

3.2   DFT-OFDM SYSTEM

3.2.1 The basic concepts of Fourier transform

If s(t) is a periodic function with period T that has a finite energy per period is

expressed by the following equation(i.e., $\int_{t_0}^{t_0+T} |s(t)^2| dt < \infty$), when resolving this

function results in equation 3-1

$$s(t) = a_0 + \sum_{n=1}^{\infty}(a_n cos2\pi nf_0 t + b_n sin2\pi nf_0 t)$$ 3-1

where t_0 represents an arbitrary time,

$$f_0 = \frac{1}{T}$$

and

$$a_0 = \frac{1}{T}\int_{t_0}^{t_0+T} s(t)dt$$

$$a_n = \frac{2}{T}\int_{t_0}^{t_0+T} s(t)cos\ (2\pi nf_0 t)dt$$

$$b_n = \frac{2}{T}\int_{t_0}^{t_0+T} s(t)sin\ (2\pi nf_0 t)dt$$

$$X_n = \sqrt{a^2{}_n + b^2{}_n}$$

$$\emptyset_n = arctan\left(\frac{-b_n}{a_n}\right)$$

where X_n is the magnitude and $\emptyset_n$ the phase, which is the angle by which the single

equivalent phasor leads a_n phasor (Harlod and Samy, 2004).

3.2.2 The Discrete Fourier Transform (DFT)

OFDM employs N_s separate subcarriers to transmit data instead of one main

carrier. Input data is grouped into a block of N bits, where $N = N_s + m_n$ and m_n is

the number of bits used to represent a symbol for each subcarrier. In order to

maintain orthogonality between the subcarriers, they are required to be spaced apart by an integer multiple of subcarrier symbol rate R_s. The subcarrier symbol rate is related to overall coded bit rate R_c of the entire system by $R_s = R_c/N$(Gupta et al., 2008). The output signal of an OFDM can be written using equation 3-2,

$$X(T) = \sum_{N=0}^{N_s-1} C_k\, e^{2\pi j(n-N_s/2)t/T_s} \qquad 3\text{-}1$$

where C_k are the complex representation of subcarrier symbols and T_s is the symbol period (Guenbacher, D. M. and Serner, A., 2001).

When the Fourier series is used in this way to represent finite-length sequence, it is called the DFT.

3.2.3 Efficient Computation of the Discrete Fourier Transform

The DFT of a finite –length sequence of length N is given by

$$X[k] = \sum_{n=0}^{N-1} x[n]\, W_N^{kn}, \quad k = 0,\ 1,\dots\ N\text{-} \qquad\qquad 3\text{-}2$$

where $W_N = e^{-j(2\pi/N)}$, and the inverse discrete Fourier transform is given by

$$x[n] = \frac{1}{N}\sum_{k=0}^{N-1} X[k]\, W_N^{-kn} \quad n= 0,\ 1,\dots,\ N\text{-}1 \qquad\qquad 3\text{-}3$$

In equations (3-3) and (3-4), both $x[n]$ and x[k] may be complex, and also the expressions on the right-hand sides of these two equations differ only in the sign of the exponent of W_N and in the scale factor 1/N.

Direct evaluation of the DFT expression in equation 3-3 provides the parameters for the following discussion. If the equation 3-3 is used as the formula for computation of DFT, N complex multiplications and (N-1) complex additions are required to compute each value of the DFT. This is because x[n] is complex. To compute all N values therefore it requires a total of N^2 complex multiplications and N (N-1) complex additions. Expressing Eq. (3-3) in terms of operations on real numbers, we obtain, the resulting expression represented by equation 3-5

$$X[k] =$$

$$\sum_{n=0}^{N-1}\left[\left(\mathcal{R}e\{x[n]\}\mathcal{R}e\{W_N^{kn}\} - \mathfrak{I}m\{x[n]\}\mathfrak{I}m\{W_N^{kn}\}\right) + j\left(\mathcal{R}e\{x[n]\}\mathcal{R}e\{W_N^{kn}\} - \right.\right.$$

$$\left.\left.\mathfrak{I}m\{x[n]\}\mathfrak{I}m\{W_N^{kn}\}\right)\right] \qquad 3\text{-}4$$

Where, K = 0, 1... N-1,

which shows that each complex multiplication requires four real multiplications and two real additions, and each complex addition require two real additions. Therefore, for each value of k, the direct computation of X[k] requires 4N different values of k. The direct computation of the discrete Fourier transform of a sequence x[n] requires $4N^2$ real multiplications and N (4N-2) real additions. Besides the multiplications and additions called by (3-5), the digital computation of the DFT on general–purpose digital computer or with special–purpose hardware also requires the ability for storing and accessing the N complex input sequence values x[n] and values of the complex coefficients W_N^{kn}. Since the amount of computation time is approximately proportional to N^2, it is evident that the number of arithmetic operations required for computing the DFT by the direct method becomes very large for large values of N. For this reason, the computational procedures that reduce the number of multiplications and additions by using FFT and IFFT become the point of interest for the researchers.

3.2.4 The Specifications for DFT
Some of the main specifications of the DFT system for consideration are discussed below:

The Fourier series are defined as solutions of partial differential equation, under prescribed boundary conditions. Decomposing a given function into an infinite but discrete set of harmonic components represents the resolution of Fourier series. The

transform of signal is often called the Fourier spectrum when it decomposes into a sine wave of different frequencies and phases. $f^\wedge(k)$ can be defined as the Fourier transform of function f(x) in the space and wave number domains where x represents the space variable and k is the wave number. The trigonometric kernel exp (-ikx), is one of the important features in the Fourier transform that oscillates indefinitely. So that, the localized information contained in the signal space f(x) is widely distributed among $f^\wedge(k)$ in the Fourier transform space. It is almost impossible to study its properties from those of $f^\wedge(k)$ when there are computational or observational errors involved in the signal f(x). The Fourier transform of signal does not reflect the change of the wave number with space or of frequency with time. Therefore, it does not contain any local information. The Fourier transform does not aid investigation of the problem simultaneously in both time (space) and frequency (wave number) domains.

Having to use separate analyses for time and frequency resolution in DFT and DCT systems make Fourier transform analysis seem inadequate for studying the physical problems in spite of some of the remarkable successes. This is considered as the major weakness of the Fourier transform analysis. It is therefore necessary for a single transform to give complete time and frequency domains (or space and wave number) of the signal, which can be used to describe the energy density of signal simultaneously in both time and frequency domains.

3.2.5 Generation of Subcarriers using The Inverse Fast Fourier Transform (IFFT)

An OFDM signal consists of the sum of subcarriers that are modulated by using phase shift keying (PSK) or quadrature amplitude modulation (QAM). If d_i are the complex QAM symbols, N_s is the number of subcarriers, T the symbol duration,

and f_c the carrier frequency, then one OFDM symbol starting at $t = t_s$ can be written as:

$$\begin{cases} s(t) = R_E \left\{ \sum_{I=\frac{N_s}{2}}^{N_s} d_{i+\frac{N_s}{2}} exp \left(j2\pi \left(f_c - \frac{i+0.5}{T} \right) (t - t_s) \right) \right\} & ,t_s < t \le t_s + T \\ s(t) = 0 & ,t < t_s \ and \ t > t_s + T \end{cases}$$

3-5

In the literature, often the equivalent complex baseband notation is used for representing OFDM signal, which is given by equation 3-6. In this representation, the real and imaginary parts correspond to the in phase and quadrature parts of the OFDM signal, which have to be multiplied by a cosine and sine of the desired carrier frequency to produce the final OFDM signal, as given below.

$$\begin{cases} s(t) = \sum_{t=\frac{N_s}{2}}^{\frac{N_s}{2}-1} d_{i+\frac{N_s}{2}} exp \left(j2\pi \frac{i}{T} (t - t_s) \right), t_s < t \le t_s + T \\ s(t) = 0, & t < t_s \ and \ t > t_s + T \end{cases}$$

3-6

where d_i are the complex QAM symbols, Ns is the number of subcarriers, T the symbol duration, and s(t) is a signal OFDM. Fig.3.1 shows the block diagram of an OFDM modulator. Here, the increasing data symbols are translated from serial to parallel and then each symbol is modulated by a subcarrier which is orthogonal to its neighbours.

$$\exp^{(-j\pi N_s(t-t_s)/T)}$$

$$\exp^{(j\pi(N_s-2)(t-t_s))/T}$$

$$\exp^{(-j\pi N_s(t-t_s)/T)}$$

Serial
To
parallel
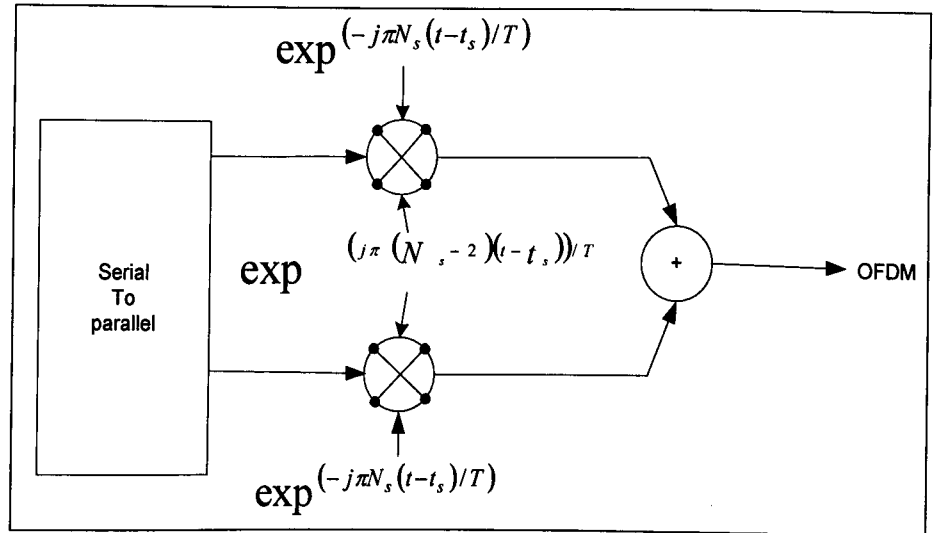
OFDM

Figure3-2 OFDM MODULATOR

As an example, Fig.3.2 shows four subcarriers within one OFDM signal. In this example, all subcarriers have the same phase and amplitude but, in practice, the amplitudes and phases will be modulated differently for each subcarrier. Note that each subcarrier has exactly an integer number of cycles in the interval T, and the number of cycles between adjacent subcarriers differs by exactly one. This property accounts for the orthogonality between the subcarriers. For instance, if the jth subcarrier from Eq. 3-6 is demodulated by down converting the signal at a frequency of j/T and then integrating the signal over T seconds, the result presented by Eq. 3-7. By examining the result from Eq. 3-7, it can be seen that a complex carrier is integrated over T seconds. For the demodulated subcarriers this j, in the integration, gives the desired output $d_{j+N/2}$(multiplied by a constant factor T), which is the QAM value for those demodulated subcarriers. For all the other subcarriers, the integration is zero, because the frequency differences (i-j)/T produce an integer number of cycles within the integration interval T, such that the integration result is always zero.
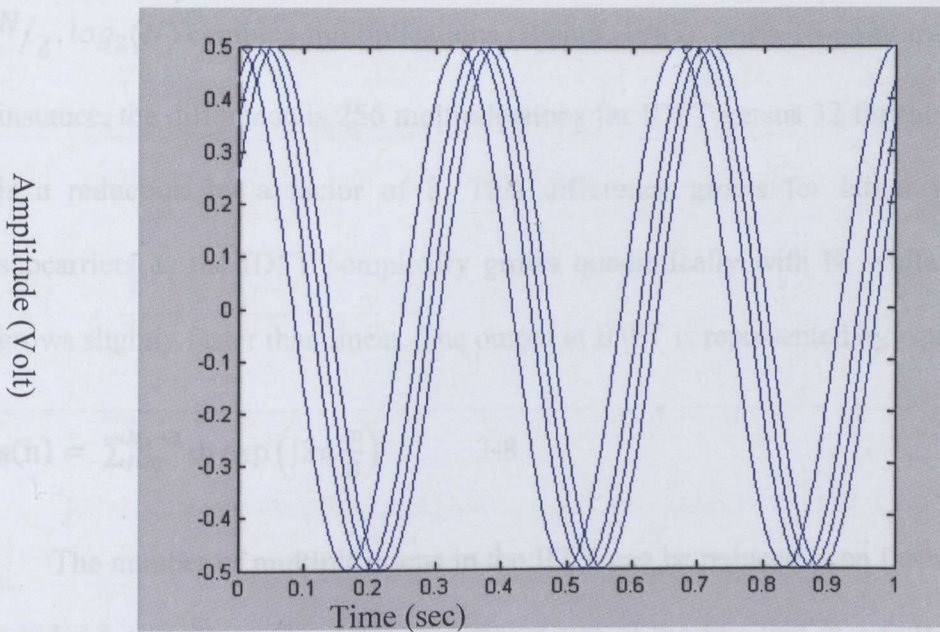
Figure 3-3 Example of Four subcarriers within one OFDM symbol, the y-axis is

amplitude and the x-axis is time

$$\int_0^{\frac{N_S}{2}+1} \exp^{(-j2\pi\frac{S((t-t_s))}{T}} \sum_{i=\frac{N_S}{2}}^{\frac{N_S}{2}+1} d_{i+\frac{N_S}{2}} \exp\left(j2\pi\frac{i}{T}(t-t_s)\right) dt$$

$$= \sum_{i=\frac{N_S}{2}}^{\frac{N_S}{2}+1} d_{i+N_S/2} \int_{t_s}^{t_s+\tau} \exp\left(j2\pi\frac{i-j}{T}(t-t_s)\right) dt = d_{j+N_S} \qquad 3\text{-}7$$

The complex baseband OFDM signal as defined by Eq. 3-8 is, in fact, nothing more than the Fourier transform of N_S numbering QAM input symbols. The time discrete equivalent is the inverse discrete Fourier transform (IDFT), which is given in Eq. 3-5 where the coordinate for time t is replaced by the number n.

In practice, this transform can be implemented very efficiently by using the inverse fast Fourier transform (IFFT). An N point IDFT requires a total of N^2 complex multiplications, which actually translate to phase rotations. Therefore, the IFFT drastically reduces the amount of calculations by exploiting the regularity of the operations in the IDFT. Using the radix -2 algorithms, an N-point IFFT requires only

$N/_2 \cdot log_2(N)$ complex multiplications (Blahut, 1985). For a 16-point transform, for instance, the difference is 256 multiplications for IDFT versus 32 for the IFFT. This is a reduction by a factor of 8. This difference grows for larger numbers of subcarriers as the IDFT complexity grows quadratically with N, while IFFT only grows slightly faster than linear. The output at IDFT is represented by equation 3-9.

$$s(n) = \sum_{i=0}^{N_s-1} d_i \exp\left(j2\pi \frac{in}{N}\right) \qquad 3\text{-}8$$

The number of multiplications in the IFFT can be reduced even further by using a radix-4 algorithm. This technique makes use of the fact that in a four-point IFFT there is only multiplication by (1, -1, j, -j), which actually does not need to be implemented by a full multiplier, but rather using a simple add or subtract and switch of real and imaginary parts in the case of multiplication –j. In this radix-4 algorithm, the full Fourier transform is split into a number of such trivial four-point transforms, and only non-trivial multiplications have to be performed between the stages of these four-point transforms. In this way, an N-point FFT using the radix-4 algorithm only requires (3/8) N ($log_2 N - 2$) complex multiplications or phase rotations and $log_2 N$ complex additions. in simplest representation, the N-point FFT will require 1.5 phase rotations and 6 additions. Non-trivial phase rotations largely establish that the implementation of a complex multiplication is at least an order of magnitude larger than the complexity of an addition.

3.3   DCT-OFDM SYSTEMS

3.3.1 Discrete Cosine Transform DCT

A signal represented by a set of cosinusoidal functions can be used on orthogonal basis to implement the multi carrier modulation (MCM) scheme, and this scheme can be synthesized using a discrete cosine transform (DCT) (Schuchet, et al 2001).

A signal from the cosinusoidal functions set $\cos(2\pi n F_\Delta t)$, n=0,1,....., N-1 will be used as the orthogonal basis to implement MCM in DCT. The minimum frequency spacing F_Δ is required to satisfy the following condition, given by equation 3-10:

$$\int_0^T \sqrt{\frac{2}{T}}\cos(2\pi k F_\Delta t) \sqrt{\frac{2}{T}}\cos(2\pi m F_\Delta t)\, dt = \begin{Bmatrix} 1, k = m \\ 0 \;\; k \neq m \end{Bmatrix} \qquad\qquad 3\text{-}9$$

the duration is $\frac{1}{2T}$ Hz for this spacing frequency [Tan, P., 2006]. However, it is worth noting that in DCT-OFDM system, if the data symbols d_n are obtained by real valued modulation formats, such as PAM and BPSK, the baseband DCT-OFDM signal x (t) is still a real value. The output signal of DCT based OFDM can be written as using equation 3-11.

$$X(t) = \sqrt{\frac{2}{N_s}}\sum_{n=0}^{N_s-1} d_n \beta_n \cos\left(\frac{n\pi t}{T_s}\right) \quad 3\text{-}10$$

Here, d_0, d_1, ...d_{N_s-1} are N_s independent data symbols obtained from a modulation constellation, and using equation 3-12.

$$\beta_n = \begin{cases} \frac{1}{\sqrt{2}} & , & n = 0 \\ 1 & , & n = 0, 1, ..., N_s \end{cases}$$

3-Error! Bookmark not defined.

3.3.2   Efficient Computation of the Discrete Cosine Transform

The time duration of the N transmitted symbols is T_s, and $T = T_s/N$ is the time duration per information symbol. The kth subcarrier waveform can be written as:

$$\cos\left(2\pi\frac{n\pi t}{2T_s} + \frac{k\pi}{2N}\right)$$

Sampling the ki^{th} subcarrier at time instants $t = n\,T = nT_s/N$, where $n = 0, \dots, N-1$, gives the discrete–time representation $\cos\left(\pi\frac{nk}{2N} + \frac{k\pi}{2N}\right)$. The modulated discrete-time waveform is given by equation 3-13

$$x_n = \sum_{n=0}^{N-1} X_k\, T_k(n), \; n = 0, \dots, N-1 \quad 3\text{-}11$$

Equation (3-14) is an inverse discrete cosine transform (IDCT), where the discrete cosine transform (DCT) is given by

$$x_k = \sum_{n=0}^{N-1} X_n\, T_n(n) \qquad\qquad\qquad\qquad 3\text{-}12$$

The orthogonal property of the DCT is

$$\sum_{n=0}^{N-1} T_p(n)T_q(n) = \begin{cases} 1, & p = q \\ 0, & p \neq q \end{cases} \qquad\qquad 3\text{-}13$$

This data represented by x_k can be referred to as the frequency domain data. The subcarriers $T_k(n)$ of the frequency domain data x_k are mutually orthogonal among them. A more intuitive representation of IDCT is shown in Fig 3-3. Note that frequency difference between neighbouring sub-carriers of the IDCT modulated signal is $\Delta f = \frac{1}{2T_s}$.

| X_k → | DCT | X_k → | Phase modulator | $s(t)$ | Add Guard | | Channel | | Remove Guard | $r(t)$ | Oversampling |

Channel estimatio

r_k

| $\bar{X}_k$ | IDCT | X_n | Phase detector | Y_n | IFFT | Y_k | Equaliser | R_k | FFT |
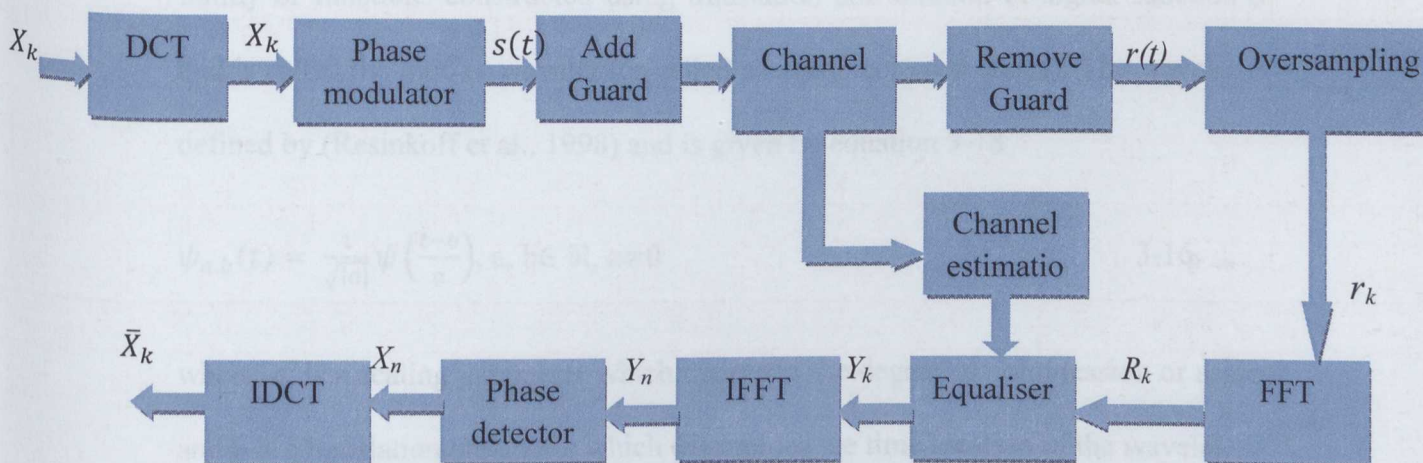
Figure 3-4 Constant envelop multicarrier modulation

As seen in figure 3-3, with the frequency-domain data (X_k) as input to the DCT, the output (x_n) of the IDFT can be viewed as time-domain data. The time–domain data sequence (x_n) is applied as input to a phase modulator to generate the band pass waveform having the complex envelope described by equation 3-16

$$s(t) = \sqrt{\frac{E}{T}}\, e^{j\emptyset(t)} \qquad \text{3-14}$$

with a phase given by,

$$\emptyset(t) = 2\pi h \sum_{n=0}^{N-1} x_n\, q(t - nT) \qquad \qquad \text{3-15}$$

However, if the data symbols d_n are obtained by real-valued modulation formats, such as PAM and BPSK, the baseband DCT-OFDM signal x (t) is still a real signal.

3.4 DWT-OFDM SYSTEMS
3.4.1 The wavelet transform

The wavelet transform is a type of technique derived from the Fourier transform. The most important difference between these two transformations is that individual wavelet functions are localized in space, while Fourier sine and cosine

functions are not (Zhang, H., et al 2007). It is based on the idea of wavelet as a family of functions constructed using translation and dilation of signal function ψ and is called the mother wavelet (or called as affine coherent states). The wavelet is defined by (Resinkoff et al., 1998) and is given by equation 3-18

$$\psi_{a,b}(t) = \frac{1}{\sqrt{|a|}}\psi\left(\frac{t-b}{a}\right), \text{a, b} \in \mathfrak{R}, \text{a} \neq 0 \qquad\qquad 3\text{-}16$$

where, a, is a scaling parameter which measures the degree of compression or scale, and b is a translation parameter which determines the time location of the wavelet.

3.4.2 Discrete Wavelet Transform (DWT)

The discrete wavelet transform represents a function by a countable set of wavelet coefficients, which correspond to points on a two-dimensional grid or lattice of discrete points in the scale-time domain indexed by m and n. If the set $\left(\Psi_{m,n}(t)\right)$ defined by (Eq.3-18) is complete in $L^2(\mathbb{R})$(Hilbert space of finite energy functions) for some choice of ψ, a, and b, then the set is called an affine wavelet. Then, we can express any f (t) $\in L^2(\mathbb{R})$ as the superposition by using equation 3-19.

$$f(t) = \sum_{m,n=-\infty}^{\infty}\left(f,\psi_{m,n}\right)\psi_{m,n}(t) \qquad\qquad 3\text{-}17$$

3.4.3 The Orthogonal Base Property

To satisfy orthonormal bases in order to operate as wavelet transform, these filters must be orthogonal and normal to each other. By assigning 'h' as HPF filter coefficients and 'g' as LPF filter coefficients, the orthogonal basis can be satisfied via four possible ways of the dot products as follows (Abdullah et al., 2009) through equations 3-20 to 3-23:

$$< g.g^* >= 1 \qquad\qquad\qquad\qquad\qquad\qquad 3\text{-}18$$

$$< h.h^* >= 1 \qquad\qquad\qquad\qquad\qquad\qquad 3\text{-}19$$

$$< g.h^* >= 0 \qquad 3\text{-}20$$

$$< h.g^* >= 0 \qquad 3\text{-}21$$

Where, the first two terms are related to the normal property, and the last two are for orthogonal property. The asterisk sign indicates that the coefficients are conjugated. Both filters are also assumed to have perfect reconstruction property. This means that the input and output of the tow filters are expected to be the same.

3.4.4   Representation of Wavelet-based OFDM

The system uses DWT and IDWT in the receiver and transmitter function, respectively. The output of the IDWT at the receiver can be represented (Strang, G., and Nguyen, T., 1997) by equation 3-24.

$$s(k) = \sum_{m=0}^{\infty} \sum_{n=0}^{\infty} S_m^n \, 2^{m/2} \psi(2_k^m - n) \qquad\qquad\qquad 3\text{-}22$$

where, S_m^n are the wavelet coefficients and $\psi_{m,n}(t)$ is the wavelet function with compression factor of m and n times shift for each subcarrier with translation and dilation of signal function ψ (number k, $0 \leq k \leq N\text{-}1$). The wavelet coefficients are the representations of signal pulses in scale and position or time. The scale is related to the frequency. Low scale represents compressed wavelet, which means that the signal is rapidly changing, or the signal is in high frequency. On other hand, high scale represents stretched wavelet, which means that the signal is slowly changing, or the signal is of low frequency. Thus, the sequence X_m is translated to S_m^n before it is processed in IDWT. At the receiver side, the process is reversed. The output of discrete wavelet transform (DWT) is given by equation 3-25.

$$S_m^n = \sum_{k=0}^{N-1} s(k) \, 2^{m/2} \psi(2_k^m - n) \qquad 3\text{-}23$$

The sequence S_m^n is decoded to X_m in order to recover the data at the demodulator. When orthogonality between carriers is lost after transmitting a signal through a non-uniform channel, the amount of interference between carriers in wavelet systems is much lower than in Fourier systems since the side lobes contain much less energy (Sandberg, S.D., and Tzannes, M.A., 1995) due to the absence of guard bands. Also, due to the high spectral containment properties of wavelet filters, DWT-OFDM can better combat narrowband interference and is inherently more robust with respect to ICI than traditional DFT-OFDM (Ahmed, N., 2000). So, the classic notion of a guard band does not apply to wavelets; hence data rate can surpass those of FFT implementations. Therefore, due to overlapping nature of wavelet properties, this wavelet based OFDM system is not affected by delay spreads in the channel. The great reduction in side-lobe levels is another main motivation behind the recent trend towards using wavelets in OFDM systems.

3.4.5 Efficient Computation of the Discrete Wavelet Transform

In wavelet based OFDM, the impulse response of a deterministic (and possibly time-varying) channel can be modelled by a linear filter h(t). Whereas, the match filtering is represented by replacing $f_k(t)$ *and* $f_i(t)$ by $w_k(t)$ *and* $w_i(t)$. $w_k(t)$ represents the wavelet carrier in IDWT operation with k sub channels to match with carrier i. Thus, the received signal is defined by equation 3-26.

rw (t) = yw(t)*h(t) + n(t)

$$= \sum_{k=0}^{K-1} d_k w_k^i + \sum_{i=0}^{g-1} \sum_{k=0}^{K-1} d_{k,i} \, w_k^i(t - lk) + n(t) \quad 3\text{-}24$$

where k is wavelet filter rank (sampling rate), $w_k(t) = w_k(t)*h(t)$ and g(g>1) is the wavelet *genus* so that k_g is the filter order (number of taps in that sub-band). After the matched filter with carrier i, the signal becomes as given in equation 3-27

$$\langle rw(t), w_i(t) \rangle = \sum_{k=0}^{K-1} d_k \langle w_k^i(t), w_i(t) \rangle + \sum_{i=0}^{g-1} \sum_{k=0}^{k-1} d_{k,i} \langle w_k^i(t - lk), \rangle w_i(t - lk) + \langle n(t), f_i(t) \rangle = \sum_{k=0}^{k-1} d_k p_{k,0}(0) + \langle n(t), f_i(t) \rangle$$

$$= d_k p_{i,i}(0) + \sum_{\substack{k=0 \\ k \neq i}}^{K-1} d_k p_{k,i}(0) + \sum_{i=0}^{g} \sum_{\substack{k=0 \\ k \neq i}}^{K-1} d_{k,l} p_{k,i}(l) + n''(t) \qquad 3\text{-}25$$

where, $d_{k,l} p_{k,i}(0)$ is the recovered data with correlation term $p_{i,i}(0)$. The term $\sum_{\substack{k=0 \\ k \neq i}}^{K-1} d_k p_{k,i}(0)$ is the interference due to the discrete filters that are no longer orthogonal to one another with correlation term $p_{k,i}(0)$, and $\sum_{i=0}^{g} \sum_{\substack{k=0 \\ k \neq i}}^{K-1} d_{k,l} p_{k,i}(l)$ is the interference term with distorted $p_{k,i}(l)$ due to the overlapped nature of wavelet transform. These two terms become 0, and only the first and last terms would appear if the channel has no distortion. The decoder would possibly obtain almost correct signal when the two terms are zero.

3.5   Choice of Performance measurement Parameters

The choice of various performance measurement parameters is a trade-off between various, often conflicting requirements. For example, we can consider bandwidth, bit rate, and delay-spread. To start with, the delay-spread directly dictates the guard time and, as a rate, the guard time should be about two to four times the root-mean-square of the delay-spread. The value depends on the type of coding and QAM modulation. Higher order QAM (for example 64-QAM) is more sensitive to ICI and ISI than QPSK; whereas heavier coding reduces the sensitivity to such an interference (Nee, 2000). Now that the guard time has been set, the symbol duration

can be fixed. To minimize the reduction in the signal-to- noise ratio (SNR) caused by the guard time, it is desirable to have the symbol duration much larger than that of the guard time. It cannot be arbitrarily large, however, because of the possible increase in implementation complexity, sensitivity to phase noise and frequency offset (Pollet et al., 1995) as well as in the peak- to-average ratio (Pauli et al., 1997) (Rapp, 1991b). Hence, a practical design choice is to make the symbol duration at least five times the guard time, which implies a –3dB SNR loss due to the guard time.

After the symbol duration and guard time are fixed, the number of subcarriers should be fixed as the required -3dB bandwidth divided by the subcarrier spacing, which is the inverse of the symbol duration less the guard time. Alternatively, the number of subcarriers   may be determined by the required bit rate divided by the bit rate per subcarrier. The bit rate per subcarrier is defined by the modulation type (e.g., 16QAM), coding rate, and symbol rate (Nee, 2000).

3.5.1 Relation between BER, EVM and SNR

Bit rate (sometimes written bitrate, data rate or as variable R) (Skalar, 1994) is the number of bits that are conveyed or processed per unit of time. The bit rate is quantified using bits per second (bit/s or bps) or multiple bits per second (Mbit/s, Gbit/s, and Tbit/s) or (Mbps, Gbps and Tbps).

Bit error rate (BER), error vector magnitude (EVM) and signal to noise ratio (SNR) are common performance metrics for assessing the quality of communication (Abdullah and Hussain, 2007). The latter can be measured using the bit error rate (BER), which gives a simple one-to-one binary decision as to whether a bit is erroneous or not. SNR is a direct measure of the relative power of the noise compared to the signal. Since noise is modelled as a source of all errors in the simplistic Gaussian noise channel model, SNR can be used to predict the

performance of the system in terms of correctness of the reception. Due to the simplicity of comparison, BER has been a major choice of engineers, industries and researchers (Kai-ming et al., 2005),(MAHMOUD and , Abdullah and Hussain, 2007).

EVM is defined as the root-mean-square (RMS) value of the difference between a collection of measured symbols and ideal symbols. (Abdullah et al., 2009). On the other hand, BER performance against SNR is the popular performance criterion that is used in today's communications systems. Since BER, calculations can often be avoided for large packets; EVM can give the desired performance metric before the demodulation can actually take place. This can be done without any major change in the algorithm in adaptive systems, since BER is a direct consequence of EVM. For performance measures for systems with small packet communication, BER versus SNR can be easier and more useful due to complex mathematical operations that need to be done in the digital signal processor for calculation of EVM.

3.5.1.1 Bit error ratio

The probability of error in terms of the number of erroneous bits per number of bits is described as Bit Error Rate (BER), which is a commonly used performance metric. Assuming M-ary modulation with coherent detection in the Gaussian noise channel and perfect recovery of the carrier frequency and phase, it can be shown (Nee, 2000) using equation 3-28,

$$P_b = \frac{2\left(1-\frac{1}{L}\right)}{\log_2 L} Q\left[\sqrt{\left[\frac{3\log_2 L}{L^2-1}\right]\frac{2E_b}{N_0}}\right] \qquad \text{3-26}$$

where, L is the number of levels in each dimension of the M-ary modulation system,

Eb is the energy per bit and No/2 is the noise power spectral density. Q[.] is the

Gaussian co-error function and is given by(Pollet et al., 1995) equation 3-29,

$$Q(x) = \int_{-\infty}^{\infty} \frac{1}{\sqrt{2\pi}} e^{\frac{-y^2}{2}} dy \qquad \text{3-27}$$

Supposing filter as raised cosine pulses with sampling at data rate, Equation (3-29)

also gives the bit error rate in terms of signal to noise ratio as represented by

equation 3-30

$$P_b = \frac{2\left(1-\frac{1}{L}\right)}{\log_2 L} Q\left[\sqrt{\left[\frac{3\log_2 L}{L^2-1}\right]\frac{2E_b}{N_0 \log_2 M}}\right] \qquad \text{3-28}$$

where Es/No is the signal to noise ratio for the M-ary modulation system and raised

cosine pulse shaping at data rate. Equation 4 defines the BER performance in terms

on SNR

3.5.1.2 BER upper Bound

Without considering AWGN the received signal on each subcarrier can be

recognized as a sum of the expected signal df and ICI signal I if a frequency error df

exists, which can be calculated using equations 3-31 and 3-32:

$$df = S_o\, a_0 \hspace{6cm} \text{3-29}$$

$$I = \sum_{k=1}^{N-1} s_k\, a_k \hspace{2cm} \text{3-30}$$

where df the channel frequency error is normalized by the subcarrier frequency separation and denoted by df, s_k - ICI coefficient function as shown in equation 3-33 below,

$$s_k = \frac{\sin(\pi df)}{N\sin(\frac{\pi}{N}(df-k))} exp\left[j\frac{\pi}{N}((N-1)df + k\right) \hspace{2cm} \text{3-31}$$

where a_k is the amplitude of side lobes being modulated by the N subcarriers.

$|d+I_{max}|$ and $|d-I_{max}|$ are two limit values between which the amplitude of the received signal lies, where I_{max} is the maximum ICI signal with respect to df as shown in equation 3-34.

$$I_{max} = \sum_{k=1}^{N-1} |s_k|$$

3-Error! Bookmark not defined.

The frequency error possible that $I_{max} > d$ occurs when it is sufficiently large. In such a case, a data decision error can be made even in the absence of AWGN.

Critical frequency error is df value where the condition $I_{max} = d$ holds. This critical frequency error is a function of N, for example: it takes the value df =0.17 for N=32 and df=0.10forN =256. Since I_{max} is a function of N, therefore its upper bound also varies as the function of N (Latif and Gohar, 2006) (Ho and Yeh, 1970) .

3.5.2 The signal to noise ratio

The relative measure of the signal power (meaningful information) compared to the noise power (unwanted signal) is a signal to noise ratio (SNR) expressed by equation 3-35

$$SNR = \frac{P_{signal}}{P_{noise}} \qquad \text{3-32}$$

where, P is the average power. Within the same system bandwidth, both signal and noise power must be measured at the same and equivalent points in a system. The SNR is defined in decibels as in equation 3-36.

$$SNR_{decibel} = 10\,log_{10}\left(\frac{P_{signal}}{P_{noise}}\right) = P_{signal,dB} - P_{noise,dB} \qquad \text{3-33}$$

Meanwhile, the SNR measures the ratio between an arbitrary signal level (not necessarily the most powerful signal possible) and noise. The dynamic range measures the ratio between the strongest undistorted signal via a channel and the minimum discernible signal. Therefore, the concepts of signal-to-noise ratio and dynamic range are closely related.

In most instances, the SNR is taken to indicate an average signal-to-noise ratio, as it is possible that (near) instantaneous signal-to-noise ratios will be very differently considered. The concept can be understood as normalizing the noise level to 1 W (0 dB) and measuring how far the signal 'stands out'.

Supposing Gaussian noise model for wireless channels and complex signals, SNR can be defined as in equation 3-37

$$SNR = \left[\frac{\frac{1}{T}\sum_{t=1}^{T}[(I_t)^2+(Q_t)^2]}{\frac{1}{T}\sum_{t=1}^{T}\left[|n_{I,t}|^2+|Q_{Q,t}|^2\right]}\right]$$

3-Error! Bookmark not defined.

where I_t and Q_t are the in-phase and quadrature signal amplitudes of the M-ary modulations, $n_{I,t}$ and $Q_{Q,t}$ are the in-phase and quadrature noise amplitudes of the complex noise being considered.

An alternative definition of SNR is the reciprocal of the coefficient of variation (which is a normalized measure of dispersion of a probability distribution), i.e., the ratio of mean to standard deviation of a signal or (Latif and Gohar, 2006) (Ho and Yeh, 1970), given by equation 3-38.

$$SNR = \frac{\mu}{\sigma} \qquad\qquad 3\text{-}34$$

where μ is the signal mean or expected value and σ is the standard deviation of the noise, or an estimate thereof. Notice that such an alternative definition is only useful for variables that are always non-negative (such as photon counts and luminance).

3.5.2.1 SNR and E_s/N_0

Equation (3-37) above shows a direct measure of SNR, which can be used in Monte Carlo simulation procedures for large symbol streams, such that T >> N, where N is the number of unique modulation symbols. Often these estimates are simplified by considering the measure of the ratio of variances of signal and the noise, when both are zero mean processes. For systems, which are sampled at data rate, E_s/N_0 gives the signal to noise ratio directly, where E_S is the symbol energy and $N_0/2$ gives the noise power spectral density. This means that, for every update in the adaptive algorithm, it can be noted that E_S = log2 M Eb; for such systems E_b/N_0 can be seen as a normalized measure of the energy per symbol per noise power spectral density (E_s/N_0) given by equation 3-39

$$\frac{E_b}{N_0} = \frac{E_s}{\rho N_0} \qquad\qquad 3\text{-}35$$

where E_s is the energy per symbol in joules and ρ is the nominal spectral efficiency in (bit/s)/Hz. E_s/N_0 is also commonly used in the analysis of digital modulation

schemes. The two quotients are related to each other according to the following equation 3-40:

$$\frac{E_s}{E_b} = \frac{\frac{E_s}{N_0}E_b}{N_0} log_2 M \qquad 3\text{-}36$$

where M is the number of alternative modulation symbols.

Note that the energy is per bit, not the energy per information bit.

E_s/N_0 can further be expressed as by equation 3-41:

$$\frac{E_s}{N_0} = \frac{C}{N}\frac{B}{f_s} \qquad 3\text{-}37$$

where

C/N is the carrier-to-noise ratio

B is the channel bandwidth in Hertz.

f_s is the symbol rate in baud or symbols per second.

Converting the value to the corresponding signal-to-noise ratio (SNR) involves, the number of bits per symbol (k), number samples (nsamp), and the over sampling factor. The factor k is used to convert E_b/N_0 to an equivalent E_s/N_0, which is the ratio of symbol energy to noise power spectral density. The factor nsamp is used to convert E_s/N_0, in the symbol rate bandwidth, to an SNR.

3.5.2.2 The Related bandwidth with SNR

The output of the modulator as average power is given by equation 3-42.

$$P = E_s/T_s \qquad\qquad 3\text{-}38$$

where E_s the average energy of the modulator signals. Each signal carrier is a $\log_{\frac{E_s}{E_b}} M$

information bit. Then the average power is given by equation 3-43.

$$\therefore P = \frac{\log_2 M E_b}{T_s} = E_b \qquad\qquad 3\text{-}39$$

The definition SNR can be considered as the ratio between the average signal

power and the average noise power over the signal bandwidth is given by equation 3-

44.

$$SNR = \frac{P}{N_0 B_w} = \left(\frac{E_b}{N_0}\right) \cdot \left(\frac{R_b}{B_w}\right) \; 3\text{-}40$$

For higher SNR, the error probability can be closely approximated by a

complementary error function erfc $[d_{min}/(2\sqrt{N_0})]$, where d_{min} is the minimum

Euclidean distance between any two elements of the modulator signal set (Burr,

2001).

The parameter γ, which is related to the power efficiency (γ) of a modulation

scheme, expresses how efficiently a modulation scheme uses the available signal

energy to generate minimum Euclidean distance. γ is defined as by equation 3-45:

$$\gamma = \frac{d_{min}^2}{4E_b} \qquad\qquad 3\text{-}41$$

The above equation provides an approximation to error probability that is

asymptotically tight with large SNR.

3.6 Performance evaluation of the OFDM techniques

3.6.1 ICI analysis for DCT and DFT -OFDM systems operating in the presence of carrier frequency offset (CFO)

In MCM systems, it is well known that carrier frequency offset (CFO), caused by oscillator mismatch or Doppler effects, destroys the subcarriers' orthogonality, and results in a substantial bit error rate (BER) degradation (Pollet et al., 1995). In addition, CFO will introduce inter carrier interference ICI in both DCT and DFT – OFDM systems. CFO causes a number of impairments, including attenuation and rotation of each of the subcarriers, and ICI between subcarriers. Due to the anti-symmetry characteristics introduced, in DCT-OFDM, full-range CFO estimation is achieved. Another advantage of using DCT-OFDM is that it can provide more accurate and robust CFO estimation than the DFT-OFDM (Tao et al., 2007).

Normally, in an OFDM system, there are N subcarriers with a symbol period of T. In the ith symbol period, the N complex values $a_{0,1} \dots a_{N-1,i}$ modulate N subcarriers, when the system uses a number of different types of modulation of subcarriers within OFDM, such as phase shift keying (PSK) and quadrature amplitude modulation (QAM). This analysis does not depend on the mapping of the data to be transmitted to the complex values $a_{0,1} \dots a_{N-1,i}$, and is therefore applicable to all forms of modulation which can be used within OFDM. Frequency offset alone does not cause ISI. Often a cyclic prefix (CP) is used in the OFDM system in order to eliminate ISI and ICI caused by errors in sampling time or distortion in the channel (Armstrong, 1999).

The DCT operation distributes more energy to the desired subcarrier and less energy to the ICI than the DFT operation. Therefore, the desired subcarrier suffers from less ICI coming from neighbouring subcarriers in DCT-OFDM than in the DFT-OFDM system (Peng and Beaulieu, 2006).

The sequence of ICI coefficients is given as $S_{n,k} = S_{n,k}^I + jS_{n,k}^Q$ in DCT-OFDM,

and are given by equations 3-46 to 3-52

$$S_{n,k}^I = \frac{1}{2N}\beta_k\beta_n[\overline{\psi}(n+k-\varepsilon) + \overline{\psi}(n-k-\varepsilon) + \phi(n+k+\varepsilon) + \phi(n-k+\varepsilon)]$$ 3-42

$$S_{n,k}^Q = \frac{1}{2N}\beta_k\beta_n[\Gamma(n+k-\varepsilon) + \Gamma(n-k-\varepsilon) \wedge (n+k+\varepsilon) \wedge (n-k+)]$$ 3-43

$$\overline{\psi}(x) = \frac{sin\left(\frac{\pi x}{2}\right)cos\left(\phi-\frac{\pi x}{2}\right)}{sin\left(\frac{\pi x}{2N}\right)}$$ 3-44

$$\overline{\phi}(x) = \frac{sin\left(\frac{\pi x}{2}\right)sin\left(\phi-\frac{\pi x}{2}\right)}{sin\left(\frac{\pi x}{2N}\right)}$$ 3-45

$$\Gamma(x) = \frac{sin\left(\frac{\pi x}{2}\right)cos\left(\phi+\frac{\pi x}{2}\right)}{sin\left(\frac{\pi x}{2N}\right)}$$ 3-46

$$\wedge(x) = \frac{sin\left(\frac{\pi x}{2}\right)sin\left(\phi+\frac{\pi x}{2}\right)}{sin\left(\frac{\pi x}{2N}\right)}$$ 3-47

$$\beta_n = \begin{cases} \frac{1}{\sqrt{2}}, & n = 0 \\ 1, & n = 0, 1, ..., N_s \end{cases}$$ 3-48

and $\varepsilon = 2T\Delta f$. Recalling that in DCT-OFDM the subcarrier frequency spacing is

1/2T Hz, ε is the normalized frequency offset with respect to the subcarrier-

frequency spacing. There is a sequence of ICI coefficients for N—subcarrier DFT-

OFDM in the presence of normalized frequency offset $\xi = \Delta fT$. It was derived by

(Peng and Beaulieu, 2006) as:

$$F_n = \frac{sin\,\pi(n+\xi)}{N\,sin\frac{\pi(n+\xi)}{N}}e^{\frac{j\pi(N-1)(n+\xi)}{N}}$$ 3-49

3.6.2   SIR, BEP and BER in the presence of CFO in DCT and DFT –OFDM systems

The DCT-OFDM gives smaller ICI power and greater signal-to-interference

ratio (SIR) than DFT-OFDM when the system is operating in the presence of CFO

over an AWGN channel. One can consider the SIR defined as (Peng and Beaulieu, 2006) represented by equations 3-54 and 3-55 for DCT and DFT respectively.

$$SIR_{DCT}^k = \frac{(S_{k,k}^I)^2}{\sum_{\substack{n=0 \\ n \neq k}}^{N-1}(S_{n,k}^I)^2} \qquad \text{3-50}$$

$$SIR_{DFT}^k = \frac{(\Re\{F_0\})^2}{\sum_{\substack{n=0 \\ n \neq k}}^{N-1}(\Re\{F_{n-k}\})^2} \qquad \text{3-51}$$

The ICI and SIR analysis suggests that the desired subcarrier suffers less ICI coming from neighbouring subcarriers in DCT-OFDM than in DFT-OFDM. The reduced interference will lead to better bit error probability (BEP) performance, which can be observed from the BEP expression and simulation result demonstrated in (Peng and Beaulieu, 2006). In order to fully appreciate the performance of BER and BEP in the OFDM systems, we need to consider the system performance under various modulation schemes. (Peng and Beaulieu, 2006) have compared the performance of QPSK, BPSK, and QAM modulation schemes. When i1 and q1 are two bits in one QPSK symbol, the i1 BEP for the kth subcarrier can then be written as, using equation 3-56

$$P_{i1}(K) = 1/2 - \int_0^{+\infty} sin(w\sqrt{E_b}\,S_{k,k}^I) \times cos(w\sqrt{E_b}\,S_{k,k}^Q)\gamma(w)dw \quad \text{3-52}$$

Where $\gamma(w)$ is given by equation 3-57

$$\gamma(w) = \frac{e^{-\frac{1}{2}w^2\sigma^2}}{\pi w}\prod_{\substack{n=0 \\ n \neq k}}^{N-1} cos(w\sqrt{E_b}\,S_{n,k}^I)\,cos(w\sqrt{E_b}\,S_{n,k}^Q) \qquad \text{3-53}$$

According to symmetry, i1 bit and q1 bit have the same BER, hence, the BER for the kth subcarrier is given by equation 3-58

$$P_{b,QPSK}(K) = \frac{1}{2}P_{i1}(k) + \frac{1}{2}P_{q1}(k) = P_{i1}(k) \qquad \text{3-54}$$

Note that the BER is a function of the subcarrier index k. This is because the ICI is a function of the subcarrier index. The average BER is given by equation 3-59

$$P_{b,QPSK}(K) = \frac{1}{N}\sum_{k=0}^{N-1} P_{b,QPSK}(K) \quad \text{3-55}$$

By eliminating the term that contains $S_{n,k}^Q$ in (3-57), one can obtain the expression of BEP in the case of BPSK modulation, as given by equation 3-60

$$P_{b,BPSK} = \frac{1}{2} - \int_0^{+\infty} \frac{sin\sqrt{E_b}wS_{k,k}^I}{\pi w} e^{-\frac{1}{2}w^2\sigma^2} \times \prod_{\substack{n\neq k \\ n=0}}^{N-1} cos\left(w\sqrt{E_b}\,S_{n,k}^I\right) dw \quad \text{3-56}$$

In addition, for 16-ary QAM the i1 BEP can be written

$$P_{i1} = \frac{1}{2} - \int_0^{+\infty} cos(2wdS_{n,k}^Q)\,cos(wdS_{k,k}^Q) \times sin(2wdS_{k,k}^I)\,cos(wdS_{k,k}^I)\,\beta(w)d$$

3 – Error! Bookmark not defined.

For i2 bit, the error probability is given by equation 3-62

$$P_{i2} =$$

$$\frac{1}{2} -$$

$$\int_0^{+\infty} 2sin\,(2wd)\,sins(2wdS_{k,k}^I)\,sin(wdS_{k,k}^I)\,cos(2wdS_{k,k}^Q)\,cos(wdS_{k,k}^Q)\,\beta(w)dw$$

3-57

It is noted that the i1 bit has the same BEP as the q1 bit, and i2 bit has the same BEP as q2 bit. Therefore, the average BEP can be given as in equation 3-63

$$P_{b,16-QAM} = \frac{1}{2N}\sum_{k=0}^{N-1}[P_{i1}(k) + P_{i2}(k)] \quad \text{3-58}$$

$S_{n,k}^I$ with $\Re\{F_{n-k}\}$, and $S_{n,k}^Q$ with $\Im F_{n-k}$ in (3-54), (3-60), and (3-61) give the BEPs of the kth subcarrier for DFT-OFDM with subcarrier modulation formats BPSK, QPSK, and 16-QAM, respectively.

3.6.3 Normalised Energy Spectral Density and the meaning of normalised frequency

It can be shown that the components in the Fourier transform are orthogonal, and therefore, the normalised energy of a non-periodic signal s(t) can be calculated in the frequency domain using equation 3-64

$$E_s = \int_{-\infty}^{\infty} |S(f)|^2 \, df \qquad\qquad 3\text{-}59$$

where, E_s is the total energy of the signal. The quantity $|S(f)|^2$ is the normalised energy spectral density (it shows how normalised energy is distributed through the frequency band). Note that this quantity is a density and its units are (Harlod and Samy, 2004) volts^2/Hz^2, which can also be expressed as volts^2-sec/Hz. $|S(f)|^2$ is also represented by the symbol $\Psi(f)$,

$|S(f)|^2 \equiv \Psi(f)$ = Normalised energy spectral density

To find the normalized energy within a given frequency band, we merely integrate the energy spectral density over that frequency band. The most important parameter of a coding or modulation scheme is the bandwidth requirement, which is determined by the spectrum of the modulated signal usually presented as a plot of power spectral density (PSD) against frequency (Harlod and Samy, 2004).

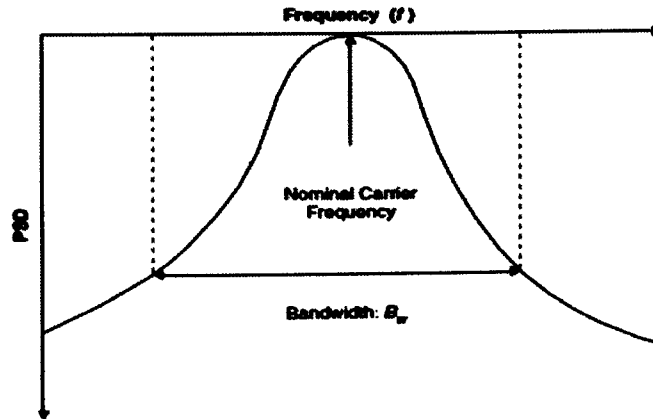An example of an ideal PSD graph is given in figure 3.4.

Figure 3-5. PSD versus frequency

As shown in figure 3.4, the power spectral density (PSD) should be zero outside the band occupied; however, this can never be achieved in reality, and so the spectrum extends beyond the band. This may be due either to the practical implementation of filters, or to the inherent characteristics of the modulation scheme. Therefore, the bandwidth B_u, must be defined such that the signal power falling outside the band is below a certain threshold, which is determined based on the tolerance of the system to adjacent channel interference. The design of modulation selection and coding scheme for a system should be based on the following factors:

- Bit error rate probability, P_b

- Bandwidth efficiency, η

- Signal-to-noise density ratio, E_b/N_0 (E_b is the energy per bit, and N_0 is the noise density).

The definition of bandwidth of a signal is the width of the band frequency, which contains a sufficient number of the signal frequency components, so as to reproduce the signal without an unacceptable amount of distortion. The bandwidth efficiency (or spectrum efficiency) of a coding and modulation scheme is how much

of the bandwidth requirement can be achieved by the system. This can be expressed as the information bit rate R_b, per unit bandwidth, and is measured in bits/sec/Hz (bps/Hz)and is given by equation 3-65:

$$\eta = \frac{R_b}{B_w} \qquad\qquad\qquad 3\text{-}60$$

"Normalisation" means to scale everything by some sensible common factor. The normalised frequency is the frequency divided by the sampling frequency in radians, which is the Nyquist rate. So, the number of samples per cycle is the reciprocal of the normalised frequency and gives the number of times the signal is sampled in one cycle.

3.7 The peak to-average power ratio (PAPR)

3.7.1 Introduction

An OFDM signal consists of a number of independently modulated subcarriers, which can give a large peak-to-average power ratio (PAPR) when added up coherently. When N signals are added with the same phase, they produce a peak power that is N times the average power. The peak power is defined as the power of a sine wave with amplitude equal to the maximum envelope value. Hence, an unmodulated carrier has a PAPR of 0 dB. An alternative measure of the envelope variation of a signal is the Crest factor, which is defined as the maximum signal value divided by the RMS signal value. For an unmodulated carrier, the Crest factor is 3 dB. This 3 dB difference between PAPR Crest factors also holds for other signals, provided that the centre frequency is large in comparison with the signal bandwidth (Nee, 2000).

However, a large PAPR brings disadvantages such as increased complexity of the analog-to-digital and digital-to-analog convertors and reduced efficiency of

the RF power amplifier. To reduce the PAPR ratio, several techniques have been proposed, which basically can be divided into three categories. First, there are signal distortion techniques, which reduce the peak amplitudes simply by nonlinearly distorting the OFDM signal at or around the peaks. Examples of distortion techniques are clipping, peak windowing and peak cancellation. The second category is coding technique, which uses a special forward-error correcting code set that excludes OFDM symbols with a large PAPR. The third technique is based on scrambling each OFDM symbol with different scrambling sequences and selecting the one that gives the smallest PAPR (Nee, 2000) .

In addition, the peak to-average power ratio (PAPR) of OFDM signals can be reduced by the use of pre-processing and post-processing techniques. One such technique (Jun and Stuber, 2002) uses constrained coding and/or selective mapping techniques to pre-process transmitted data to reduce the PAPR. In (Wilkinson and Jones, 1995) (van Nee, 1996), Golay complementary codes are used to reduce the PAPR of OFDM. Coding can also be combined with phase shifting to reduce the PAPR (Tarokh and Jafarkhani, 2000). Post-processing techniques usually clip the OFDM signal in an appropriate way so that clipped signals can be stored at the receiver. A comprehensive survey of PAPR reduction technique is presented in (Nee, 2000).

So, in a significant number of MCM systems, there is a possibility of high peaks in the transmitted signals, which emphasises the necessity to increase the dynamic range of the corresponding linear amplifier of the communication system or otherwise to clip the signals. The clipped signal yields an undesirable inter-carrier and out-of-band radiation (Paterson and Tarokh, 2000) and thus results in degraded

system performance. Thus, such transmission schemes using orthogonal base with high peaks must be avoided.

Although the DWT-OFDM provides many advantages, the transmitted signal in the system does not have the constant envelope. Envelope variation is to be controlled, to avoid operating the transmission amplifiers near their non-linear saturation regions. If hard limiter is employed to limit the peaks, the orthogonality of the constituent terminal functions is destroyed, resulting in potentially unacceptable performance. One of the metrics used to quantify large envelope variation is peak-to-average-power ratio (PAPR) value (Baxley and Zhou, 2004). So, a good performance of an OFDM system with respect to PAPR is vital for the performance measurement of the system.

3.7.2 PAPR in DWT system

In wavelet-based OFDM, the IFFT and FFT blocks are replaced by an inverse discrete wavelet transform (IDWT) and discrete wavelet transform (DWT), respectively. In Fourier based OFDM, there are M independent sub channels via a K = 2M point IFFT operation (when the conjugate symmetry condition is imposed). The wavelet transform converts real numbers to real numbers, and hence binary signalling must be used in each sub channel. To keep the same data rate in the wavelet-based system, K independent binary sub channels are multiplexed together via a K point IDWT (Khalid and Shah, 2006).

The PAPR of the DWT-OFDM signal can be defined as in equation 3-66

$$PAPR = \frac{max|S(t)|^2}{\overline{|S(t)|^2}} \qquad\qquad 3\text{-}61$$

where $\overline{|S(t)|^2}$ denotes the transmitted signal mean power.

PAPR analysis is based on its cumulative distribution with respect to the number of binary combinations at the transmitter input (Khalid and Shah, 2006).

By far, wavelet based multi-carrier modulation (MCM) also called wavelet (filter bank) based OFDM (WOFDM) system seems to offer most of the advantages and suffers from fewer disadvantages when compared to the other OFDM systems. In the WOFDM systems, the orthogonality is satisfied by orthogonal wavelet filter (filter bank) (Strang et al., 1996) and no guard interval (cyclic prefix) is needed, thus enhancing the bandwidth efficiency by 20% compared to conventional OFDM systems. Besides (Technologies, 2001), additional bandwidth efficiency (8%) in WOFDM systems is also provided since pilot tones are not necessary.

(Muller and Huber, 1997) proposed the use of piecewise scales transform (PST) using the complementary cumulative distribution function (CCDF) of PAPR of signals.

By using PST, the average power of the transmitted signals is enlarged while their peak is kept unchanged; the reduction in PAPR should be very limited to avoid large companding distortion as shown in the following equation 3-67

$$PAPR_n = \frac{\max\limits_{k,m1}\left[|S_{k,m}|^2\right]}{E\left[|S_{k,m}|^2\right]} \qquad\qquad 3\text{-}62$$

where E[ ] denotes the expectation.

The channel is modelled as an additive white Gaussian noise (AWGN) with zero mean and $N_0/2$ variance.

Therefore, as shown in equation 3-67 above, better performance may be achieved against the trade-off between the reduction in PAPR and the BER of the system, by changing not only the peak value but also the average power of the transmitted signal.

3.7.3   The theoretical analysis of the PARP reduction method

The discrete wavelet transform (DWT) is a type of batch processing, which analyses a finite domain signal by breaking up the initial domain into two parts: the detail and approximation domain (Mallat, 1999). The approximation domain is then successively decomposed into detail and approximation domains. (Zhang et al., 2007) have used the properties of the discrete wavelet transform (DWT). DWT generally is scattered, i.e. a wavelet basis provides an efficient approximation of uniformly regular signals. This means only a few coefficients of DWT dominate the representation. Using this property in WMCM systems means that the PAPR can be reduced with little reconstruction loss. The transmitter of a WMCM system is shown in Fig.3-3. Let x (n) be the signal obtained after orthogonal modulation. Then, the PAPR can be defined as in the following equation 3-68,

$$PAPR_{(dB)} = 10\,log_{10}\frac{max_n\{|x(n)|^2\}}{E\{|x(n)|^2\}} = 10log_{10}\frac{max\{|x(n)|^2\},n=0,1,...,N-1}{\frac{1}{N}\sum_{n=0}^{N-1}|x(n)|^2} \qquad 3\text{-}63$$

Since wavelet transforms always concentrate energy on some given number of bases, we can introduce equation 3-69 to represent the energy concentrated in a wavelet.

$$\begin{cases} x_T(n) = 0 \, if \, |x(n)|^2 < T \\ x_T(n) = x(n) \, if \, |x(n)|^2 \geq T, \end{cases} \qquad 3\text{-}64$$

a threshold T and compare it with the energy of each orthogonal base. Then lets us define a new sequence

$$x_1(i) = x_T(n), x_T(n) \neq 0 \text{ i=0, 1... N-M-1: n=0, 1... N-1 } \quad 3\text{-}65$$

Reconsidering (3-67), the PAPR can now be written (Zhang et al., 2007) using equation 3-71,

$$PAPR_N = 10\,log_{10}\,g(n)\,,g(n) = 10log_{10}\frac{max\{|x(n)|^2\},n=0,1,...,N-M-1}{\frac{1}{N-M}\sum_{n=0}^{N-M-1}|x(n)|^2} 3\text{-}66$$

Let the threshold T fulfil the inequality $T < \frac{1}{N}\sum_{n=0}^{N-M-1}|x(n)|^2$.

Then, there exists the condition expressed by equation 3-72,

$$\frac{1}{N}\sum_{n=0}^{N-M-1}|x(n)|^2 < \frac{1}{N-M}\sum_{n=0}^{N-M-1}|x(n)|^2. \qquad\qquad 3\text{-}67$$

From (3-68), (3-71) and (3-72), we obtain

$$PARP > \boldsymbol{PAPR_N}. \qquad\qquad 3\text{-}68$$

Equation (3-71) expresses the reduction in PAPR, as the denominator is reduced more than the numerator. As mentioned earlier, the wavelet transform can concentrate most of the energy in the main lobe, so that there is very little energy in the side lobes. This means that the condition imposed on the threshold T can always be satisfied. Therefore, we can exploit this property of the wavelet transform to reduce the PAPR. Equations (3-66)-(3-71) show, that this method is effective in reducing the PAPR. The only difficulty with this method is choosing the proper threshold T. From equations 3-69 and 3-70 it is easy to realize that the higher the value of T is, the larger M becomes which results in a lower PAPR value. On the other hand, the higher the value of T is, the higher are the distortions of the transmitted signals, which results in higher information loss and in BER performance distortions. Given a certain value of T, different wavelet basis functions perform differently in reducing PAPR, due to their characteristics (Zhang et al., 2007).

For implementing in the receiver, we only need an additional forward transfer channel, which carries the label information of subspace whose energy is set to zero. Then, we pad zeros in subspaces, which are set to zero at the transmitter (Zhang et al., 2007b).

3.7. 3.1 Using CCDF with DWT/DCT based OFDM within 64QAM/64DAPSK modulation for PAPR measurement

Clipping the amplitude of the transmitted signal that exceeds a desired threshold is the simplest technique to control the peak-to-average power ratio. This technique however produces a significant Out-of-Band Interference (OBI) and is also a highly non-linear process. Companding is a good remedy for OBI, which means 'soft' compression of the amplitude of the transmitted signal. This is also an attractive option to compand the DWT-OFDM and DCT-OFDM signals. Furthermore, this technique not only reduces the high PAPR, but also improves the performance bandwidth efficiency of the system.

The effectiveness of a PAPR reduction technique can be measured by using the complementary cumulative distribution function (CCDF), which is defined as the probability of PAPR exceeding certain threshold. This can be expressed as:

CCDF = Probability (PAPR > $p0$), where $p0$ is the threshold.

The value of CCDF is directly proportional with the number of sub-carriers in the OFDM signal. So, the CCDF of parameter could be used to measure the PAPR value in the proposed OFDM system. The proposed combination of DWT system with 64DAPSK modulation scheme has been demonstrated to have reduced PARP level.

3.8 AWGN channel

An additive white Gaussian noise (AWGN) channel model is the one where the only impairment to communication is a linear addition of a Gaussian distribution of amplitude. It is also characterised by a wideband with a constant spectral density (expressed as watt per hertz of bandwidth) which is also described as white noise.

This simple model does not account for frequency selectivity, fading, nonlinearity, interference or dispersion. However, it produces tractable mathematical models, which are useful for gaining insight into the underlying behaviour and simplicity of a system before these other phenomena are considered.

Wideband Gaussian noise comes from celestial source such as the sun and from many other natural sources, such as the thermal vibrations of atoms in conductors (referred to as Johnson-Nyquist or thermal noise), black body radiation from the earth and other warm objects.

The normal (or Gaussian) distribution is a continuous probability distribution that has a bell-shaped probability density function, known as informally the bell or Gaussian function is given by equation 3-73

$$f(x, \mu, \sigma^2) = \frac{1}{\sigma\sqrt{2\pi}} e^{-\frac{1}{2}\left(\frac{x-\mu}{\sigma}\right)^2} \quad \text{3-69}$$

The parameter σ^2 is the variance and μ is the mean or expectation (location of the peak). σ is known as the standard deviation. The unit normal distribution or the standard normal distribution is the distribution with $\mu = 0$ and $\sigma^2 = 1$. Usually, a normal distribution is used as a first approximation to describe real-valued random variables that cluster around a signal mean value.

AWGN is a suitable model for most of the satellite and deep-space communication links. However, for most of the terrestrial wireless channels, due to the effects of multipath, terrain blocking, interference, etc., the AWGN is not a suitable model. Currently AWGN is also used to represent the background noise of the channel in modern terrestrial radio communication systems.

Band limited AWGN cannot be ignored in modern communication systems. Statistical analysis reveals that the amplitudes of the real and imaginary contributions are independent variables, when the modelling band limited AWGN is in the phasor domain, which follows the Gaussian distribution model.

3.9 Rayleigh channel

A channel can be modelled as the physical processes that modify the signal being transmitted. For example, a channel in wireless communications can be modelled by incorporating the reflection of the signal from every object in the environment. Simulating external interference and/or electronic noise in the receiver, a sequence of random numbers might also be added. Statistically, a communication channel is modelled with three variables for repsenting an input alphabet, an output alphabet, and for each pair *(i, o)* of input and output elements a transition probability *p (i, o)*. Statistical and physical modelling can also be combined. Often, for example, the channel is modelled by a random attenuation (known as fading) of the transmitted signal, in wireless communications, followed by additive noise. The underlying physical processes capture the change in signal power as the attenuation term is simplified over the course of the transmission. The noise in the model captures external interference and/or electronic noise in the receiver. If the attenuation term is complex it also describes the relative time a signal takes to get through the channel. The Rayleigh fading process, in which the gain of each wireless channel experiences independent variation while remaining constant within a frame, considers the multipath fading channel which is frequency nonselective. The correlation function of the Rayleigh fading process which was generated according to the Jakes model is given (Jakes, W. C., 1974) by equation 3-74

$$R(\tau) = J_0(2\pi f_D \tau) \hspace{3cm} \text{3-70}$$

where f_D is the maximum Doppler shift of the fading signal caused by the mobile motion. The Doppler shift is given by $f_D = v/\lambda$, where v is the velocity of the mobile and λ is the wavelength of the carrier. In most cases, the normalized maximum Doppler shift $f_D T$ is used as the measure for the fading rate, where T denotes the symbol duration (Der-Zheng and Che-Ho, 2001).

The model assumes that N equal-strength rays arrive at a moving receiver with uniformly distributed arrival angles a. If a transmitted signal is x, then the received signal y can be written as using equation 3-75

$$y = hx + n \hspace{3cm} \text{3-71}$$

where $h = h_c + jh_s$ is the complex channel coefficient, $n = n_c + jn_s$ is the complex additive white Gaussian noise, and h and n are assumed to be zero mean statistically independent complex Gaussian random variables (h_c, h_s, n_c and n_s are independent). In addition, the noise is assumed to have zero mean and unit variance (noise power is normalized to unit).

The equivalent-baseband signal at receiver is given by (Der-Zheng and Che-Ho, 2001) equation 3-76

$$y(t) = \sqrt{\frac{\Gamma_s}{2}} e^{j(\Delta wt + \Theta)} f(t) . \sum_{i=-\infty}^{\infty} \sum_{k=0}^{L-1} s_k^{(i)} g_T[t - (iL + k)T] + w(t) \hspace{1cm} \text{3-72}$$

Where $g_T(t)$ the pulse-shaping is filter and Γ_s denotes the average received signal-to-noise ratio (SNR) per symbol. Thus, the average SNR per bit is given by equation 3-77

$$\Gamma_b = \Gamma_s / \log_2 M \qquad \text{3-73}$$

$w(t)$ is a complex Gaussian process whose real and imaginary components have the same power spectral density (PSD) which represents the combined distortion introduced into the desired signal in the fading channel. $\Delta wt = 2\pi \Delta f$ and Θ are frequency offset in radians and residual phase error introduced during demodulation, respectively.

Rayleigh distribution is derived from two zero-mean statistically independent normally distributed random variables μ_1 and μ_2, each having a variance σ_0^2, i.e., μ_1, $\mu_2 \sim N(0, \sigma_0^2)$, according to $\zeta = \sqrt{\mu_1^2 + \mu_2^2}$. Then ζ represents a Rayleigh distributed random variable. The probability density function (Kai-ming et al., 2005) is given by equation 3-78

$$p_\zeta(x) = \frac{x}{\sigma_0^2} e^{\frac{x^2}{2\sigma_0^2}}, \quad x \geq 0 \qquad \text{3-74}$$

Flat Rayleigh channel with Jakes' power spectral density is used in simulation. The frequency range of the Jakes' power spectral density is limited to the range $|f| \leq f_{max}$, f_{max} denotes the maximum Doppler frequency due to the motion of the receiver or transmitter. Generation of two coloured Gaussian random processes is based on a superposition of a finite number of harmonic functions according to the Rice method. The Monte Carlo Method (MCM) has been employed for computation of the model parameters such as Doppler coefficients, discrete Doppler frequencies and Doppler phases.

When combined, the resultant phasor's magnitude is a Rayleigh distribution random variable, while the phase is uniformly distributed from 0 to 2π.

3.10 Related bandwidth with transmission speed

The pulse width of transmitted data represented by this directly proportional to the transmission speed. Also, when the pulse width is large, the first zero crossing in the first zero crossing in the spectrum is lowered while shorter width increases the same. In a digital communication system transmitting rectangular impulses as shown in figure 3-5, the location of the first zero crossing in the magnitude spectrum is directly related to the bandwidth required. For that, quantitatively examining communication system trade-offs involving bandwidth versus transmission speed provides the techniques and insight necessary to begin (Harlod and Samy, 2004) .
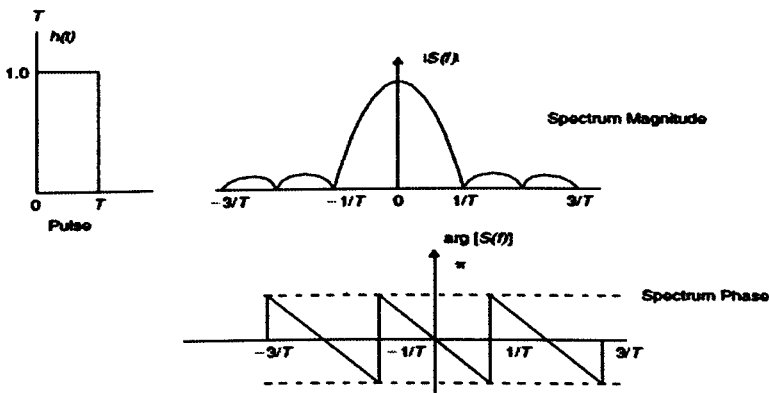

Figure 3-6. Rectangular pulse and its spectrum

The bit period symbolized as $T = 1/r_b$, as shown in Fig.3-5, is the amount of time between the two adjacent bits or the pulses, where r_b is a source out putting bits per second. While the pulses should not overlap, they should be as wide as possible (this minimizes bandwidth). This is accomplished by selecting a pulse width of $\tau = T$. Pulses will be overlapping when $\tau > T$, so that pulses do not overlap when $\tau < T$ but bandwidth is wasted (since bandwidth is proportional to τ).

3.11 Summary

The advantages offered by DCT over DFT technique (Al-Dhahir, N., and Minn, H., 2005) the excellent spectral compaction and energy concentration

properties. This in turn, leads to improved performance with interpolation-based channel estimation and in the presence of narrow-band interference and residual frequency offsets. In addition, it can result in improved adaptive filtering convergence. So, the DCT is widely adopted in image/video coding standards (e.g. JPEG, MPEG). It has been demonstrated that DCT when used with frequency-selective channels results in a better integrated system design and could mean reduced implementation cost. Also the DCT uses only real value processing as opposed to the complex-valued operation in DFT. This reduces the signal processing complexity, especially for real pulse-amplitude modulation (PAM). The DFT based processing also suffers from in-phase/quadrature (I/Q) imbalance problems which can cause significant performance degradation.

In this research, DWT system has been demonstrated to offer the best features for digital wireless communication. It has an inherent advantage of not requiring CP and as a result has good bandwidth efficiency. Also, DWT provides side lobs of much lower magnitude than those of Discrete Fourier transforms [Resnikoff, H.L., et al 1998], and can better combat narrowband interference. The system is also inherently more robust with respect to ICI than traditional DFT-OFDM, and offers simplicity of receiver design.

Chapter 4

Design of a novel hybrid OFDM system using DWT technique with DAPSK scheme for wireless communication systems

4.1   Introduction

The coherent demodulation techniques used in the current mobile network design lead to increased system complexity and signalling overhead. This results from the need for the channel estimation procedure to be updated at every OFDM symbol, leading to a large amount of transmitted pilot tones being generated. A decision directed channel estimation approach reduces the signalling overhead considerably, but is very sensitive to erroneous decision on the data symbols due to the changes in channel characteristics (Toender, Georgi et al. 2006).

To avoid using any channel estimation, equalization and tracking techniques, differential modulation schemes can be used, encoded in time or frequency domain. In this case, even if a time variant radio channel is considered, no pilot signals and no radio channel estimation procedures are needed, which reduces the system complexity significantly. Therefore in practice, differential amplitude and phase shift keying (DAPSK) is a very attractive technique for high-rate transmission in a mobile radio environment (Rohling and Engels 1995), since differential detection instead of coherent detection can be employed. The DAPSK scheme consists of DASK and DPSK, by which the information bits are partially carried on the amplitude and partially on the phase (Suzuki, Mi et al. 1995) and has superior performance compared to both the schemes.

One of the major advantages of the DWT is system is that the wavelet based system does not need a cyclic prefix to deal with delay spreads of the channel due to

the overlapping nature of wavelet properties. As a result, it has higher spectral containment than the DFT-OFDM and DCT-OFDM systems discussed in the previous chapters. Moreover, the DWT is widely used for data compression. Wavelet based still image compression methods not only out-perform traditional methods, but also possess built-in scalability so that single bit stream can be transmitted progressively and decoded from coarse to fine resolution (Guo 1998). In addition a great reduction in the side-lobe levels achieved by this system is the motivation behind the recent trend in using the wavelet in the OFDM system. While DWT-OFDM provides many advantages, the transmitted signal does not have a constant envelope.

Therefore, in this research work, it is proposed to develop a novel hybrid OFDM system using DWT with DAPSK modulation. The main goal in proposing this system is to achieve considerable reduction in the PARP of the OFDM system. With its major advantages of reduced PAPR and optimum BER performance in fast moving mobile environments, the newly proposed hybrid OFDM system can find a very useful application in the 4G wireless communication systems.

4.2   Proposed Transceiver and Channel Transmission systems

4.2.1   Wavelet-Based OFDM (DWT-OFDM)
The block diagram of the proposed wavelet OFDM system with the DAPSK modulation scheme is given in figure 4.1 below. In the block diagram, the blocks representing inverse discrete wavelet transform (IDWT) and DWT have replaced the blocks for IFFT and FFT in the FFT-OFDM system. The output of IDWT can be represented by the following equation 4-1,

$$s(k) = \sum_{m=0}^{\infty} \sum_{n=0}^{\infty} S_m^n \, 2^{m/2} \psi(2_k^m - n) \qquad \text{4-1}$$

where S_m^n are the wavelet coefficients and $\psi_{m,n}(t)$)is the wavelet function with compressed factor m times and shifted n times for each subcarrier (number k, $0 \leq k \leq$ N-1). Also the IDWT function can be expressed as weighted sum of functions as given by (Guo, H., 1998) equation 4-2,

$$Y = \sum_{i=0}^{N} c_i B_i \qquad \text{4-2}$$

where N is the length of the data sequence, B_i denotes the wavelet basis function W_j on various scales, and the scaling basis function S_j on the coarsest scale. As the wavelet transform is made up of compression and dilation factors, these can be represented by low pass and high pass filtering components. The scaling function S and the wavelet function W at different scales can be obtained from (Guo 1998) equations 4-3 and 4-4

$$S_{j+1} = up(S_j) * h, \quad W_{j+1} = up(W_j) * h \qquad \text{4-3}$$

With

$$S_i = h, \qquad W_i = g \qquad \text{4-3}$$

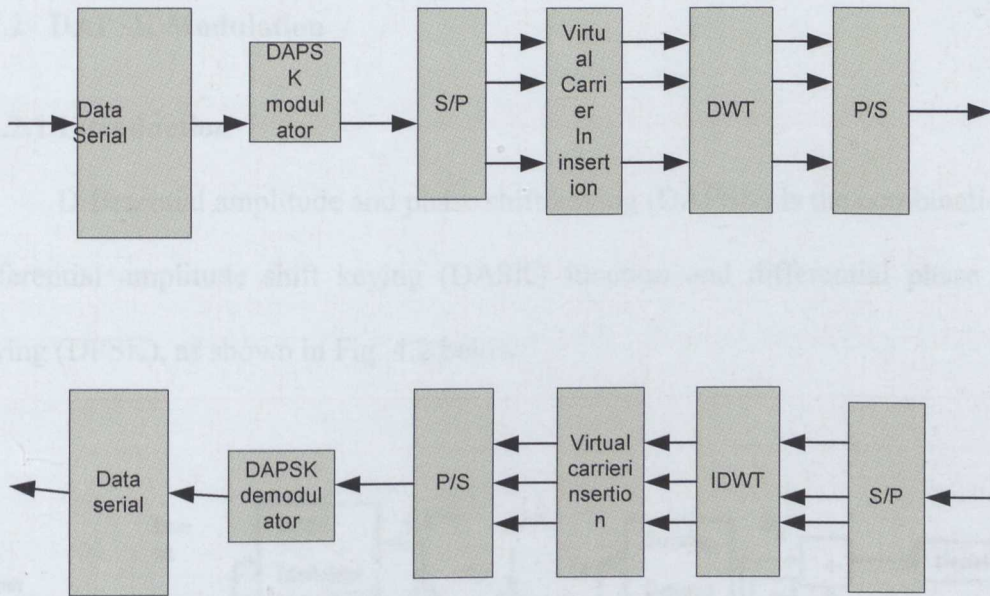where up() denotes up-sampling, and * denotes convolution.

Figure 4-1. DWT-OFDM with DAPSK transmission system

Unlike the DCT system where the basis functions are on the same scale and have the same support, the basis functions for the DWT have been increasing support at coarser scales. Also, the basis functions on the same scale are merely shifts of one another. By grouping the coefficients according to scales and enabling them, the previous equation (Guo 1998) can be rewritten using equation 4-5,

$$Y = \sum_{j+1}^{J} \sum_{i=0}^{\frac{N}{2^j}-1} c_{j,i} W_{j,i} + \sum_{i=0}^{\frac{N}{2^J}-1} d_{J,i} S_{J,i}, \qquad 4\text{-}4$$

where j is used for scale, and i is used for position within the scale, and J is the total number of decompositions.

4.2.2 DAPSK Modulation

4.2.2.1 Introduction

Differential amplitude and phase shift keying (DAPSK) is the combination of differential amplitude shift keying (DASK) function and differential phase shift keying (DPSK), as shown in Fig. 4.2 below.
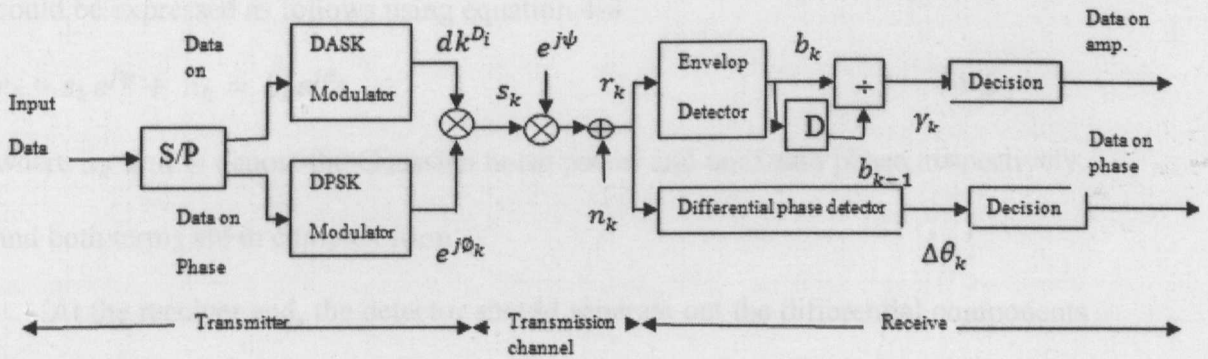

Figure 4-2 The transmission model of DAPSK scheme.

Differential amplitude and phase shift keying (DAPSK) is an efficient modulation scheme that can be implemented in wireless channel state information (CSI) at the receiver side (Yao, Zhang et al. 2005), in that the performance of the HF communication system (e.g. radio mobile environment) with differential modulation has been demonstrated to be comparatively better than those with no differential modulation. Furthermore, the differential modulation can greatly reduce the computational complexity in the demodulation process because it does not require complicated channel estimation and equalization procedures (Shuzheng, Huazhong et al. 2005).

The DAPSK scheme consists of DASK and DPSK, by which the information bits are partially carried on the amplitude and partially on the phase. The transmitted

symbol at time k is denoted as s_k , its amplitude component as a_k, and phase component as ϕ_k using equations 4-6 and 4-7,

$$s_k = ae^{j\ \phi_k}$$ 4Error! Bookmark not defined.

$$\Delta\ \phi_k = \ \phi_k - \ \phi_{k-1} \quad \text{4-5}$$

Now, let the received symbols be represented by r_k, which consists of amplitude part b_k and phase part ϕ_k. Since AWGN channel is assumed, the received symbols could be expressed as follows using equation 4-8

$$r_k = s_k e^{j\psi} + n_k = b_k e^{j\theta_k} \qquad\qquad \text{4-6}$$

where $n_k\ and\ \psi$ denote the Gaussian noise power and uncertain phase, respectively, and both terms are in complex form.

At the receiver end, the detector should separate out the differential components of amplitude and phase. This is done by using the previous symbol r_{k-1} as a reference to deduce the ratio of amplitude γ_k and the differential phase $value\ \Delta\ \phi_k$ as shown below using equations 4-9 and 4-10

$$\gamma_k = \left|\frac{\gamma_k}{\gamma_{k-1}}\right| = \frac{b_k}{b_{k-1}}$$

4-Error! Bookmark not defined.

$$\Delta\theta_k = \theta_k - \theta_{k-1}$$

4-Error! Bookmark not defined.

The conventional differential detector will deduce the transmitted data of the DAPSK signals, based on the above two equations.

4.2.2.2 The differential amplitude shift key (DASK)

The term "differential" is used here because the information is transmitted as the difference in amplitudes between the current and previous bits. When transmitting a phase amplitude modulation (PAM) through a band pass channel, it

produces an amplitude shift key (ASK). Therefore, ASK can be expressed using equations 4-11 and 4-12

$$S_{ASK}(t) = S_{baseband}(t)\,sin(2\pi f_c) \qquad\qquad 4\text{-}7$$

where $S_{baseband}(t) = \begin{cases} A & \text{\textit{when the data from the source is a "1"}} \\ 0 & \text{when the data from the source is a "0"} \end{cases}$

$$A_i = dk^{D_i} \qquad\qquad 4\text{-}8$$

where $D_i = (D_{i-1} + \Delta)mod4, D_{i-1} \in \{0,1,2,..\}$, Δ is amplitude increment and f_c represents the carrier frequency. In order to produce an energy spectral density with all its significant components in dc- to low-frequency range, PAM signals were designated '1's and '0's (where '1's are transmitted by sending the carrier signal with an amplitude of A volts, and '0's are transmitted by sending the carrier signal with an amplitude of 0 volts) to represent different amplitudes of the carrier signal using binary ASK (Abdullah, Hussain et al. 2009). Formatting information to represent ASK is based the amplitude of the transmitted signal relative to the carrier; while for DASK, it depends on the amplitude of the transmitted signal relative to the previously transmitted bit. For example, when the amplitude ring increases cyclically from inner to the outer ring, the increment between rings also increases. Thus, the amplitude of the signal can be expressed as demonstrated in (Kai-ming, Wen-bo et al. 2005) .

Power spectral density for ASK has two such curves; one centred at $-f_c$ (the carrier frequency) while the other is centred at f_c. The bandwidths for both ASK and PAM is calculated based on the percentage of in-band power required to maintain a certain degree of accuracy. The percentage of in-band power required to maintain a certain degree of accuracy will be the bandwidth for both ASK and PAM. The

bandwidth of $2r_b$ (the number of bits output by the source per second) for the ASK contains 95% of the signal's power, while a bandwidth of r_b contains 90% of the signal's power for PAM. This means, the bandwidth for ASK is twice that of the PAM signal, since due to the symmetry of components the frequency range occupied by the PAM signal spectrum to the left of 0 Hz is now shifted to the right of 0 Hz in the ASK spectrum. As a result in order to obtain 95% in-band power for an ASK signal, the channel must be capable of reliably transmitting all frequency components ranging from (f_c-2r_b) to $(f_c + 2r_b)$, which means a bandwidth of $4r_b$.

4.2.2.3 The differential phase shift key (DPSK)

The DPSK scheme is based on the difference between the phase of the transmitted signal relative to that of previously transmitted bit. A one-bit initialization period at the beginning of each transmission is required for DPSK. The concept of differential encoding can easily be extended to the constellation for mixed amplitude/phase modulation. Let $a \in A$ be the differential symbol drawn from the signal set A and s the current state of the encoder (the reference symbol). The transmitted symbol $\chi \in X$ is produced from the tuple (a, s) encoder. The operator $\otimes$ specifies the relation between a and s (Fisher, Lamp et al. 1999) given by equation 4-13

$$\chi = s \otimes a, \qquad\qquad\qquad 4\text{-}9$$

where "$\otimes$" is a non-commutative operation as shown below.
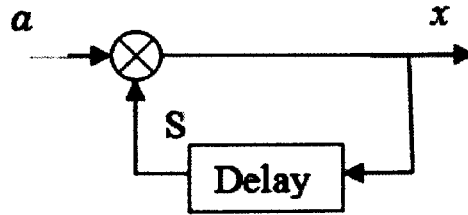
$$\otimes: X \times A \rightarrow X,$$

Figure 4-3 differential encoder

In the above figure 4-3, for the traditional DPSK, "$\otimes$" is simply the complex multiplication. Considering the classical DPSK for the encoder state, let the differential symbol $a = r_j e^{j\varphi_m}$ and $s = r_i e^{j\varphi_n}$. So that the lead transmitted symbol is given by Equation 4-14 (and, thus, implicitly the operator "$\otimes$")

$$x = s \otimes a = r_i e^{j\varphi_n} \otimes r_j e^{j\varphi_m} \triangleq r_{(i+j)mod\alpha} e^{j\varphi(n+m)mod\beta} = s_k \qquad \text{4-10}$$

where r_k is the received signal, which consists of amplitude part b_k and phase part $\emptyset_k$.

4.2.2.4 The M-DAPSK scheme modulation

M-DAPSK modulation is a combination of N-DPSK and K-DASK, where M = N*K. The encoder will produce organisation output into sets of four bits binary data $c_m^{(0)}$, $c_m^{(1)}$, ..., $c_m^{(q)}$, where q = $2^{N/2}$. Mapping these data to the complex value set s_m, equation 4-15 represents the set S_m

$$S_m = r_m exp\ (j\Delta\varphi_m) \qquad \text{4-11}$$

where $\Delta\varphi_m$ and r_m represent phase transition factor and amplitude transition factor, respectively.

The phase transition factor $\Delta\varphi_m$ in the transmitted complex value S_m means

applying Gray mapping of three–bit binary data $c_m^{(0)}$, $c_m^{(1)}$, $c_m^{(2)}$ for 8–DPSK

modulation according to Table 4-1 (Harlod and Samy 2004)

Table 4-1 Natural Binary to Gray code

Input decimal	Input binary	Gray decimal	Gray Binary
0	0000	0	0000
1	0001	1	0001
2	0010	3	0011
3	0011	2	0010
4	0100	6	0110
5	0101	7	0111
6	0110	5	0101
7	0111	4	0100
8	1000	12	1100
9	1001	13	1101
10	1010	15	1111
11	1011	14	1110
12	1100	10	1010
13	1101	11	1011
14	1110	9	1001
15	1111	8	1000

Table 4.2 Amplitude choice for DAPSK modulation

$|x_i|$		Amplitude bits $b_{i,4}$, $b_{i,5}$			
		00	01	11	10
$|\tilde{x}_i|$	1	1	a	a^2	a^3
	a	a	a^2	a^3	1
	a^2	a^2	a^3	1	a
	a^3	a^3	1	a	a^2

The amplitude transition factor r_k for each transmitted signal in Table 4.2 is multiplied by ak-1, which is the amplitude of the previous transmitted complex symbols. A ring factor α in M–DAPSK modulation is defined using equation 4-14

$$\alpha = a_H/a_L \qquad\qquad 4\text{-}12$$

where a_H and a_L ($a_L <$ a_H) represent the two amplitude levels of the modulated signals. Therefore, the transmitted complex symbol d_m is given by (Harlod and Samy 2004) equation 4-17

$$d_m = a_m \, exp(j\varphi_m) = s_m d_{m-1} = r_m \, exp(j\Delta\varphi_m) * a_{m-1} \, exp(j\varphi_{m-1}) =$$

$$r_m a_{m-1} \, exp[j(\Delta\varphi_m + \varphi_{m-1})] \qquad 4\text{-}13$$

where d_{m-1} represents the previously transmitted complex symbols.

The received complex symbol $\hat{d}_m$ is divided by the previous received complex symbol, to obtain the differential complex value S_m.

where r_m is the received signal, which consists of amplitude part b_m and phase part $\emptyset_m$. Since the additive white Gaussian noise (AWGN) channel is assumed, the received symbols hold the relation as follows:

$$r_m = s_m e^{j\psi} + n_m = b_m \, e^{j\emptyset_m} \qquad 4\text{-}14$$

where n_m and ψ denote the Gaussian noise with power n and uncertain phase, respectively, both with complex form.

The previous symbol r_{k-1} in the differential detector is used as the reference to detect the difference between the phase $\Delta\theta_m$ and the ratio of amplitudes γ_m represented by equations 4-19 and 4-20 respectively.

$$\Delta\theta_m = \theta_m - \theta_{m-1} \qquad\qquad 4\text{-}15$$

$$\gamma_m = \left|\frac{r_m}{r_{m-1}}\right| = \frac{b_m}{b_{m-1}} \qquad\qquad 4\text{-}16$$

The conventional differential detector will detect the transmitted data on DAPSK signals (Suzki et al., 1995) based on those two values.

4.3 Mathematical model of the DWT-OFDM system with DAPSK modulation
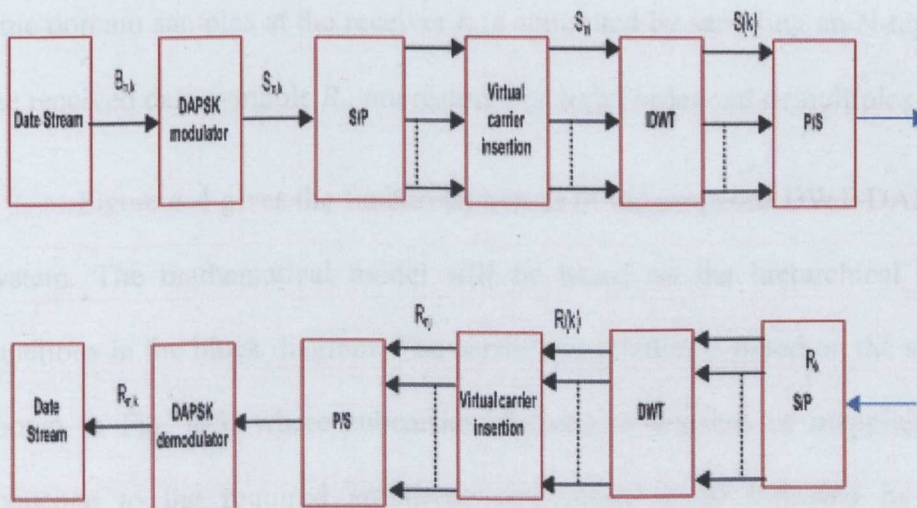
Figure 4-4 Communication System model

The DAPSK modulation process in the block diagram represented by figure 4-4 can be visualised as a series of mapping of the amplitude and phase components. This is shown in figure 4-5 below.

$(b_1, b_2, \ldots, bm)_{n,k}$ → [Mapping] → Bn,k → [Differential Encoding] → Sn,k
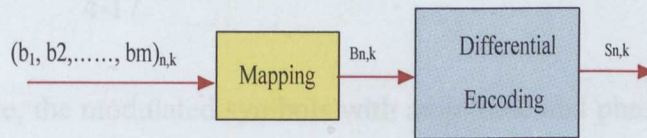
Figure 4-5 Block diagram of linear subcarrier modulation

Modulation is achieved as a mapping of serial data stream as data symbols having a symbol rate of $\frac{1}{T_s}$, via a general phase and amplitude modulation scheme; demultiplexing is obtained as result of mapping the symbols into a vector of N data symbols S_0 to S_{N-1}. The parallel data symbol is N times longer than the serial symbol of duration T_s. The coefficients S_0 to S_{N-1} are constants in an OFDM system and are computed via the inverse DWT (IDWT) of the data symbol vector. Samples of the OFDM symbols are transmitted sequentially over the channel at a symbol rate of $\frac{1}{T_s}$ such as the S_n in the time domain. A spectral decomposition of the received time domain samples at the receiver r_n is computed by sampling an N-tap DWT, and the received data symbols R_n are restored in serial order and demultiplexed.

Figure 4-4 gives the functional blocks of the proposed DWT-DAPSK-OFDM system. The mathematical model will be based on the hierarchical flow of the functions in the block diagram. The carrier modulation is based on the system block shown in Fig. 4-5, where subcarrier modulation consists of mapping the binary sequence to the required amplitude and phase space followed by differential encoding. Differential encoding can be expressed (Rohling, May et al. 1999) using equation 4-21

$$S_{n,k} = B_{n,k} \cdot S_{n-1,k} \qquad \text{4-17}$$

Therefore, the modulated symbols with amplitude and phase components can be represented using complex notation as given below by the equation 4-22 below.

$$B_{n,k} = \left\{ a^{A'} \cdot e^{j\Delta\varphi p} \middle| \begin{array}{l} A' \in \{-N_{a+1}, \ldots\ldots, N_a - 1\} \\ p \in \{0, \ldots\ldots, N_P - 1\} \end{array} \right\} \qquad \text{4-18}$$

The subscripts n and k refer to the time and number of subcarriers in the OFDM block considered, and $B_{n,k}$ is the complex coded sequence describing the transition between the different amplitude and phase states in the constellation diagram. Note that the amplitudes are spaced by a factor a. The number of amplitude circles is represented by $N_a = 2^{m_a}$, and the number of phase constellation points per amplitude circle is given by $N_p = 2^{m_p}$, so the number of signal states is calculated as M $= N_a \cdot N_p = 2^m$. $\Delta\varphi$ is deviation angle for two successive points in one circle on the constellation.

DAPSK can be described as a differentially encoded APSK (Der-Zheng and Che-Ho 2001) (Weber 1978), the signal-space diagram of which is defined by the complex signal set, given by equation 4-23

$$S_{n-1,k} = \lambda \cdot \mu^{a_{n,k}} \cdot e^{j(\frac{2\pi}{N_p})b_{n,k}} \qquad \text{4-19}$$

Where $\mu > 1$ is the fixed ring ratio, and the number of bits per DAPSK signal m = $m_a + m_p$. $a_{n,k}$ and $b_{n,k}$ indicate the amplitude and phase levels of the transmitted DAPSK signal, $S_{n,k}$, respectively. $\lambda = \sqrt{N_a(\mu^2 - 1)/(\mu^{2N_a} - 1)}$ is the normalized gain of signals; the average transmitted signal power is normalized to unity.

By substituting equations 4-22 and 4-29 in equation 4-21 yields equation 4-24

$$S_{n,k} = \lambda . \mu^{a_{n-1,k}} . e^{j(\frac{2\pi}{Np})b_{n-1,k}} \left\{ a^{A'} \left| \begin{array}{l} A' \in \{-3, \dots, 3\} \\ p \in \{0, \dots, 15\} \end{array} \right. \right\} . e^{j\Delta\varphi p} \qquad \text{4-20}$$

Eq. (4-24) will be the output signal for DAPSK modulator, but after the virtual carrier insertion block yields (Der-Zheng and Che-Ho 2001) (Weinstein and Ebert 1971) the equation 4-25.

$$S_{nj} = \frac{1}{\sqrt{N}} \sum_{k=0}^{N-1} S_{n,k} e^{j2\pi nk/N} \qquad \text{4-21}$$

In order to obtain the signal map of DWT with DAPSK substituting equation (4-24) in Eq. (4-25) the OFDM symbol in DFT is represented by equation 4-26

$$S_{nj} = \frac{1}{\sqrt{N}} \sum_{k=0}^{N-1} \left\{ a^{A'} \left| \begin{array}{l} \lambda . \mu^{a_{n-1,k}} . e^{j\left(\frac{2\pi}{Np}\right)b_{n-1,k}} \\ A' \in \{-3, \dots, 3\} \\ p \in \{0, \dots, 15\} \end{array} \right. \right\} . e^{j\Delta\varphi p} e^{j2\pi nk/N} \qquad \text{4-22}$$

Rearranging equation 4-26 yields equation 4-27

$$S_{nj} = \frac{\lambda}{\sqrt{N}} \left\{ a^{A'} \left| \begin{array}{l} A' \in \{-3, \dots, 3\} \\ p \in \{0, \dots, 15\} \end{array} \right. \right\} . e^{j\Delta\varphi p} \sum_{k=0}^{N-1} \mu^{a_{n-1,k}} . e^{j\left(\frac{2\pi}{Np}\right)b_{n-1,k}} e^{j2\pi nk/N}$$

$$= \frac{\lambda}{\sqrt{N}} \left\{ a^{A'} \left| \begin{array}{l} A' \in \{-3, \dots, 3\} \\ p \in \{0, \dots, 15\} \end{array} \right. \right\} . e^{j\Delta\varphi p} \sum_{k=0}^{N-1} \mu^{a_{n-1,k}} e^{j2\pi(\frac{b_{n-1,k}}{Np} + \frac{nk}{N})}$$

$$= \varepsilon \sum_{k=0}^{N-1} \mu^{a_{n-1,k}} e^{j2\pi(\frac{b_{n-1,k}}{Np} + \frac{nk}{N})} \qquad \text{4-23}$$

where $\varepsilon = \frac{\lambda}{\sqrt{N}} \left\{ a^{A'} \left| \begin{array}{l} A' \in \{-3, \dots, 3\} \\ p \in \{0, \dots, 15\} \end{array} \right. \right\} . e^{j\Delta\varphi p}$

So, equation (4-27) represents the output of the inverse discrete wavelet transform (IDWT) which is represented by (Abdullah and Hussain 2007) (Strang and Nguyen 1997) as given by equation 4-28

$$s(k) = \sum_{c=0}^{\infty} \sum_{d=0}^{\infty} S_c^d 2^{c/2} \psi(2_k^c - c) \qquad \text{4-24}$$

where $\{S_c^d\}$ are the wavelet coefficients and $\psi(t)$ is the wavelet function with a compression factor of c and shifted d times for each subcarrier (number k, $0 \leq k \geq N - 1$). The wavelet coefficients are representations of signals in scale and position or time. The scale is related to the frequency. Low scale represents compressed wavelet which means that the signal is rapidly changing, or the signal is high frequency. On the other hand, high scale represents stretched wavelet which means that the signal is slowly changing, or the signal is in low frequency. Since, the IFFT output is the sum of the received signal in discrete frequency by equation 4-29

$$x_k = \frac{1}{\sqrt{N}} \sum_{m=0}^{N-1} X_m e^{j2\pi km}/N \qquad\qquad 4\text{-}25$$

X_m is a sequence in the discrete time domain, and $\{ X_m | 0 \leq m \leq N - 1 \}$ are complex numbers in discrete frequency domain. Thus, X_m, which is a sequence in discrete time domain in FFT, can be represented to $\{S_c^d\}$ before it is processed in the IDWT block.

Therefore by substituting Eq. (4-26) in Eq. (4-28) we obtain the modulated signal yields equation 4-30

$$s(k) = \sum_{c=0}^{\infty} \sum_{d=0}^{\infty} \varepsilon \sum_{k=0}^{N-1} \mu^{a_{n-1,k}} e^{j2\pi(\frac{b_{n-1,k}}{N_p} + \frac{nk}{N})} 2^{c}/2 \, \psi(2_k^c - c) \qquad 4\text{-}26$$

So equation (4-30) represents the mathematical model that is proposed for the IDWT DAPSK transmitted signal .

In the receiver side the complex received signal is (Rohling, May et al. 1999) represented by equation 4-31

$R_{n,k} = S_{n-1,k}.B_{n,k}H_{n,k}+N_{n,k}$ 4-27

where $H_{n,k}$ is channel transfer factors and $N_{n,k}$ is additive noise signal.

If differential encoding is used in the transmitter, the demodulation can be performed either non-coherently (nc) or quasi-coherently (qc). With non-coherent demodulation the decision is based on the quotient of two successive symbols and is given by equation 4-32

$$D_{n,k}^{nc} = \frac{R_{n,k}}{R_{n-1,k}} = \frac{S_{n-1,k}.B_{n,k}H_{n,k}+N_k}{S_{n-1,k}.H_{n-1,k}+N_{n-1,k}}$$ 4-28

Since, $S_{n,k} = S_{n-1,k}.B_{n,k}$ it is substituted in numerator of equation 4-32

$R_{n,k} = S_{n,k}H_{n,k} + N_k$.

In general, successive channel transfers are strongly correlated so that $H_{n,k} \approx H_{n-1,k}$ and therefore cancel down in (4-31) (if the noise is neglected). Unfortunately, $D_{n,k}^{nc}$ is affected twice by the noise power than $D_{n,k}^c$ (decision with coherent demodulation), leading to a higher BER than coherent demodulation (with perfect channel state information). Note that, with no coherent demodulation, no channel estimation has to be performed. Thus, the computation complexity in the receiver is relatively low.

To determine the data in sub-channel k, the transmitted waveform needs to be matched with carrier n (Ahmed 2000; Abdullah and Hussain 2007)as represented by equation 4-33

$$\langle y(t), f_n(t) \rangle = \sum_{k=0}^{K} d_k \langle f_k(t), f_n(t) \rangle \qquad \qquad 4\text{-}29$$

where y(t) is the transmitted via IFTT, $f_k(t)$ the complex exponential used in the IFFT operation or $e^{j2\pi km/K}$ (K being the size the size of FFT), d_k the data projected on each carrier, and $\langle y(t), f_n(t) \rangle$ equals 1 when k=n and 0 when k ≠n.

In a typical communication system, data is transmitted over a dispersive channel. The impulse response of a deterministic (and possibly time-varying) channel can be modelled by a linear filter (t) as shown using equations 4-34 and 4-35

$$r(t) = y(t)*h(t)+n(t) \qquad 4\text{-}30$$

$$= \sum_{k=0}^{K-1} d_k f'_k + n(t) \qquad \qquad 4\text{-}31$$

f'_k being the distorted carriers due to the dispersive channel and n(t) is additive white Gaussian noise.

In wavelet-based OFDM, the same conversion as for the DFT using match filtering is performed except that the $f_k(t)$ is the complex exponential used in the IFFT operation $e^{j2\pi km/K}$ (K being the size of FFT), and the coefficients are replaced with $W_k(t)$ and $W_n(t)$; $W_k(t)$ being the wavelet carrier in IDWT operation with sub-channels to match with carrier n. Therefore, the received signal is expressed as by equations 4-36 and 4-37

$$r_w(t) = y_w(t)*h(t)+n(t) \qquad 4\text{-}32$$

$$= \sum_{k=0}^{K-1} S_{n,k} W'_k(t) + \sum_{l=0}^{K_g-1} \sum_{k=0}^{K-1} S_{n,k,l} W'_k(t-lk) + n(t) \qquad \qquad 4\text{-}33$$

where K is the wavelet filter rank (sampling rate), $W'_k(t) = W(t)*h(t)$, and g(g>1) is the wavelet genus so that K_g is the filter order (number of taps in that sub-band).

After matched filtering with carrier n, the signal is represented by equations 4-38 and 4-39.

$$\langle r_w(t), W_n(t)\rangle = \sum_{k=0}^{K-1} S_{n,k} \langle W'_k(t), W_n(t)\rangle + \sum_{l=1}^{K_g} \sum_{k=0}^{K-1} \langle W'_k(t-lk), W_n(t-lk)\rangle + n(t), f_n(t) \qquad 4\text{-}34$$

$$= \sum_{k=0}^{K-1} S_{n,k}\, p_{k,0}(0) + \langle n(t), f_n(t)\rangle \quad = \quad S_K p_{k,n}(0) + \sum_{\substack{k=0\\k\neq n}}^{K-1} S_{n,k} p_{k,n}(0) +$$

$$\sum_{n=1}^{K_g} \sum_{\substack{k=0\\k\neq n}}^{K-1} S_{n,k,l}\, p_{k,n}(l) + n''(t) \qquad\qquad\qquad\qquad 4\text{-}35$$

where $S_K p_{n,n}(0)$ is the recovered data with correlation term $p_{n,n}(0)$. The term $\sum_{\substack{k=0\\k\neq n}}^{K-1} S_{n,k} p_{k,n}(0)$ is the interference due to the distorted filters that are no longer orthogonal to one another with correlation term $s\, p_{k,n}(0)$, and $\sum_{n=1}^{K_g} \sum_{\substack{k=0\\k\neq n}}^{K-1} S_{n,k,l}\, p_{k,n}(l)$ is the interference term with correlation $p_{k,n}(l)$ due to the overlapped nature of wavelet transform. These two terms become zero, and only the first and last terms would appear if the channel has no distortion. The decoder would possibly obtain an almost correct signal when the terms are zero.

In this chapter, the mathematical representations of DWT, DASK and DPSK schemes have been discussed briefly. Using those mathematical representations as basic building blocks, a new mathematical model for the complete DWT-DAPSK system has been proposed and verified analytically.

Chapter 5

Simulation and Analysis

5.1 Introduction

A novel hybrid DWT-OFDM system with DAPSK modulation has been proposed and a mathematical model for the system has been presented in chapter 4. The block diagram was presented in figure 4-4. In this chapter, this proposed system has been simulated using Matlab simulink package and also verified using Matlab programming. The results of the DWT system are compared with those of DCT and DFT OFDM systems using various types of modulation schemes. The performance of the systems is compared in terms of Bit-Error-Ratio (BER), Peak-to-Average-Power-Ratio (PAPR) and Power Spectral Density (PSD).

The parameters used in this simulation are: ring ratio of phase constellation $(a=\mu)=1.4$, number of carriers n=64, symbol length N=64, number of possible amplitude levels Na=4, number of possible phase levels Np=16, and deviation angle $\Delta\varphi = 22.5$ .The power spectral density (PSD) is measured with window type Hann and Buffer size 90. A random binary stream was used for the input data and modulated data were transmitted over AWGN and Rayleigh transmission channels. The results were achieved using an array mapping of 64 subcarriers, a message size of 10, and symbol rate of 1e9 over AWGN transmission channel. Rayleigh channels were considered with a direct path delay vector of [0-2e-3], an average path gain vector of [0-3], and Doppler spectrum types of both flat fading and selective frequency fading. In addition, the number of samples considered for the symbols is 1000. The number of samples was fixed at this value so that the simulation results could be obtained in a reasonable amount of time, because if the number of samples for the sub carriers and symbols were larger, the time for running the simulations will be longer. However, it has been verified that any larger number of samples for both the parameters does not make significant difference to the results.

5.2 Spectrum of the transmitted signals

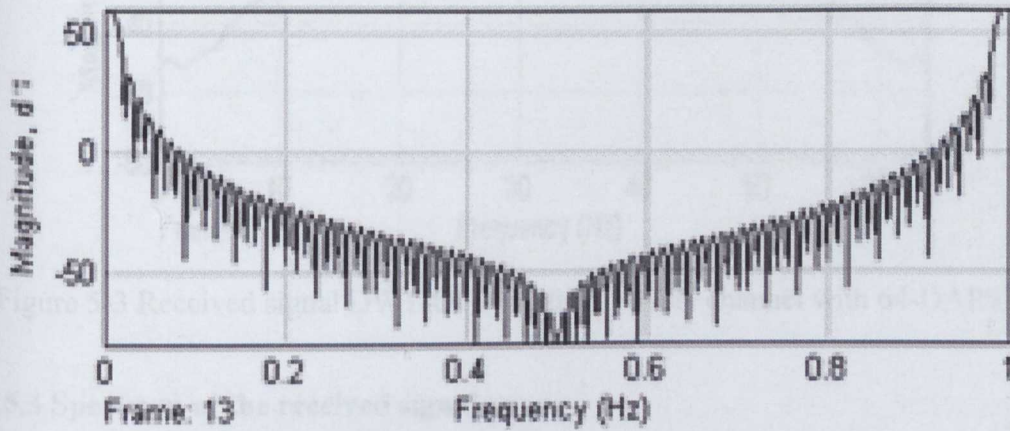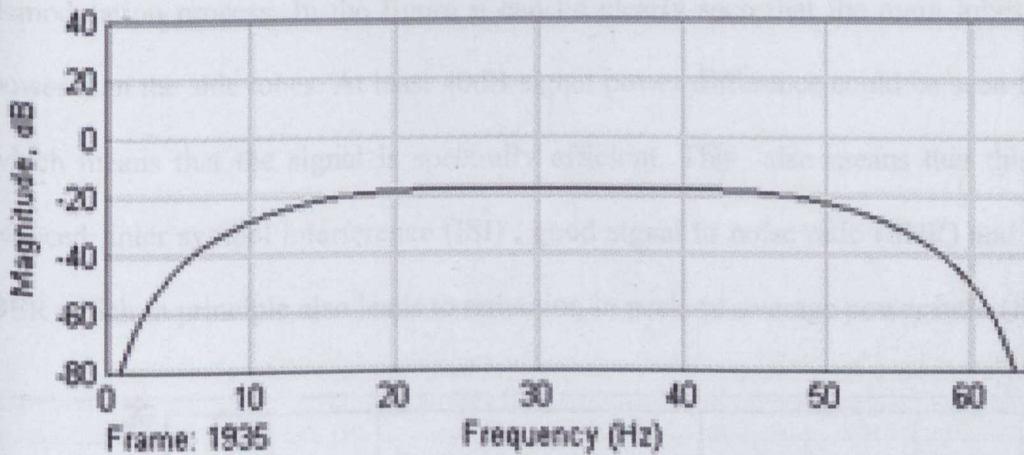Figure 5-1. 64DAPSK modulated signalbefor the wavlet transformation

Figure 5-2.Transmitted signal at the IDWT-OFDM before AWGN channel with 64-DAPSK modulation

Figure 5-1 represents the output at the DAPSK block in figure 4-1. Figure 5-2 shows the output of the transmitter after the IDWT and DAPSK modulator, the signal spectrum covering a wide frequency range. Figure 5-3 shows the effect of noise introduced by the AWGN channel on the signal spectrum as measured at the receiver side of the channel. A reduction in the amplitude, at the two ends of the spectrum can be seen in the figure.
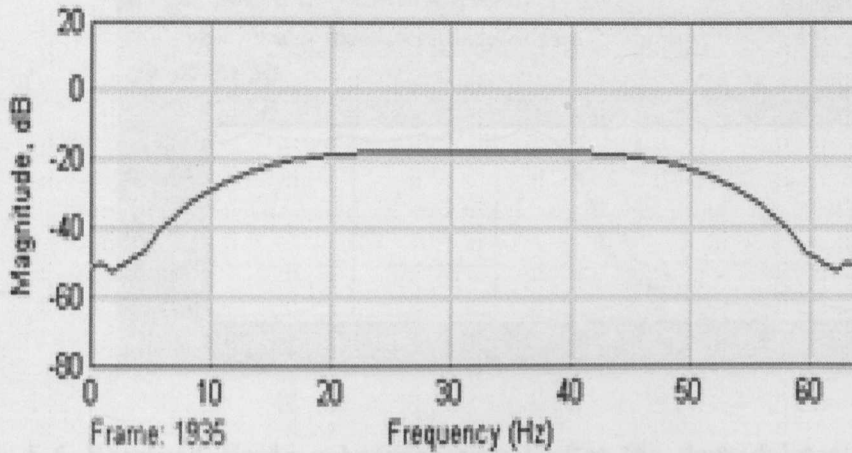
Figure 5-3 Received signal DWT-OFDM after AWGN channel with 64-DAPSK modulation

5.3 Spectrum of the received signal

Figure 5-4 represents the 64-series of DWT data at the receiver end before the demodulation process. In the figure it can be clearly seen that the main lobes have higher power than the side lobes. At least 40dB signal power difference could be seen from fig. 5-4, which means that the signal is spectrally efficient. This also means that this system has reduced inter symbol interference (ISI) , good signal to noise ratio (SNR) and thus reduced BER which in principle also leads to reduction in peak–to-average power ratio (PAPR).
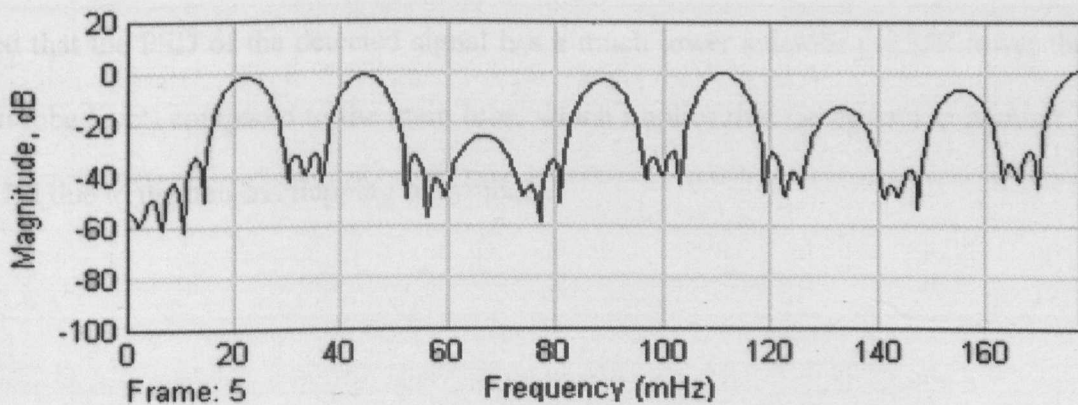
Figure 5-4 Received signal at the output of DWT block in the DWT-OFDM system
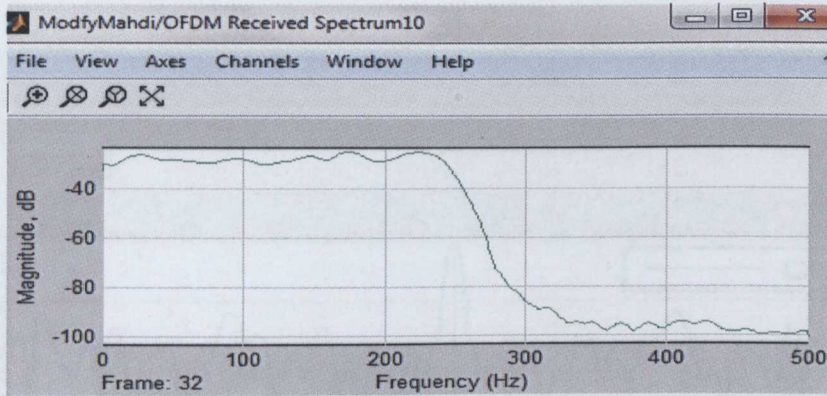
Figure 5-5 Received single subcarrier signal after the demodulator in the DWT-OFDM system

Finally, figure 5-5 shows the output at the receiver end, after the demodulator. This spectrum has good bandwidth efficiency as can be seen from the wide bandwidth of a single subcarrier signal in figure 5-5. However, the information streams are still spectrally efficient with negligible effect due to inter carrier interference (ICI).

5.4 PSD of the transmitted and received random binary streams

Figures 5-6 and 5-7 represent the power spectral density (PSD) of the random binary input stream and the detected signal stream at the receiver, respectively. In this case, it can be noted that the PSD of the detected signal has a much lower sidelobs (~25dB lower than the main lobe level) compared to the main lobe, which implies that the system is immune to ICI and ISI due to the non-overlapping of symbols.
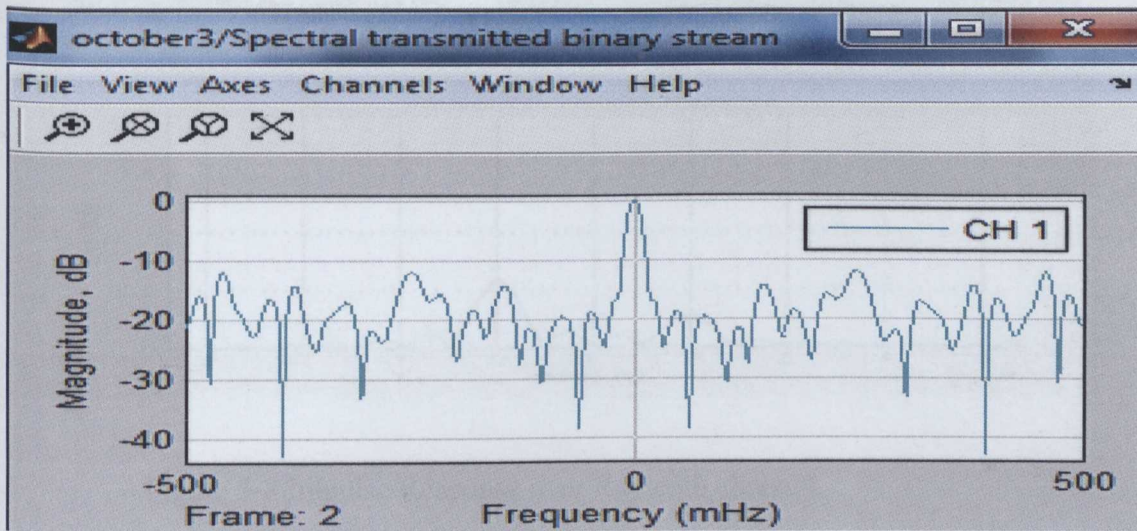
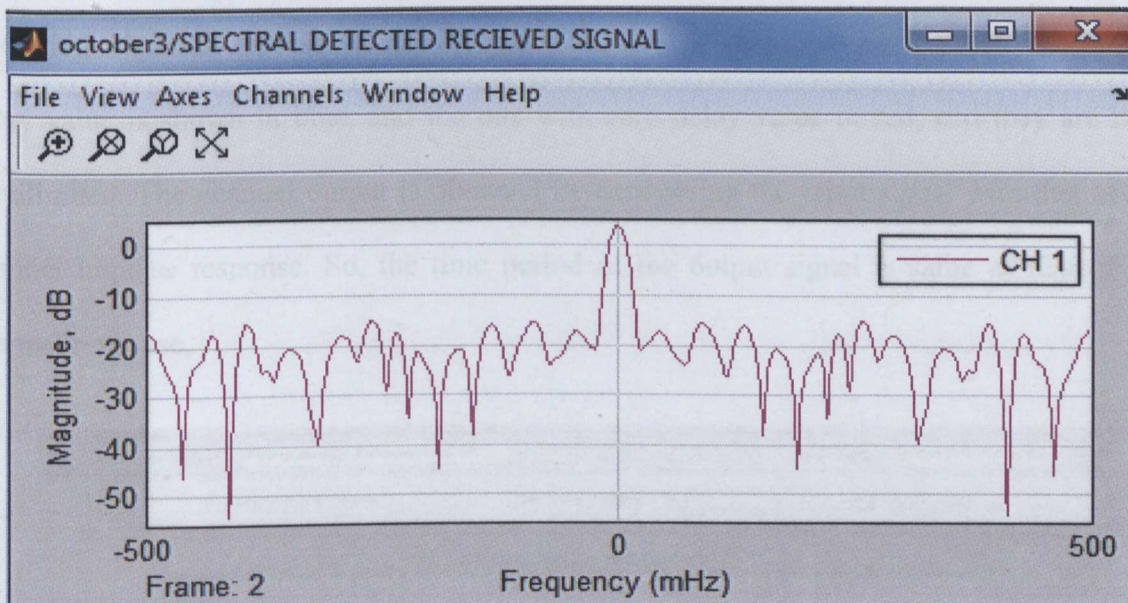Figure 5-6 PSD of the transmitted binary stream

Figure 5-7 PSD of the detected signal

5.5 Performance over the Rayleigh channel

Figures 5-8 and 5-9 represent the impulse response and the frequency response of the modulated signal over a multipath fading Rayleigh channel respectively.
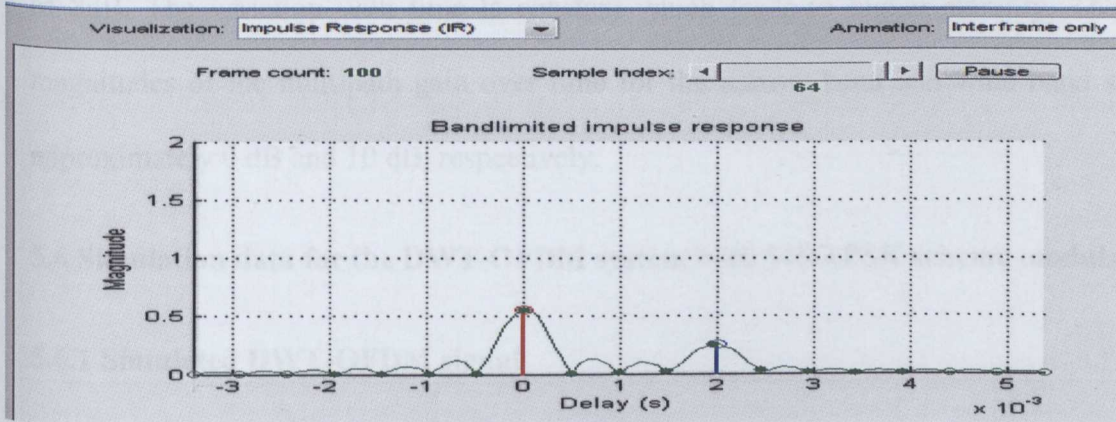
Figure 5-8 Impulse Response over Rayleigh channel

Figure 5-8 shows the magnitudes of two impulse responses of the channel namely, the bandlimited channel response and infinite bandwidth channel response. The infinite bandwidth signal is represented by the green curve. The multipath component with largest delay value is shown in blue, and the one with zero delay value in red, and they are both bandlimited. The channel output is obtained by convolving the input signal with that of the channel impulse response. So, the time period of the output signal is same as that of the channel response.
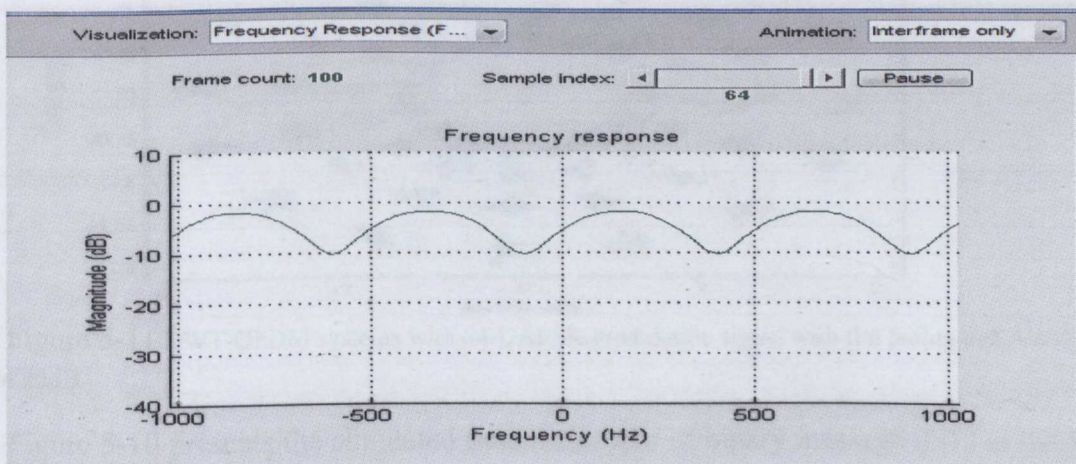

Figure 5-9 Frequency Response over Rayleigh channel

Figure 5-9 shows the frequency response of the transmitted signal over Rayleigh channel; it is represented by a convex sequence of pulses, each with a wide band of 500Hz and a peak

of 8dB. The variation with time is constant which leads to higher stability. The varying

magnitudes of the multipath gain over time for the narrow band and wide band signal are

approximately 0 dB and 10 dB, respectively.

5.6 Simulation data for the DWT-OFDM system with 64DAPSK scheme modulation
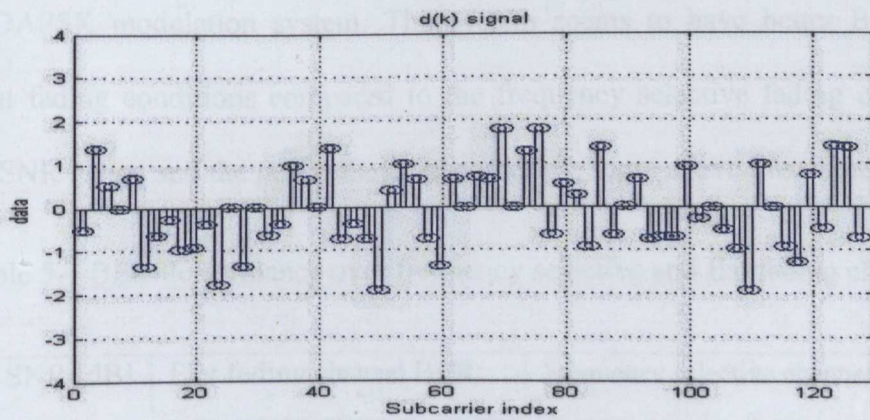
5.6.1 Simulated DWT-OFDM signal

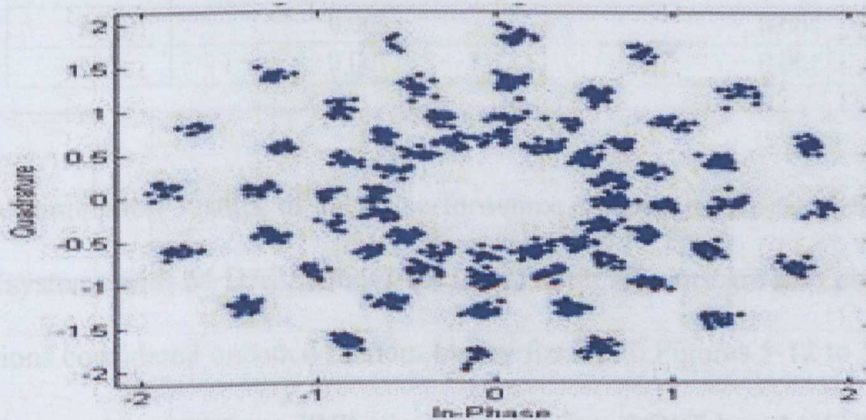Figure 5-10 simulated d (k) signal for DWT

Figure 5-11 DWT-OFDM systems with 64-DAPSK modulation signal with flat fading and AWGN at SNR of 25dB

Figure 5-10 presents the simulated random stream of binary message d (k) at the DWT

transformation block. Fig. 5-11 shows the constellation of the signal through DWT-OFDM

system with 64-DAPSK scheme modulation over flat fading and AWGN channels at SNR of

25dB. In the I-Q coordinate system, this is seen as distributed rings with an amplitude factor a

=1.6, which is the ratio between the current symbol and previous. Here, the distances between symbols are equal, which leads to non-overlapping subcarriers with no ISI. This in turn leads to simple decision criteria at the receiver and thus simplifies the receiver design.

5.6.2 BER and PAPR performance of the received signal

Table 5-1 presents the simulation results of BER values for a range of SNR values under both flat fading and frequency selective fading channel conditions for the DWT-OFDM with 64DAPSK modulation system. The system seems to have better BER performance under flat fading conditions compared to the frequency selective fading channel for up to 26dB of SNR value, and the performance becomes the same above this value.

Table 5-1 BER Performance over frequency selective and flat fading channel

SNR [dB]	Flat fading channel BER	Frequency selective channel BER
5	0.291	0.296
10	0.198	0.204
15	0.084	0.082
20	0.018	0.020
26	0.001	0.004
28	0.001	0.001

The simulation results of these performance characteristics for the DWT and DCT-OFDM systems with 64 DAPSK/64QAM modulation schemes are also presented below. The simulations considered uncoded random binary for input. Figures 5-12 to 5-14b represent the simulation results of BER vs. SNR for DWT, DCT and DFT based OFDM systems with 64 DAPSK over AWGN channel or/and with Rayleigh flat fading or frequency selective fading channels. From these figures it can be noted that the DWT system achieves a BER of 10^{-3} for an SNR value of at least 4dB less than that requiered by DCT and DFT systems under all channel conditions.
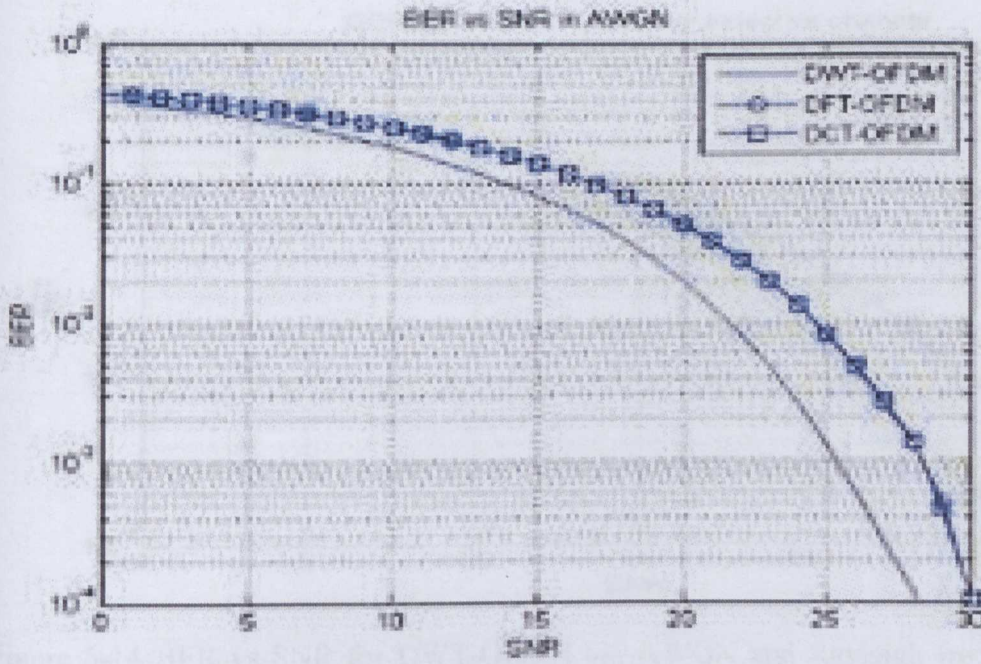
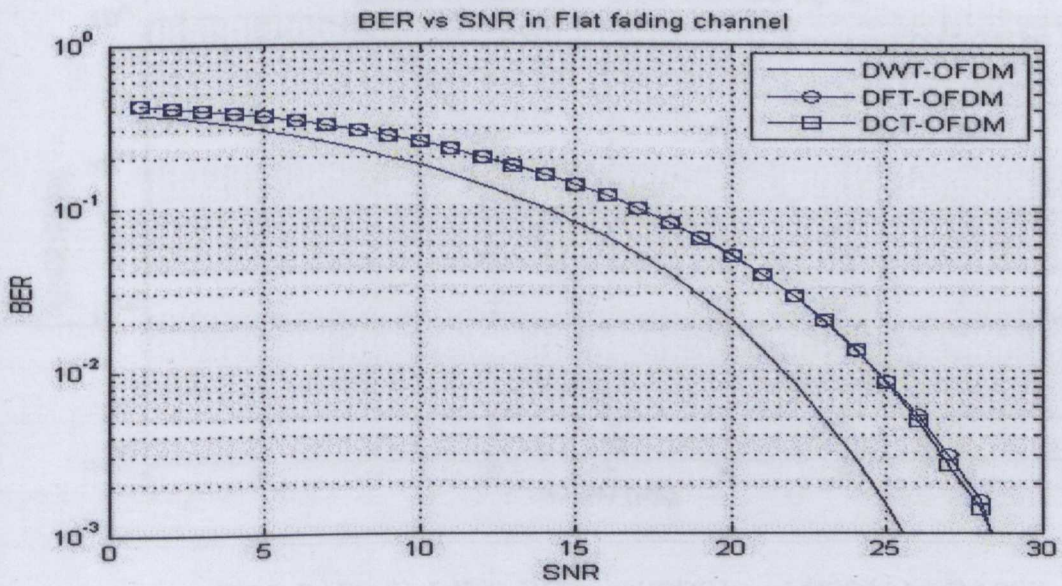Figure 5-12 BER vs SNR for DWT-OFDM via AWG

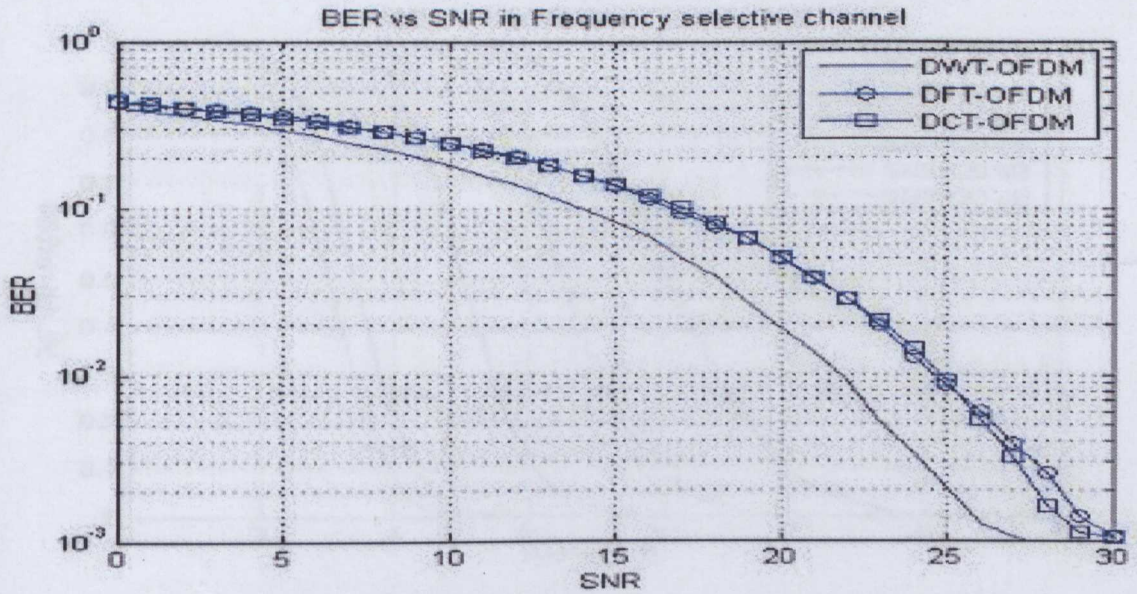Figure 5-13 BER vs SNR for DWT-OFDM via   AWGN and Rayleigh flat fading

Figure 5-14 BER vs SNR for DWT-OFDM via AWGN and Rayleigh frequency selective
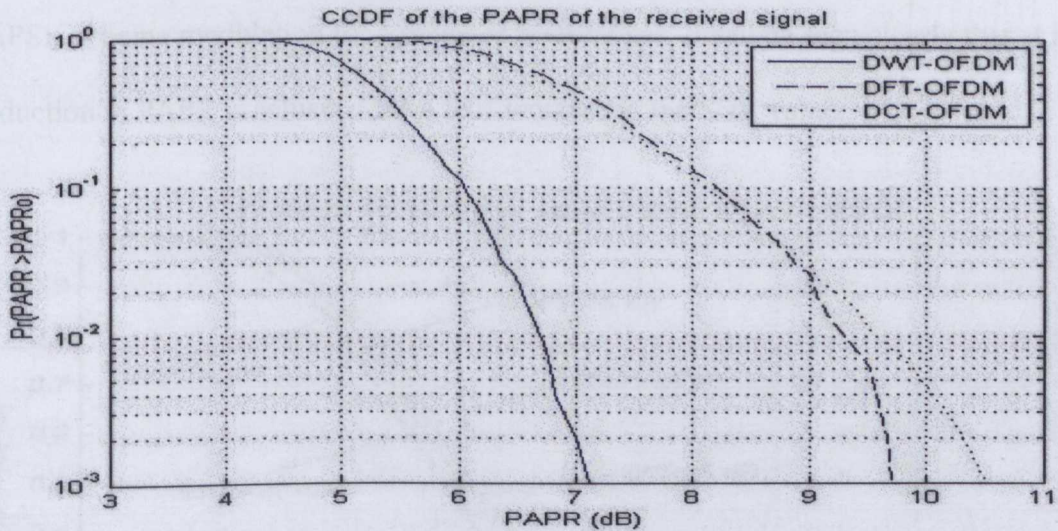
channel

Figure 5-15 PAPR for DWT, DCT, and DFT based OFDM 64-DAPSK

Figure 5.15 illustrates the PAPR characteristics for DWT, DCT, and DFT based OFDM

systems with 64-DAPSK modulation, using cumulative complementary distribution function

(CCDF). From this figure it can be noted that the DWT system shows at least 5 dB reduction

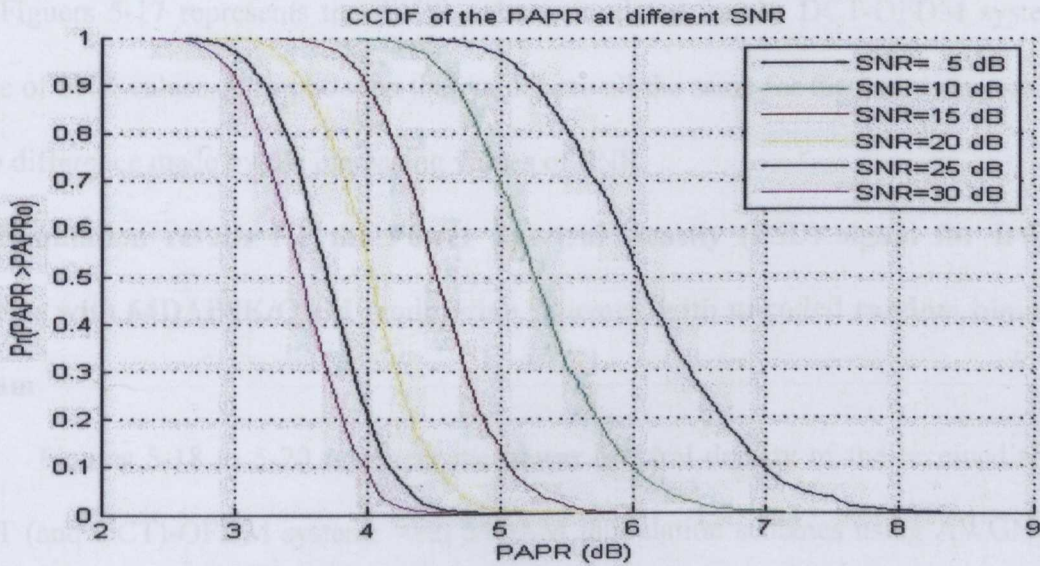in PARP compared to DFT and DCT systems.

Figure 5-16 PAPR for DWT, DCT, and DFT based OFDM systems for a range of SNR values

Figure 5-16 presents the PAPR characteristics for the DWT-OFDM system with 64DAPSK scheme modulation for a range of SNR values. It can be seen clearly that at least 1 dB reduction in PAPR is achieved for a 5dB increase in the SNR value.
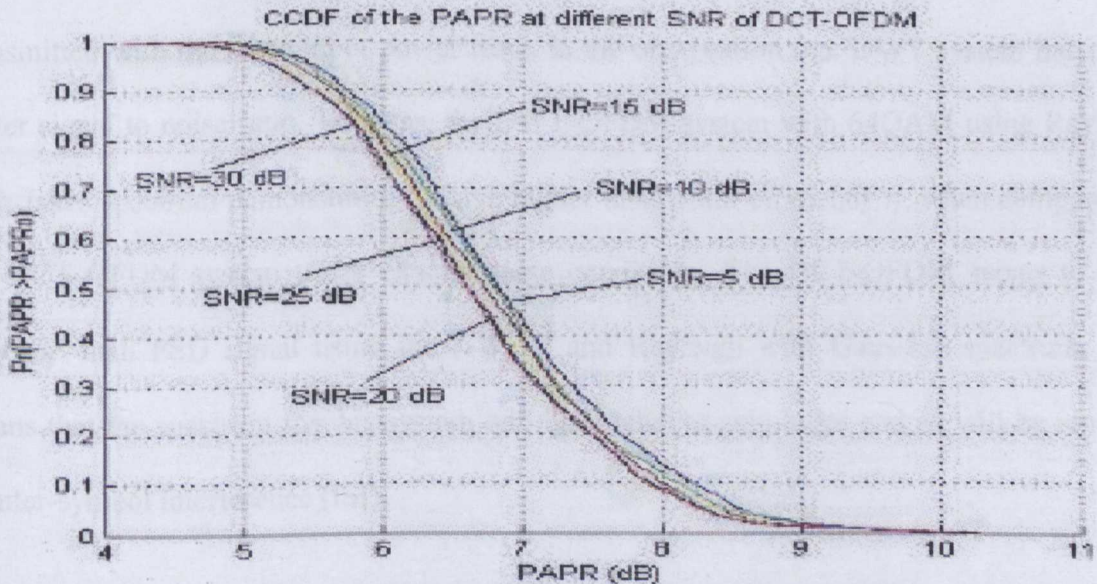

Figure 5-17 PAPR using CCDF for DCT -OFDM with 64-DAPSK for different values of

SNR

Figuers 5-17 represents the PAPR values simulated for the DCT-OFDM system for a range of SNR values. It can be seen that values are all the same for the entire range, and there is no difference made by the increasing values of SNR.

5.7 Simulation results for the Power Spectral Density (PSD) signal for DWT/DCT systems with 64DAPSK/QAM modulation schemes, with uncoded random binary input stream

Figures 5-18 to 5-20 represent the power spectral density of the received signal for DWT (and DCT)-OFDM systems with 64QAM modulation schemes using AWGN channel with Gaussian spectrum and Rayleigh channel with Jakes spectrum. The simulation results indicate that the DWT-OFDM with 64QAM scheme has higher signal power than the DCT based OFDM system using the same modulation scheme. It is also clearly seen that the power spectral density (PSD) for DWT-OFDM is approximately 20-40dB/rad/sample better than the DCT-OFDM system when using the 64QAM scheme modulation via AWGN transmission channel type. This huge difference in PSD between the received signals which were transmitted with the same input power leads to the observation that DWT system has much better signal to noise ratio. Whereas, the DWT-OFDM system with 64QAM using Rayleigh with Jakes spectrum demonstrates to have higher bandwidth efficiency η when compared to the DCT OFDM system under exactly same conditions. The DCT-OFDM seems to have better η than PSD signal using the AWGN and Rayleigh with Gaussian spectrum. This means that the spectrum for this system will have smaller side-lobes and so will be immune to inter-symbol interference (ISI).

Periodogram Power Spectral Density Estimate DWT/DCT with 64QAM with channel AWGN

Figure 5-18 Power spectral densities for DWT and DCT systems with 64QAM modulation schemes over AWGN channel

Periodogram Power Spectral Density Estimate DWT/DCT with 64QAM (Rayliegh,GAUSSIAN)
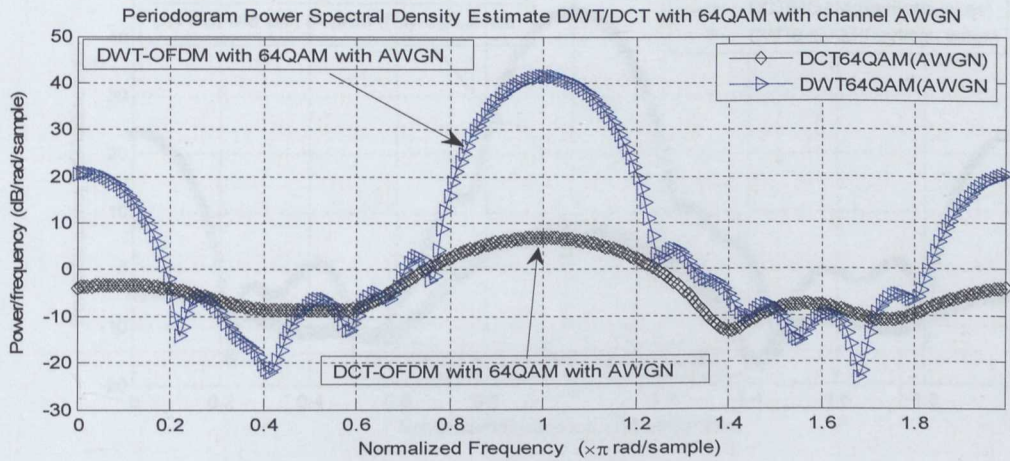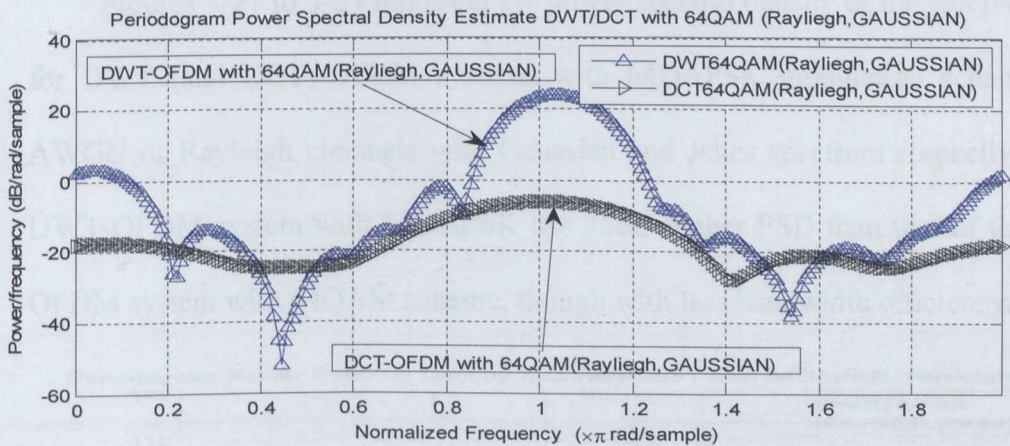

Figure 5-19 Power spectral densities for DWT and DCT systems with 64QAM modulation schemes over Rayleigh (GAUSSIAN) channel
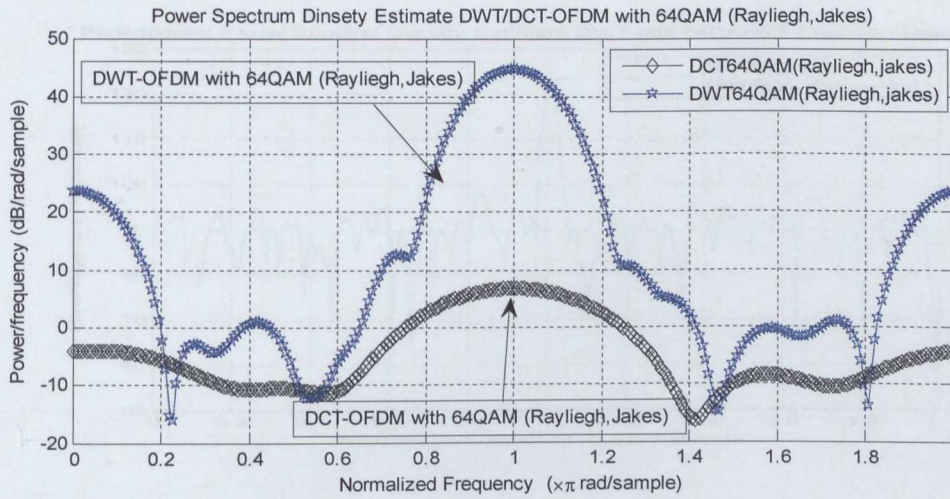
Figure 5-20 Power spectral densities for DWT and DCT systems with 64QAM modulation schemes over Rayleigh (Jakes) channel

Figures 5-21 to 5-23 represent the power spectral density of the received signal for DWT (and DCT)-OFDM systems with 64DAPSK modulation scheme using AWGN or Rayleigh channels with Gaussian and Jakes spectrum respectively. The DWT-OFDM system with 64DAPSK has 75dB higher PSD than that of the DWT-OFDM system with 64QAM scheme, though with less bandwidth efficiencyη.
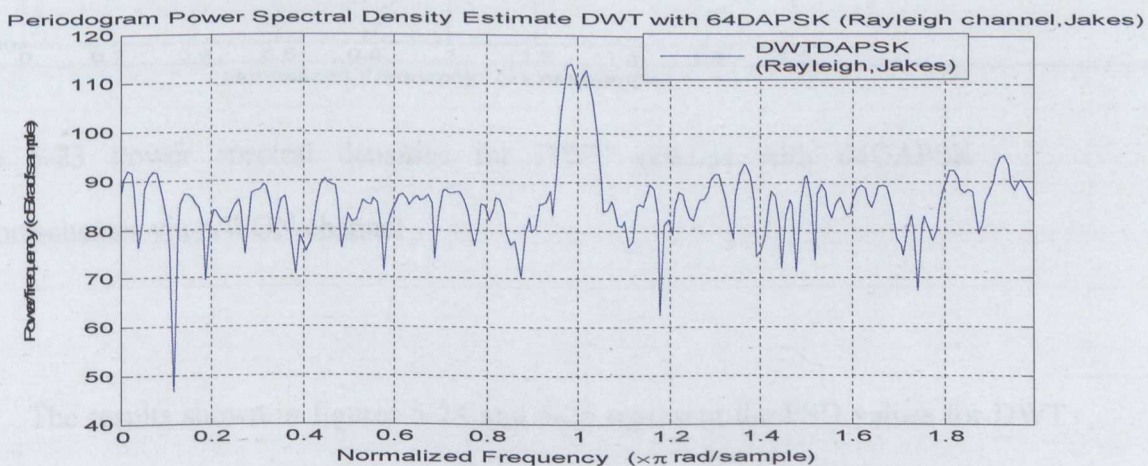
Figure 5-21 Power spectral densities for DWT system with 64DAPSK modulation over Rayleigh (Jakes) channel
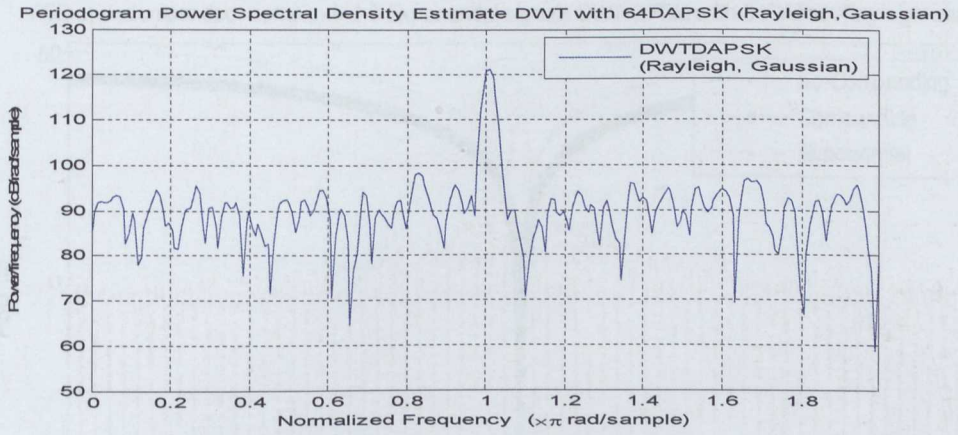
Figure 5-22 Power spectral densities for DWT system with 64DAPSK modulation over Rayleigh (Gaussian) channel
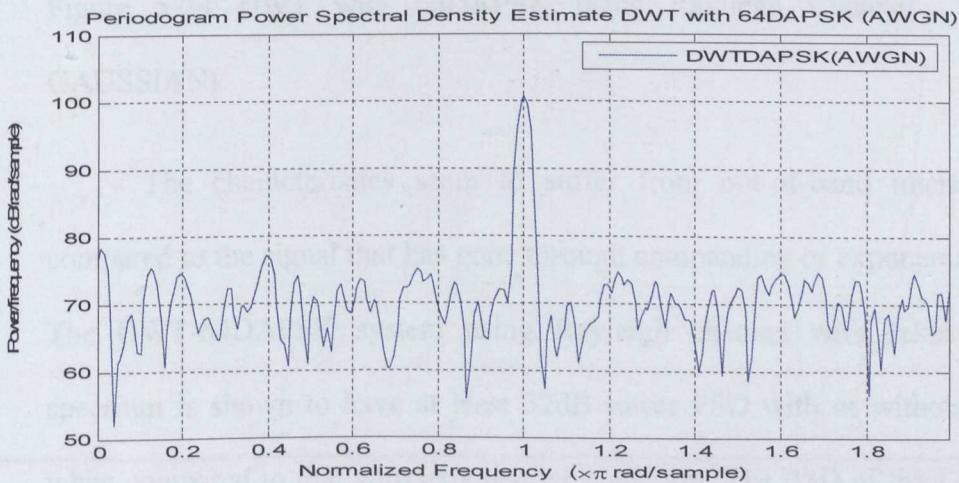
Figure 5-23 Power spectral densities for DWT systems with 64DAPSK modulation schemes via AWGN channel

The results shown in figures 5-24 and 5-25 represent the PSD values for DWT system with various signal manipulations to reduce PAPR. Figure 5-24 represents the DWT-OFDM system with 64DAPSK scheme using Rayleigh Channel for the signal with exponential processing, and with and without Companding.

PSD of nocompanded, companded & Exponantial signals DWT-OFDM with 64DAPSK Rayleigh channel
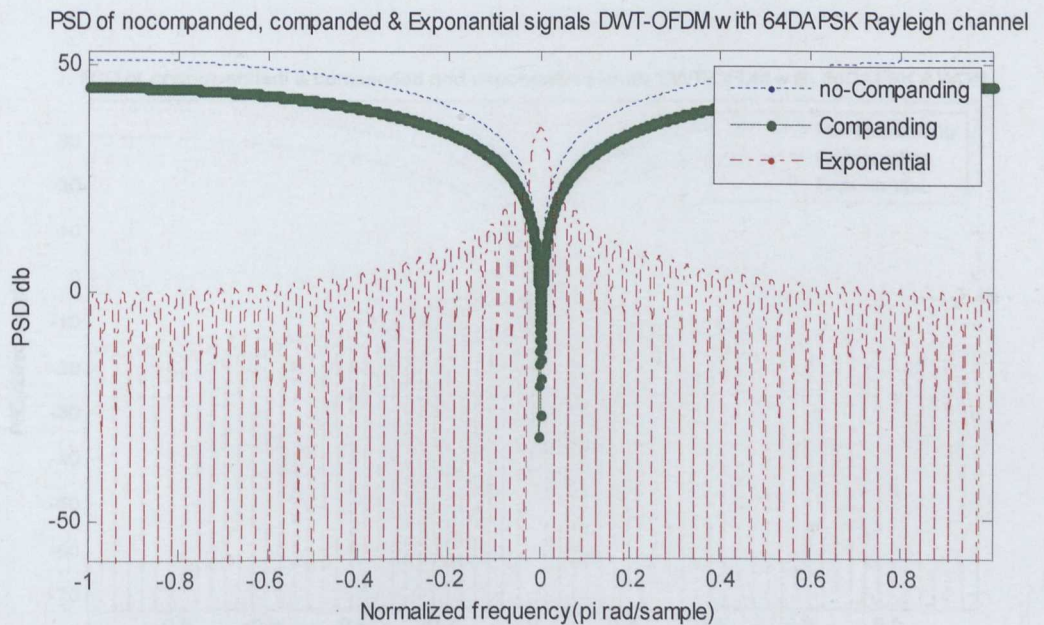
Figure 5-24 DWT with 64DAPSK using Rayliegh Channel (JAKES and GAUSSIAN)

The characteristics seem to suffer from out-of-band interference (OBI) compared to the signal that has gone through companding or exponential transforms. The DWT-64DAPSK system using Rayleigh channel with Jakes or Gaussian spectrum is shown to have at least 32dB lower PSD with or without companding when compared to that with exponential transform. The PSD of the DWT and DCT OFDM systems were also simulated with and without μ-law companding, and exponential transforms.

when compared to that with or without companding.

PSD of nocompanded l & companded and exponantial signals DWT-OFDM w ith 64DAPSK AWGN
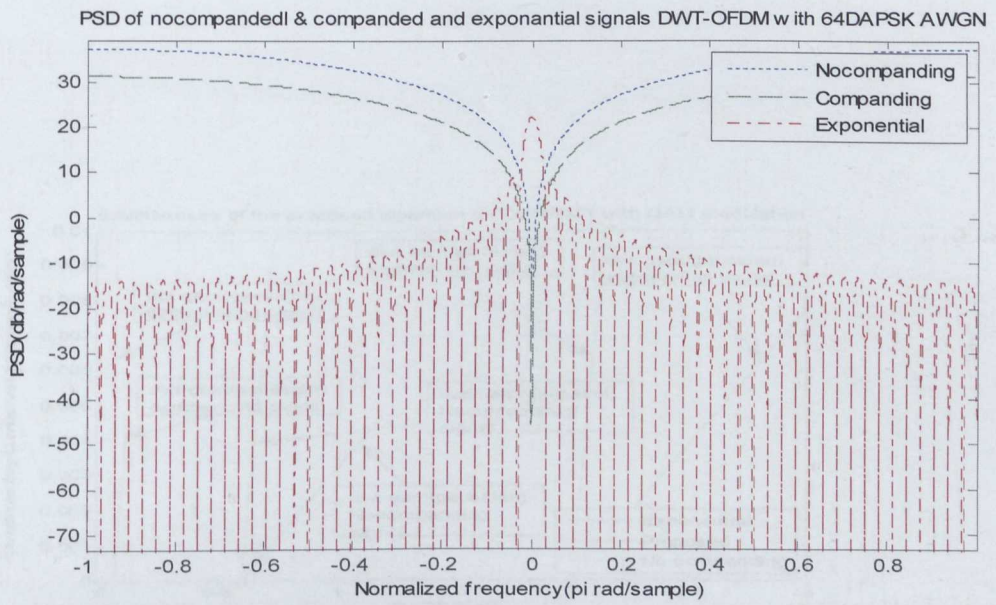
Figure 5-25 PSD for DWT with 64DPASK over AWGN channel

Figures 5.25 and 5-26 represents the DCT-OFDM system with 64DAPSK and

64QAM schemes respectively over Rayleigh Channel and AWGN channels. The

DCT-64QAM is shown to have at least 15dB lower PSD with exponential transform

PSD of nocompanded, companded and exponatial signals DCT-OFDM w ith 64QAM
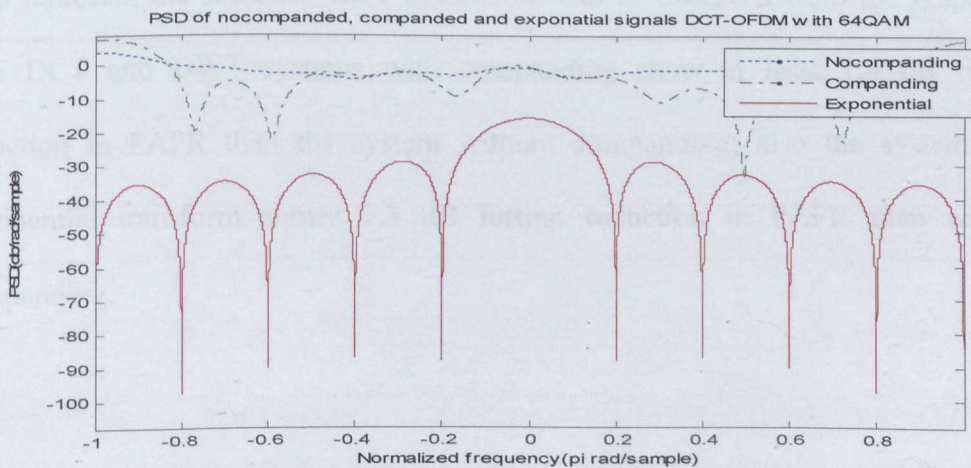
Figure 5-26 PSD for DCT with QAM Rayleigh's channel(GAUSSIAN and JAKES)

and AWGN

when compared to that with or without companding.
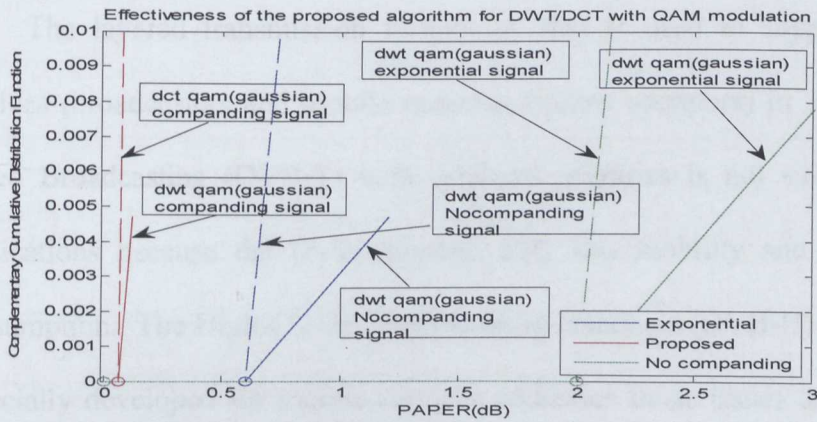
Fig.5-27 CCDF for DWT/DCT with QAM for no-companding,

companding and Exponential transformations

In figure 5-27, continuous lines represent the complementary cumulative distribution (CCDF) vs. PAPR performance for DWT systems, whereas the dashed lines represent the same for DCT systems. It can be observed from the graph that both DCT and DWT systems with companding show at least 1.9 dB further reduction in PAPR than the system without companding; also the system with exponential transform shows 1.3 dB further reduction in PAPR than without companding.

Chapter 6

Performance evaluation of DWT-DAPSK for DVB-T application

6.1 Introduction

The layered transmission technology that is used to support the multiple services (broadcasters and mobile communications operators) in Terrestrial Digital Video Broadcasting (DVB-T) with different priorities is not suitable for mobile applications because the DVB supports only low mobility and has high power consumption. The Digital Video Broadcasting-Handheld (DVB-H) system, which is especially developed for mobile services addresses those issues and provides high speed.

Recent research investigations identify the OFDM to be most suitable for the upcoming DVB-H system and wireless communication systems due to its excellent robustness against impairments due to frequency-selective fading channels (Ladebusch and Liss, 2006).

Recently, the OFDM systems have attracted considerable research attention as a suitable candidate for the next-generation digital television terrestrial broadcasting systems (DTTB) and the 4th generation mobile receivers. The OFDM system has been successfully implemented by (Yang and Wang, 2012), (Martoyo and Jondral, 2002) and (L. Dai et al., 2012) in the wireless broadcasting applications such as Digital Video Broadcasting (DVB) and Digital Audio Broadcasting (DAB). The above mentioned systems have demonstrated data rates in the range of 40 Mbits/s and the DTTB system could deliver 40 GB of contents to unlimited number of local servers. In (Ladebusch and Liss, 2006), the ETSI-BRAN system employs DVB-T transmission technique for HIPERLAN 2 (high performance local area networks). A

DVB-T system supports networks covering portable mobile receivers in buses, cars, and indoor receivers (Ladebusch and Liss, 2006).The digital dividend has been designated as a matter of controversy between broadcasters and mobile communications operators which occupy part of it as desired (Kalogirou et al., 2009). Therefore, future mobile communication systems with data rates far beyond that is employed in Universal Mobile Telecommunication system (UMTS) can be realised using OFDM for the transmission technique.

6.2 Simulation results of DWT/DCT with 64DAPSK/QAM in DVB-T systems

When the input data of the DWT-OFDM system block (presented in chapter 4) is changed to that of DVB-T, created by using a trellis code with length = 256 and Fs=1000, the bandwidth efficiency and PAPR of the system has improved. These simulation results are presented in figures 6-1 to 6-4.
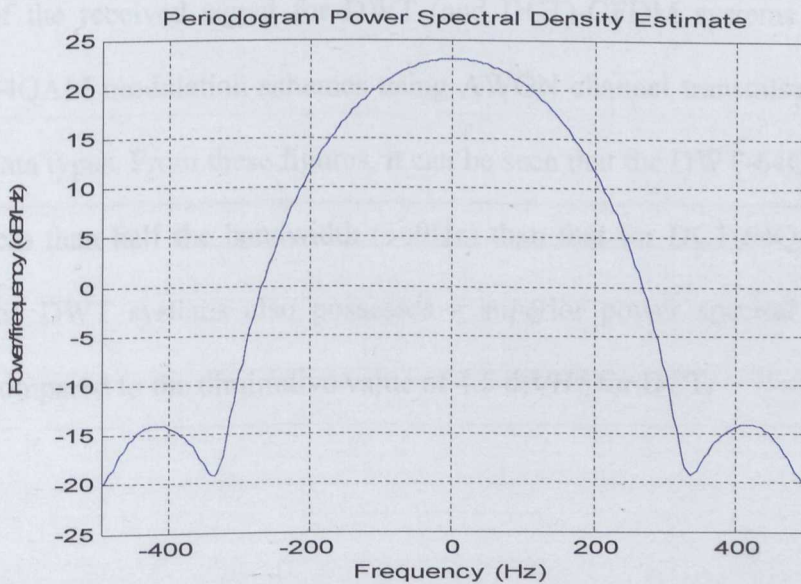
Figure 6-1 Power spectral density of DWT system with 64QAM modulation over AWGN channel
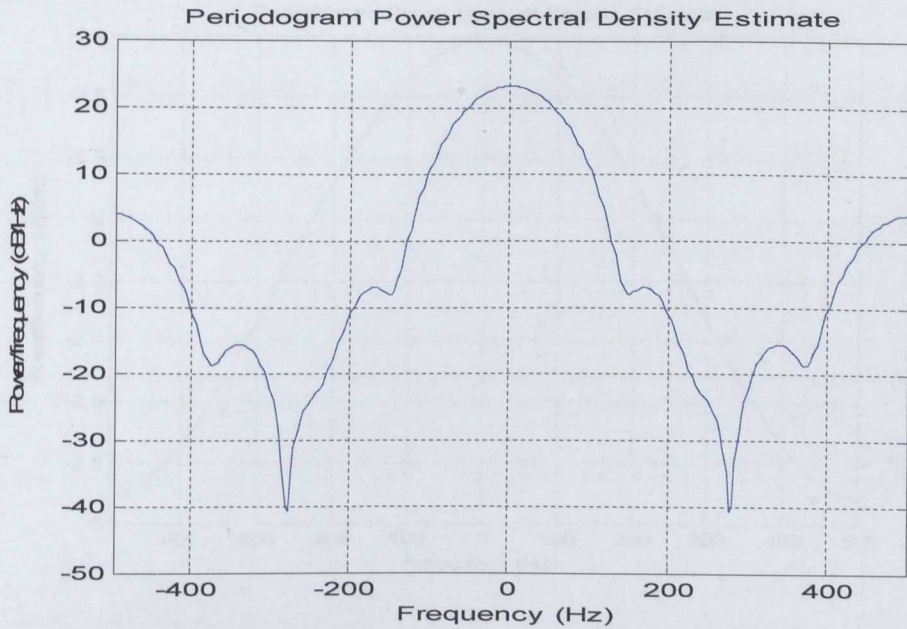
Figure 6-2 Power spectral density of the DCT system with 64QAM modulation over AWGN channel

Figures 6-1 to 6-4, depict the simulation results for the power spectral density of the received signal for DWT (and DCT)-OFDM systems with 64DAPSK and 64QAM modulation schemes using AWGN channel transmission for DVB-T input data types. From these figures, it can be seen that the DWT-64QAM system occupies less than half the bandwidth (369Hz) than that for DCT-64QAM system (800Hz); the DWT systems also possesses a superior power spectral density of 65dB/Hz compared to the diminutive value of 4.5 dB/Hz for DCT.

Periodogram Power Spectral Density Estimate
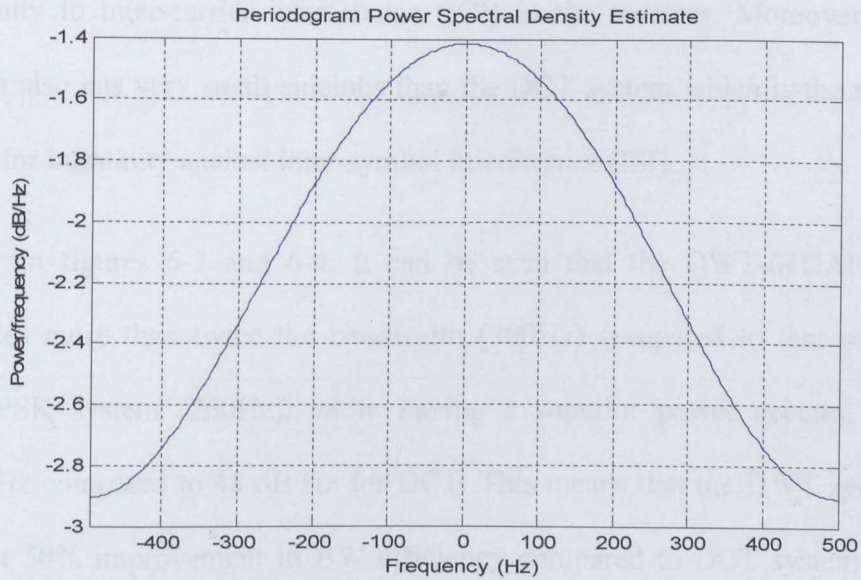
Figure 6-3 Power spectral density for DWT system with 64DAPSK modulation via AWGN channel using trellis code

Periodogram Power Spectral Density Estimate
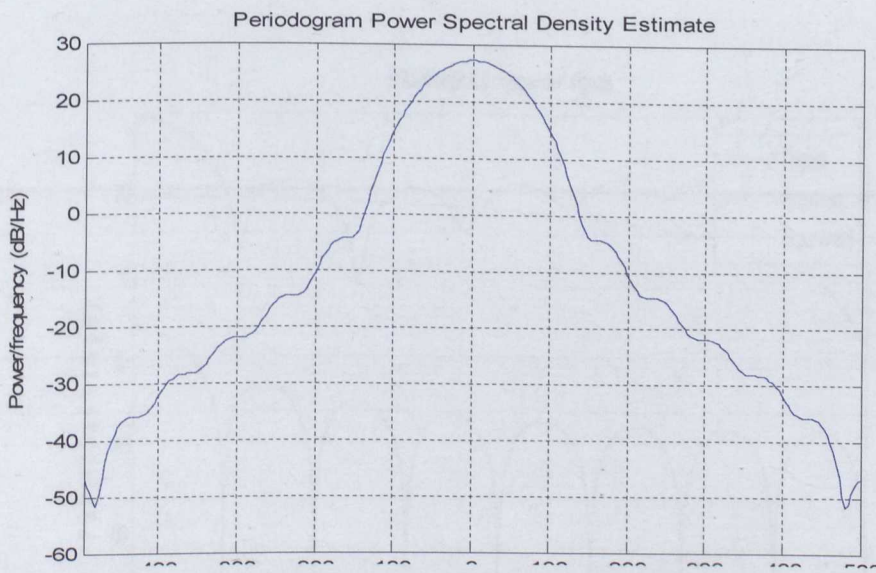
Figure 6-4 Power spectral density for DCT system with 64DAPSK modulation via AWGN channel using trellis code

It also can be seen from these figures that the DWT system possesses at least 7 times better BW efficiency than the DCT system. This high BW efficiency ensures

immunity to inter-carrier interference (ICI) in the receiver. Moreover, the DWT system also has very small sidelobs than the DCT system which is the representing factor for immunity against inter-symbol interference (ISI).

From figures 6-3 and 6-4, it can be seen that the DWT-64DAPSK system occupies more than twice the bandwidth (700Hz) compared to that of the DCT-64DAPSK system (260Hz), while having a superior power spectral density of 88dB/Hz compared to 48 dB/Hz for DCT. This means that the DWT system shows at least 50% improvement in BW efficiency compared to DCT system. This high BW efficiency ensures immunity against inter carrier interference (ICI) in the receiver. Moreover the DWT system has 50% less power in the sidelobs compared to DCT system, which results in improved immunity against inter symbol interference (ISI) than the DCT system.
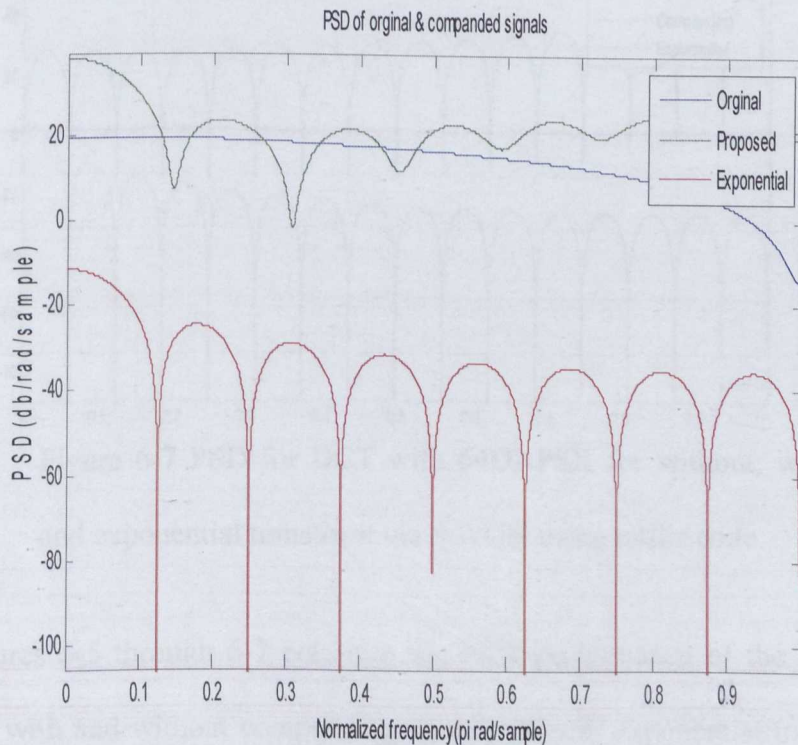
Figure 6-5 PSD for DWT with QAM for without, with companding and exponential

lower PSD compared with the system having with no companding. It also has 25 dB lower PSD with the system having companding. The overall performance of the DCT with QAM modulation is not as good as that of the DWT system. It shows a means 5 dB difference from both non-companding & companding processes. In fig.6-7 this shows that DCT with DAPSK performance is similar same, in that DCT-DAPSK has lower (10 dB) PSD compared to non-companding and non-companding processes.

Figure 6-6 PSD for DCT with QAM for without, with companding
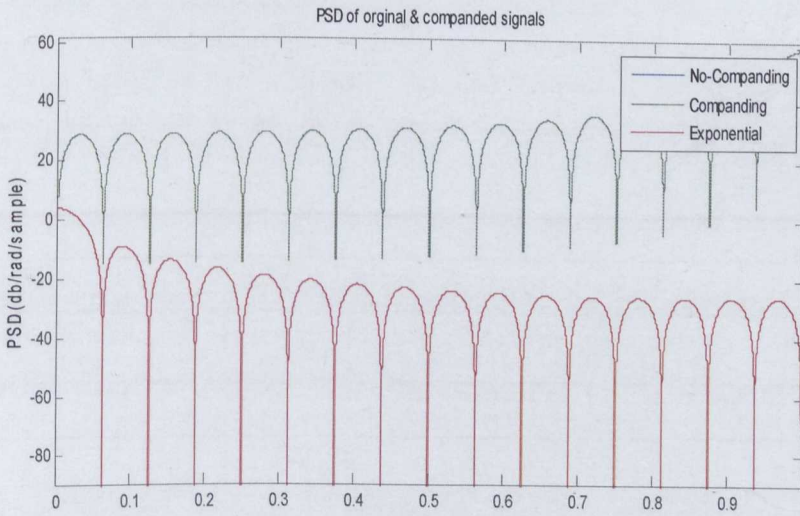
Figure 6-7 PSD for DCT with 64DAPSK for without, with companding

and exponential transform via AWGN using trellis code

Figures 6-5 through 6-7 compare the PSD performance of the DWT & DCT

systems with and without companding to that of with exponential transform. From

these figures, it is seen that DWT-QAM system with exponential transform has 35dB

lower PSD compared with the same system with no companding. It also has 25 dB lower PSD with the system having companding. However, the performance of the DCT with QAM modulation is not as good as that of the DWT system. It shows a meagre 5 dB difference from both non-companding & companding processes. In fig.6-7, it is shown that DCT with DAPSK performance is slighter better, in that DCT-DAPSK has lower (10 dB) PSD compared to companding and non-companding processes.

Chapter 7

Conclusion and suggestions for future expansion

In this research work, a novel hybrid DWT-OFDM system with 64DAPSK modulation scheme has been proposed to achieve reduced peak-to-average power ratio (PAPR) for high speed mobile network applications. A mathematical model for the whole system has been derived based on the existing mathematical representations for individual component blocks. The functional blocks have been simulated using Matlab Simulink software package and the results were also verified using Matlab programming. The simulation results demonstrate that the proposed system is not only spectrally more efficient, but also shows significant improvement in BER and PAPR performance compared to the traditional DCT and DFT systems under the same simulation conditions.

From the simulation results, the proposed DWT-OFDM system using 64DAPSK modulation scheme is demonstrated to have at least 20 to 40dB/rad/sample higher spectral density (PSD) in the received signal compared to that of the DCT-OFDM under the same simulation conditions. This leads to the observation that the DWT-OFDM system possesses much better signal-to-noise ratio (SNR) than the DCT-OFDM systems.

Moreover, the DWT-OFDM system with 64QAM using Rayleigh with Jakes spectrum demonstrates to have higher bandwidth efficiency η when compared to the DCT OFDM system under exactly the same conditions. However, the DCT-OFDM seems to have better η than PSD signal using the AWGN and Rayleigh with Gaussian spectrum. This means that the spectrum for this system will have smaller side-lobes and so will be immune to inter-symbol interference (ISI). From the

analysis carried out, it can be noted that the DWT system achieves a BER of 10^{-3} for an SNR value of at least 4dB less than that requiered by DCT and DFT systems for all different channel conditions.

Most importantly, the proposed DWT-DAPSK system was demonstrated to achieve at least 3 to 7 dB reduction in PAPR compared to the DCT and DFT systems respectively. Also, adding further signal processing such as companding to the system has been demonstrated to reduce the PAPR further (~1.9dB) compared to the systems not employing companding. Systems using exponential transform achieved 1.3 dB less PAPR than that without any transform. These performance figures lead us to believe that the proposed combination of DWT-DAPSK system with companding or exponential transforms should be best suited for the next generation mobile communication networks. In fact such systems with reduced PAPR have been demonstrated to be very suitable for the terrestrial-digital-video-broadcasting (DVB-T) systems. Also in this research, the BW efficiency of the DWT-OFDM system with both 64QAM and 64DAPSK modulation schemes via AWGN transmission channel has been shown to be better than the DCT-OFDM system under similar conditions. The DWT system with QAM shows 7 times better BW efficiency than the DCT with QAM modulation. The DWT with DAPSK modulation has shown 100% improvement in BW efficiency than the DCT system with DAPSK. The better BW efficiency possessed by the DWT with DAPSK is an indicator of the system's immunity to inter-carrier interference (ICI) which in turn guarantees high bitrate, high quality data transmission. The DWT system also displays minimal side-lobes which contribute to its immunity to inter-symbol interference (ISI).

The proposed combination of DWT-DAPSK system with companding or exponential transforms should be best suited for the next generation mobile communication networks.

The model proposed in this research deserves further study. It would be useful if simulations could be carried out to verify the suitability of the proposed system for the 4th generation mobile networks. This work can also be extended to include cases where certain quality of services (QoS) will be required; such as lower transmission power (decreased PAPR), high spectral efficiency and better resilience to fading, optimum BER etc.

References

ABDULLAH, K. & HUSSAIN, Z. M. Performance of Fourier-based and wavelet-based OFDM for DVB-T systems. Telecommunication Networks and Applications Conference, 2007. ATNAC 2007. Australasian, 2-5 Dec. 2007 2007. 475-479.

ABDULLAH, K., HUSSAIN, Z. M. & Studies on DWT-OFDM and FFT-OFDM Systems, . international conference on communication, computer and power(ICCCP'09), 2009 Muscat.

AHMED, N. 2000. *Joint detection strategies for orthogonal frequency division multiplexing.* Master degree, Houston, Texas.

ARMSTRONG, J. 1999. Analysis of new and existing methods of reducing intercarrier interference due to carrier frequency offset in OFDM. *Communications, IEEE Transactions on,* 47, 365-369.

BAXLEY, R. J. & ZHOU, G. T. Assessing peak-to-average power ratios for communications applications. Military Communications Conference, 2004. MILCOM 2004. 2004 IEEE, 31 Oct.-3 Nov. 2004 2004. 181-185 Vol. 1.

BEAULIEU, N. C. & PENG, T. 2007. On the effects of receiver windowing on OFDM performance in the presence of carrier frequency offset. *Wireless Communications, IEEE Transactions on,* 6, 202-209.

BENVENUTO, N., CORVAYA, R., ERSEGHE, T., LAURENTI, N. & 2007. *Communication systems fundamentals and design methods,* Wiley

BINGHAM, J. A. C. 2000. *VDSL and Multicarrier Modulation West Sussex,* UK, Wiley

BLAHUT, E. R. 1985. *Fast Algorithms for Digital Signal processing,* MA, Addison – Wesley

BURR, A. 2001. *Modulation and Coding for Wireless Communications,,* NJ Prentice Hall

CAMPBELL-KELLY, MARTIN, CROARKEN, MARY, ROBSON, ELEANOR & EDS 2003

The History of Mathematical Tables From Sumer to Spreadsheets (1st ed.), New York USA, Oxford University Press

CHIU, C. T. & LIU, K. J. R. 1992. Real-time parallel and fully pipelined two-dimensional DCT lattice structures with application to HDTV systems. *Circuits and Systems for Video Technology, IEEE Transactions on,* 2, 25-37.

DER-ZHENG, L. & CHE-HO, W. DAPSK-OFDM transmissions for high date-rate digital mobile radio. Circuits and Systems, 2001. ISCAS 2001. The 2001 IEEE International Symposium on, 6-9 May 2001 2001. 417-420 vol. 2.

DILMAGHANI, R. & GHAVAMI, M. 2008. Comparison between wavelet-based and Fourier-based multicarrier UWB systems. *Communications, IET,* 2, 353-358.

DIVSALAR, D. & SIMON, M. K. 1990. Multiple-symbol differential detection of MPSK. *Communications, IEEE Transactions on,* 38, 300-308.

F.H., R., FISHER, LAMP, L. H.-J., MULLER-WEINFURTNER, S. H., HUBER, J. B. & *Coded Modulation for Differential Encoding and Non-Coherent Reception on Fading Channels,,* Germany, University Erlangen – Nurnberg.

, Wellesly-Cambridge Press.

GHARGE, S. & KRISHNAN, S. Simulation and Implementation of Discrete Cosine Transform for MPEG-4. Conference on Computational Intelligence and Multimedia Applications, 2007. International Conference on, 13-15 Dec. 2007 2007. 137-141.

GUO, H. 1998. Mapped Invers Discrete Wavelet Transform for Data Compression. *IEEE*, 1385-1387.

GUPTA, D., VATS, V. B. & GARG, K. K. Performance Analysis of DFT-OFDM, DCT-OFDM, and DWT-OFDM Systems in AWGN Channel. Wireless and Mobile Communications, 2008. ICWMC '08. The Fourth International Conference on, July 27 2008-Aug. 1 2008 2008. 214-216.

HARLOD, P. E. & SAMY, M. A. 2004. *Communication Systems analysis and Design*, Prentice Hall.

HO, E. Y. & YEH, Y. S. 1970. A new approach for evaluating the error probability in the presence of intersymbol interference and additive Gaussian noise. *BCTJ* 49, 2249-2265

HUA, Y. & GANG, W. Computation of the continuous-time PAR of an OFDM signal. Acoustics, Speech, and Signal Processing, 2003. Proceedings. (ICASSP '03). 2003 IEEE International Conference on, 6-10 April 2003 2003. IV-529-31 vol.4.

JR, P. Z. P. & HALL, P. 1987. Digital Communication Systems. Prentice Hall.

JUN, T. & STUBER, G. L. Constant envelope multi-carrier modulation. MILCOM 2002. Proceedings, 7-10 Oct. 2002 2002. 607-611 vol.1.

KAI-MING, L., WEN-BO, W., YUAN-AN, L. , 2005. High Data Ratio OFDM System with Simplified DAPSK Demodulation. *the journal of china universities of posts and telecommunications,* 12.

KHALID, S. & SHAH, S. I. PAPR reduction by using discrete wavelet transform. Emerging Technologies, 2006. ICET '06. International Conference on, 13-14 Nov. 2006 2006. 179-182.

KUMBASAR, V. & KUCUR, O. 2008. Better wavelet packet tree structures for PARP reduction in WOFDM systems. *Digital Signal Processing,* 18, 885-891

LATIF, A. & GOHAR, N. D. BER Performance Evaluation and PSD Analysis of Non-Coherent Hybrid MQAM-LFSK OFDM Transmission System. Emerging Technologies, 2006. ICET '06. International Conference on, 13-14 Nov. 2006 2006. 53-59.

LEE, K. F. & WILLIAMS, D. B. A space-time coded transmitter diversity technique for frequency selective fading channels. Sensor Array and Multichannel Signal Processing Workshop. 2000. Proceedings of the 2000 IEEE, 2000 2000. 149-152.

MAHMOUD, H. P. E. S.-S. A. & *Communication Systems and Design,* Prentice Hall.

MALLAT, S. 1999. *A Wavelet Tour of Signal Processing,* New Yourk Acadmic Press.

MOUNIR, G. & SWAMI, A. 2008. Carrier frequency synchronization for OFDM systems. Leeds: university Leeds

MULLER, S. H. & HUBER, J. B. 1997. OFDM with Reduced Peak-to-Average Power Ratio by Optimum Combination of Partial Transmit Sequences

Electronics Letters, 33, 368-369.

NEE, D. J. V., AND PARASAD, R. 2000. OFDM for Wireless Multimedia Communications. *Artech House.*

PATERSON, K. G. & TAROKH, V. 2000. On the existence and construction of good codes with low peak-to-average power ratios. *Information Theory, IEEE Transactions on,* 46, 1974-1987.

PAULI, M., AND KUCHENBECER, H. P. 1997. Minimization of the Inter modulation Distortion of a Nonlinearly Amplified OFDM signal. *Wireless Personal Communications,* 4, 93-101.

PAULI, M., PKUCHENBECER, H. & 1997. Minimization of the Inter modulation Distortion of a Nonlinearly Amplified OFDM signal. *Wireless Personal Communications,* 4, 93-101

PENG, T. & BEAULIEU, N. C. 2006. A Comparison of DCT-Based OFDM and DFT-Based OFDM in Frequency Offset and Fading Channels. *Communications, IEEE Transactions on,* 54, 2113-2125.

POLLET, T., VAN BLADEL, M. & MOENECLAEY, M. 1995. BER sensitivity of OFDM systems to carrier frequency offset and Wiener phase noise. *Communications, IEEE Transactions on,* 43, 191-193.

RAPP, C. L. 1991a. Effect of HAP- Nonlinearity on a 4- DPSK /OFDM Signal for a Digital Sound Broadcasting system. *proce. of the Second European Conference on Satellite Communication.* Belgium.

RAPP, C. L. 1991b. Effect of HAP- Nonlinearity on a 4- DPSK /OFDM Signal for a Digital Sound Broadcasting system. *proce of the Second European Conference on Satellite Communication.* Belgium

RESINKOFF, H. L., RAYMOND, J. & WELLS, O. 1998. *Wavlet analysis , the scable structure of information,* New York, Springer.

ROHLING, H. & ENGELS, V. Differential amplitude phase shift keying (DAPSK)- a new modulation method for DTVB. Broadcasting Convention, 1995. IBC 95., International, 14-18 Sep 1995 1995. 102-108.

ROHLING, M., MAY, T., BRUNINGHAUS, K. & GRUNHEID, R. 1999. Broadband OFDM radio transmission for multimedia applications. *Proceedings of the IEEE,* 87, 1778-1789.

RYU, H. G., LI, Y. & PARK, J. S. 2005. An Improved ICI Reduction Method in OFDM Communication System. *Broadcasting, IEEE Transactions on,* 51, 395-400.

SANDBERG, S. D. & TZANNES, M. A. 1995. Overlapped discrete multitone modulation for high speed copper wire communications. *Selected Areas in Communications, IEEE Journal on,* 13, 1571-1585.

SCHUCHERT, A., HASHOLZNER, R. & ANTOINE, P. 2001. A novel IQ imbalance compensation scheme for the reception of OFDM signals. *Consumer Electronics, IEEE Transactions on,* 47, 313-318.

SCHWARTZ, M. & 1990. *Information Transmission, Modulation, and Noise, 4/e,,* McGraw

SHUZHENG, X., HUAZHONG, Y. & HUI, W. 2005. Application of DAPSK in HF communications. *Communications Letters, IEEE,* 9, 613-615.

SKALAR, B. 1994. *Digital Communications Fundamental and Application,* Prentice Hall

SKLAR, B. & *Digital Communications Fundamental and Application,* Prentice Hall.

STRANG, G., & NGUYEN, T. 1996. *Wavelets and filter banks,* Massachusetts USA, Wellesley-Cambridge press

TAO, C., FEIFEI, G., NALLANATHAN, A. & TELLAMBURA, C. ML CFO and PO Estimation in DCT OFDM Systems under Non-Circular Transmissions. Communications, 2007. ICC '07. IEEE International Conference on, 24-28 June 2007 2007. 6275-6280.

TAROKH, V. & JAFARKHANI, H. 2000. On the computation and reduction of the peak-to-average power ratio in multicarrier communications. *Communications, IEEE Transactions on,* 48, 37-44.

TECHNOLOGIES, R. 2001. RM wavelet based (WOFDM) PHY proposal for 802.16.3. IEEE 802.16: Inc.

TELLAMBURA, C. 2001. Computation of the continuous-time PAR of an OFDM signal with BPSK subcarriers. *Communications Letters, IEEE,* 5, 185-187.

TOENDER, N., GEORGI, S. & ROHLING, H. Low-Complexity OFDM System with High Mobility Using DAPSK Schemes. Personal, Indoor and Mobile Radio Communications, 2006 IEEE 17th International Symposium on, 11-14 Sept. 2006 2006. 1-5.

VAN NEE, R. D. J. OFDM codes for peak-to-average power reduction and error correction. Global Telecommunications Conference, 1996. GLOBECOM '96. 'Communications: The Key to Global Prosperity, 18-22 Nov 1996 1996. 740-744 vol.1.

WANG, Z. D. & Fast algorithms for the discrete W transform and for the discrete cosine transform. IEEE Trans Acoust Speech Signal Process, 1984. 803-816

WEBER, W., III 1978. Differential Encoding for Multiple Amplitude and Phase Shift Keying Systems. *Communications, IEEE Transactions on,* 26, 385-391.

WEINSTEIN, S. & EBERT, P. 1971. Data Transmission by Frequency-Division Multiplexing Using the Discrete Fourier Transform. *Communication Technology, IEEE Transactions on,* 19, 628-634.

WILKINSON, T. A. & JONES, A. E. Minimisation of the peak to mean envelope power ratio of multicarrier transmission schemes by block coding. Vehicular Technology Conference, 1995 IEEE 45th, 25-28 Jul 1995 1995. 825-829 vol.2.

WONG, K. D., PUN, M. O. & POOR, H. V. 2008. The continuous-time peak-to-average power ratio of OFDM signals using complex modulation schemes. *Communications, IEEE Transactions on,* 56, 1390-1393.

XIAO, H., JIANHUA, L., JUNLI, Z. & JUN, G. Piecewise-scales transform for the reduction of PAPR of OFDM signals. Global Telecommunications Conference, 2002. GLOBECOM '02. IEEE, 17-21 Nov. 2002 2002. 564-568 vol.1.

XIAOYI, T., ALOUINI, M. S. & GOLDSMITH, A. Effect of channel estimation error on M-QAM BER performance in Rayleigh fading. Vehicular Technology Conference, 1999 IEEE 49th, Jul 1999 1999. 1111-1115 vol.2.

YAO, M., ZHANG, Q. T., SCHOBER, R. & PASUPATHY, S. 2005. Diversity reception of DAPSK over generalized fading channels. *Wireless Communications, IEEE Transactions on,* 4, 1834-1846.

ZHANG, H., YAUN, D. & PAETZOLD, M. 2007. Novel study on PAPRs reduction in wavelet – based multicarrier modulation systems. *Digital Signal Process,* 17, 272-279.

ZIMER, R. E., TRANTER, W. H. & 1990. *Principles of communications system modulation and noise*, WILEY.

Appendix A

Matlab code written by the candidate for simulating the mathematical model

```
nsamp=1;

snr = EbNo + 10*log10 (k) - 10*log(nsamp);

Snoisy = awgn (P,snr,'measured');

%Create a fast fading channel

h = rayleighchan (1/9600, 100);

h.DopplerSpectrum = doppler.gaussian (0.3)

h.StoreHistory = 1;        %Allow states to be stored

FadeSig = filter (h,P );%Process samples through channel

plot(h);                        %open channel visualization

%%Received Signal

Snoisy = awgn (fadeSig,snr,'measured');

Prx =Snoisy;

% Create options object and set properties

scatterplot (Snoisy);

hp = spectrum.periodogram('hann');

% Create periodgram

% Create options object and set properties

hpopts = psdopts (hp,Snoisy);

hpsd = psd(hp,Snoisy,hpopts);

figure(4)

plot(hpsd);

[H,W]=freqz(Snoisy,1,128);     %compute frequency response

mag=20*log10(abs(H));

phase=angle(H)*180/pi;         %phase angle in degrees

figure(5),clf

subplot(2,1,1),plot(W/(2*pi),mag)

title('Magnitude response of recieved DWT-OFDM')

xlabel ('Digital frequency in Hz'),ylabel ('Magnitude in dB')
```

```matlab
subplot(2,1,2),plot(W/(2*pi),phase)

title('phase response of recieved)')

xlabel('Digital frequency '),ylabel('Phase in Degrees')

title('phase response of recieved DWT-OFDM)')

Xlabel ('Digital frequency '),ylabel('Phase in Degrees')

nSamp = 8;

u1 =Snoisy;

u=reshape (u1.',1,numel(u1));

[ca] =dwt(u,'haar');

%create demodulate

hDemod = modem.qamdemod (hMod);

xrec=demodulate (hDemod,ca);

u2=xrec;

hp = spectrum.periodogram('hann');

% Create periodgram

% Create options object and set properties

hpopts = psdopts(hp,xrec);

hpsd = psd(hp,xrec,hpopts);

figure(6)

plot(hpsd);

[H,W]=freqz(xrec,1,128);    %compute frequency response

mag=20*log10(abs(H));

phase=angle(H)*180/pi;       %phase angle in degrees

figure(7),clf

subplot(2,1,1),plot(W/(2*pi),mag)

title('Magnitude response of DETECT SIGNAL')

xlabel('Digital frequency in Hz'),ylabel ('Magnitude in dB')

subplot (2,1,2),plot(W/(2*pi),phase)

title('phase response of DETECT SIGNAL)')

xlabel('Digital frequency '),ylabel('Phase in Degrees')
```

```
%air.m

in=8;

[a]=airy(in);

L=length(in);

for i=1:L;

    a(i)=cos((1/3)*(i^3)+(in(i)*i))/L;

end

%comp decomp.m

x=-0.5:0.1:0.5;

x=x(x~=0);

alp=[5 7.5 ];

figure(12),clf

for k=1:length(alp)

    A1=airy(alp(k)*abs(x));

    A0=airy(0);

    dem=(A0-A1).^2;

    beta=sqrt((x.*x)/dem);

    fx=beta.*sign(x).*(A0-A1);

    xlr={'o--','ro--','ko--'};

    figure(12),clf

    subplot(2,1,1);

    plot(x,fx,xlr{k});

    hold on;

end

legend('alp=5','alp=7.5','alp=12.5',4);

title('Companding profile of the proposed algorithm');

xlabel('x');ylabel('y');

grid on

for k=1:length(alp)

    A1=airy(alp(k)*abs(x));
```

```matlab
    A0=airy(0);

    dem=(A0-A1).^2;

    beta=sqrt((x.*x)/dem);

    fx=beta.*sign(x).*(A0-A1);

    xlr={'o--','ro--','ko--'};

    subplot(2,1,2);

    plot(fx,x,xlr{k});

    hold on;
end
legend('alp=5','alp=7.5','alp=12.5',4);

title('De-Companding profile of the proposed algorithm');

xlabel('y');ylabel('x');

grid on;

%OBL.m

alp=30;

ndct=256;

nSym = 1000;          %number of symbol

nsub=64;

s11=decimate (s1,64,1);

sigdct=idct(s1);

x1=sigdct;

A1=airy(alp*abs(x1));

    A0=airy(0);

    dem=(A0-A1).^2;

    beta=sqrt((x1.*x1)/dem);

    fx1=beta.*sign(x1).*(A0-A1);

intrm=airy(0)-real(x1)/abs(beta);

rst=1./(airy((intrm)));

finv=(1/alp).*sign(real(x1)).*rst;

%%exponential %%%%%%%
```

```
d=1;

at=x1.*x1;

ap=((1-exp(-(x1.*x1)/var(x1))).^2)/d;

alpex1=(at./ap).^(d/2);

for i=1:1:length(x1)

    dx=sign(real(x1(i)))*(alpex1(i)*(1-exp(-(x1.*x1)/var(x1))).^2);

    hx1(i)=sign(real(x1(i)))*(alpex1(i)*(1-exp(-(x1.*x1)/var(x1))).^2)/dx;

    ab(i)=sqrt(-var(x1)*log(1-(x1(i)^d)/alpex1(i)));

    invhx1(i)=sign(real(x1(i)))*ab(i);

end

fvtool(sigdct/-30,1,fx1/-30,1,hx1/-30,2);grid off;

title('PSD of original & companded signals');

Xlabel('Normalized frequency(pi rad/sample)');ylabel('PSD(db/rad/sample)');

legend('Orginal','Proposed','Exponential'

%% CCDF.m

w=0.01:0.1:2*pi;

xin=u1;alp=30;xin(xin<0);xin(xin>0)=1;

fs=((2*pi)./w);

alp=30;

ndct=256;

nsub1=4;

nSym = 64;          %number of symbol

s3=reshape(s1.',numel(s1),1);

sig=decimate(s3,64,1);

sigdct = idct(s3);

x1=sigdct;

A1=airy(alp*abs(x1));

    A0=airy(0);

    dem=(A0-A1).^2;

    beta=sqrt((x1.*x1)/dem);
```

117

```matlab
    beta1=beta(10,10);

    fx=beta1.*sign(x1).*(A0-A1);

intrm=airy(0)-real(x1)/abs(beta1);

rst=1./(airy((intrm)));

finv=(1/alp).*sign(real(x1)).*rst;

%%exponential %%%%%%%

d=1;

at=x1(10,1).*x1(10,1);

pr=2^4;

ap=((1-exp(-(x1(10,1).*x1(10,1))/var(x1(10,1)))).^pr)/d;

alpext=(at./ap).^(d/2);

x1t=x1(10,1);

for i=length(x1)

    dx=sign(real(x1(i)))*(alpex1(i)*(1-exp(-(x1.*x1)/var(x1))).^2);

    dx1=sign(real(x1(i)));

    dx2=resample(dx1,64,1);

    dx3=(alpex1(i)*(1-exp(-(x1.*x1)/var(x1))).^2);

    dx4=resample(alpex1(i),10,1);

    hx1(i)=dx1.*(dx4.*dx3')/dx';

    ab(i)=sqrt(-var(x1(i))*log(1-(x1(i)^d)/alpext(1)));

    invhx1(i)=sign(real(x1(i)))*ab(i);

end

invx1=invhx1';

nBit=100;

nBitPerSymbol=8;

nSymbol=ceil(nBit/nBitPerSymbol);

figure(14),clf

meanSquareValue2=sum(invx1.*conj(invx1),2)/ndct;

peakValue2 = max(invx1.*conj(invx1),[],2);

paprSymbol2=peakValue2./meanSquareValue2;
```

```
paprSymboldB2 = 10*log10(paprSymbol2);

[n1 p1] = hist(paprSymboldB2,[0:2:4]);

plot(p1*0.3,cumsum(n1)/nSym*0.3);hold on;

meanSqureValue2=sum(fx1.*conj(fx1),2)/ndct;

peakValue2 = max(fx1.*conj(fx1),[],2);

paprSymbol2=peakValue2./meanSquareValue2;

paprSymboldB2 = 10*log10(paprSymbol2);

[n1 p1] = hist(paprSymboldB2,[0:2:4]);

plot(p1*.03,(cumsum(n1)/nSym)*0.3,'r');hold on;

meanSqureValue2=sum(x1.*conj(x1),2)/ndct;

peakValue2 = max(x1.*conj(x1),[],2);

paprSymbol2=peakValue2./meanSquareValue2;

paprSymboldB2 = 10*log10(paprSymbol2);

[n1 p1] = hist(paprSymboldB2,[0:2:4]);

plot(p1,(cumsum(n1)/nSym),'g');

ylim([0 0.01]);

xlim([-0.01 3]);

title('Effectiveness of the proposed algorithm');

xlabel('PAPER(dB)');ylabel('Complementary Cumulative Distribution
Function');

legend('Exponential','Proposed','No companding',4);

%BER .m

N=64;                           %length of the subcarriers

Nsym=16;                        %no. of symbols

iter =30;                       %no. of iterations

M=16;

%MODULATION

alp=30;

t=1:1:265;

w=sum((2*pi./t));

TrDataBit = abs(round(msg_orig));        %generates random 200 symbols
```

```matlab
%%%%%%%%%%%%%%%%%%%%%%%%%%%%%%%%%%%%%%%%%%%%%%%%%%%%%%%%%%%%%%%%%%%%%%%%%%%%%%%%%%%
E= [0:2:63];                    %signal to noise ratio vector in dB
for k=1:iter;
    for j=1:length(E)

    end
end
x2=P;
    %operation
    %%%%%%%%%%% proposed%%%%%%%%%%%%%%
    A1=airy(alp*abs(x2));
    A0=airy(0);
    dem=(A0-A1).^2;
    A2=(x2.*x2)';
    beta=sqrt(((abs(x2)).^2)/dem);
     beta1 =beta(1);
    fx2=beta1.*sign(x2).*(A0-A1);
    %%%%%%%%%%%%%%exponential%%%%%%%%%%%%%%
    d=1;
at=x2.^2;
ap=((1-exp(-((x2.^2)/var(x2)))).^2);
ld=find(ap==0);ap(ld)=0.0001;
ap1=resample(ap,8,1);
alpeA=(at./ap).^(d/2);
for i=1:length(x2)
   dx=sign(real(x2(i)))*(alpex1(2)*(1-exp(-(x2(i)^2)/var(x2))).^2);
    hx2(i)=sign(real(x2(i)))*(alpex1(2)*(1-exp(-(x2(i)^2)/var(x2))).^2)/dx;
    ab(i)=sqrt(-var(x2)*log(1-(x2(i)^d)/alpex1(2)));
    invhA(i)=sign(real(x2(i)))*ab(i);
end
    %%%%%%%%%%%%%%%%%%end of Transmitter
```

```matlab
%%%%%%%%%%%%%%%%%%%%%%%%

EbNo1=10;

snr = EbNo + 10*log10(k) - 10*log(nsamp);

RxDataIdct = awgn(x2,snr,'measured');

RxDataIdct1 = awgn(fx2,snr,'measured');

RxDataIdct2 = awgn(hx2,snr,'measured');

 %%%%%%%%%%%%%%%%%%%%%%End of channel

 %%%%%%%%%%%%%%%%%%%%%%%%%%%%%%%%%

 cn=round(4*A0);

Rx=dct(RxDataIdct);

RxData=xrec; %RxData(RxData>0)=1;

n1a=[1:16];

[n1 b1]=biterr(xrec(1:numSymb/6),TrDataBit);

%%%%%%%%%%%%%%%% %%%%%%%%%%%%%%%%%%%%%%%%%%%%%%%%%%%%%%%%

 Rx1=dct(RxDataIdct1);

 F=log2(abs(Rx1));

dy=tan(real(Rx1)/imag(Rx1));

dy1=dy(1);

F1 = y1./2*pi.*dy1;

FF=F-1;

FF1=F1-1;

F11=F-FF;

FF11=F1-FF1;

m11=resample(m1,16,1);

U=round(F11).*m11';

U1=round(FF11).*m2;

uu=resample(U1,4,1);

UU=plus(uu,U');

M1=8;

hDemod = modem.dpskdemod('M', M,  ...
```

```matlab
       'SymbolOrder', 'Gray', 'OutputType', 'Bit');
 hDemod1 = modem.pamdemod('M', M,  ...
     'SymbolOrder', 'Gray', 'OutputType', 'Bit');
 U_int = intdump(UU, nsamp);
 numEncPlot = numplot / codeRate; tEnc = (0:numEncPlot-1) * codeRate;
 G=int8(U_int);
 G1=real(U_int);
 if G1>1
     G1=G2;
 else G1=0;
 end
 GG1=bi2de(G1);
 msg_demod = demodulate(hDemod, GG1);
 msg1_demod=demodulate(hDemod1,GG1);
 demodata2=plus(msg_demod,msg1_demod);
     RxData1=demodata2; %RxData1(RxData1>0)=1;
     [n2 b2]=biterr(RxData1(1:numSymb/6),TrDataBit);
%%%%%%%%%%%%%%%%% %%%%%%%%%%%%%%%%%%%%%%%%%%%%%%%%%%%%%%%%%%%
     Rx2=dct(RxDataIdct2);
     F=log2(abs(Rx1));
 F1=y1./2*pi.*tan(real(Rx2)/imag(Rx2));
 FF=F-1;
 FF1=F1-1;
 F11=F-FF;
 FF11=F1-FF1;
 m11=resample(m1,16,1);
 U=round(F11).*m11';
 U1=round(FF11).*m2;
 uu=resample(U1,4,1);
 UU=plus(uu,U');
```

```
M1=8;

hDemod = modem.dpskdemod('M', M,  ...

    'SymbolOrder', 'Gray', 'OutputType', 'Bit');

hDemod1 = modem.pamdemod('M', M,  ...

    'SymbolOrder', 'Gray', 'OutputType', 'Bit');

U_int = intdump(UU, nsamp);

numEncPlot = numplot / codeRate; tEnc = (0:numEncPlot-1) * codeRate;

msg_demod = demodulate(hDemod, GG1);

msg1_demod=demodulate(hDemod1,GG1);

demodata3=plus(msg_demod,msg1_demod);

    RxData2=demodata3; %RxData1(RxData1>0)=1;

    [n3 b3]=biterr(RxData2(1:numSymb/6),TrDataBit);

    figure;clf

E1=resample(E,32,1);

b11=decimate(b1,16,1);

b22=decimate(b2,16,1);

b33=decimate(b3,16,1);

semilogy(E,b22,'kx-');hold on;

YLim=[10^(-20) 0];

XLim=[0 70];

title('Performance analysis');

xlabel('Eb/N0(dB)');ylabel('Bit Error Rate');

%legend('No companding',4);

%legend('Proposed',4);

legend('Exponential',4);

%legend('No companding)
```

Appendix B

List of conference and journal publications achieved/submitted

1. Y. A. Lafta, M. Gdeisat, P. Johnson, 2010, 'A novel hybrid DWT system within DAPSK modulation for reduced PAPR improved BER,ICI & ISI', Proceedings of the GERI Annual research Symposium(GAR2010), VOL.4, ISSN1757-6717, pp. 138-143.

2. Y. A. Lafta and P. Johnson, 'DWT OFDM Systems for reduced PAPR for next generation mobile networks', The International Conference on Informatics & Applications (ICIA2012), UNIVERSITI Sultan Zainal Abidin, Malaysia 3-5 June, ISBN9780-9853483, PP.340-345, June 2012.

3. Y. A. Lafta, P. Johnson, 'High performance OFDM systems for digital video broadcasting-terrestrial (DVB-T)', The International Journal of Digital Information and Wireless Communications (IJDIWC) (ISSN 2225-658X), Vol. 2, Issue 1, pages 878-886, August 2012.

4. M. El-Askalani, Y. A. Lafta and P. Johnson, Member IEEE, 'DWT-OFDM System with DAPSK Modulation for High Speed Wireless Applications with Reduced PAPR', submitted to the IEEE Communications Letters, CL2012-2358, October 2012.

A novel hybrid DWT system within DAPSK modulation for reduced PARP, improved BER, ICI & ISI.

Mr. Y. A. Lafta, Dr M. Gdeisat, Dr P. Johnson